TRANSPORTATION RESEARCH RECORD
548

Soil and Rock Mechanics, Culverts, and Compaction

9 reports prepared for the 54th Annual Meeting of the Transportation Research Board

TRB
TRANSPORTATION RESEARCH BOARD
NATIONAL RESEARCH COUNCIL
Washington, D. C., 1975

Transportation Research Record 548
Price $4.60
Edited for TRB by Joan B. Silberman

Subject areas
33 construction
62 foundations (soils)
63 mechanics (earth mass)

The conference that is the subject of this report was approved by the Governing Board of the National Research Council acting in behalf of the National Academy of Sciences. Such approval reflects the Governing Board's judgment that the conference is of national importance and appropriate with respect to both the purposes and resources of the National Research Council.

The members of the committee selected to organiz the conference and to supervise the preparation of thi report were chosen for recognized scholarly competence and with due consideration for the balance of disciplines appropriate to the project.

Responsibility for the selection of the participants in the conference and for any summaries or recommer dations in this report rests with that committee. The views expressed in individual papers and attributed to the authors of those papers are those of the authors and do not necessarily reflect the view of the committee, the Transportation Research Board, the National Academy of Sciences, or the sponsors of the project.

Each report issuing from such a conference of the National Research Council is reviewed by an independent group of qualified individuals according to procedures established and monitored by the Report Review Committee of the National Academy of Sciences Distribution of the report is approved by the Presiden of the Academy upon satisfactory completion of the review process.

LIBRARY OF CONGRESS CATALOGING IN PUBLICATION DATA

National Research Council. Transportation Research Board.
Soil and rock mechanics, culverts, and compaction.

(Transportation research record; 548)

1. Roads–Foundations–Congresses. 2. Soil mechanics–Congresses. 3. Rock mechanics–Congresses. I. Title. II. Series.
TE7.H5 no. 548 [TE210] 380.5'085 [625.7'32] 75-37632
ISBN 0-309-02453-6

CONTENTS

FOREWORD

Although the trend is toward computer aided solutions, there are many times when graphical or chart solutions can aid engineers in checking the reasonableness of a computer answer or in a simplistic check of a proposed embankment design. Huang provides two charts, and Fang, Snitbhan, and Chen have supplied another that will aid materially in these quick check solutions.

Hagerty, Deen, Palmer, and Tockstein propose an engineering rock evaluation schema for various professionals to use in planning transportation facilities. The schema emphasizes the ease of data accumulation, storage, and retrieval.

Preloading by vacuum to accelerate the consolidation of fills constructed on soft clay soils is described by Holtz and Wager. Cost estimates and a full-scale test fill are described. It is estimated that, where applicable, this method might reduce the cost of preloading by as much as two-thirds.

Alonso and Krizek present a simulation procedure to analyze the influence of a randomly varying coefficient of permeability on the one-dimensional consolidation settlement of clay layers. Corotis, El-Moursi, and Krizek present a method for using derived distributions to develop a probabilistic model for predicting the total settlement in a compressible clay layer in terms of uncertain soil compressibility and loads. Both papers help in the opportunity for making realistic predictions when heterogeneous natural clay layers are dealt with.

Selig and Calabrese describe the instrumentation and data obtained from a large experimental buried structure. The report presents useful information regarding the magnitudes and distribution of stresses and deformations, the influence of construction procedures, and the apparent moduli of the backfill.

A rapid method of compaction control testing is proposed by Hatano and Smith, who present comparative data and time savings. Howeedy and Bazaraa describe 22 test fills that were compacted by using 7 models of vibratory compactors. For these specific conditions, they present the relationship attained for final relative density as it relates to lift thickness, coverage, force, frequency, and towing speed.

Sneddon describes a method of obtaining secant moduli, soil support values, and subgrade modulus from an analysis of triaxial data for the soils involved.

This RECORD will be of interest to soil and pavement design engineers.

STABILITY CHARTS FOR EARTH EMBANKMENTS

Y. H. Huang, Department of Civil Engineering,
University of Kentucky

Two new charts are presented for the stability analysis of earth embankments. The chart for short-term stability is based on the $\phi = 0$ analysis and can be applied to a nonhomogeneous slope composed of various soil layers, and that for long-term stability is based on the $\bar{c}$, $\bar{\phi}$ analysis and is applicable only to a homogeneous slope. The major advantage of these charts compared with those currently available is their simplicity. They can be used by practicing engineers to determine the factor of safety of a proposed embankment or to check the reasonableness of a computer solution. With discretion, the charts can be applied to a variety of cases encountered in engineering practice. Examples demonstrate the application of these charts to the stability analysis of earth embankments. The factors of safety obtained from the new charts are compared with those from the ICES-LEASE computer program, based on the simplified Bishop method, and are found to be in good agreement.

•SINCE Taylor (1) first published his stability charts in 1937, various charts have been successively presented by Bishop and Morgenstern (2), Morgenstern (3), Spencer (4), and Hunter and Schuster (5) for the stability analysis of earth slopes. These charts can be divided into two categories: those based on the total stress analysis for short-term stability, in which the pore pressure along the failure surface is not considered, and those based on effective stress analysis for long-term stability, in which the pore pressure must be prescribed. Each chart has its advantages and disadvantages; some are too simplified to bear resemblance to actual field conditions, and some are too complex and require extensive interpolations and calculations. The applications of these charts were reviewed by Hunter and Schuster (6).

Although computer programs are now available for the stability analysis of slopes, these programs generally do not serve the same purpose as stability charts. For major projects in which the shear strength parameters of the various soils are carefully determined and the geometry of the slope is complex, a computer program will provide the most economical and probably the most useful solution, even though stability charts can still be used as a guide for preliminary designs or as a rough check for the computer solution. For minor projects in which the shear strength parameters are estimated from the results of standard penetration tests or index properties, the application of sophisticated computer programs may not be worthwhile, and stability charts should be used instead.

Two new charts are presented: one for short-term stability analysis of embankments and one for long-term stability analysis. The short-term analysis is used to ensure the stability during or immediately after construction, and the long-term analysis to ensure the stability long after construction. The design of earth embankments is generally governed by short-term stability. However, long-term stability should also be considered if the embankments are subjected to steady-state seepage or rapid drawdown. In this paper, the chart for short-term stability is designed to take care of nonhomogeneous soils composed of various layers because the short-term

Publication of this paper sponsored by Committee on Embankments and Earth Slopes.

shear strength, or cohesion, usually varies appreciably from soil to soil. To simplify applications, the chart for long-term stability considers a homogeneous soil only. This consideration does not impose severe limitations because the long-term shear strength, i.e., effective cohesion and effective friction angle, does not change significantly in a given region, and average values can usually be used. Examples demonstrate the application of the charts to the stability analysis of earth embankments. The solutions obtained from the charts are compared with those from the ICES-LEASE computer program (7), based on the simplified Bishop method, and are found to be in good agreement.

TOTAL STRESS ANALYSIS

The total stress analysis is used to evaluate the short-term stability of embankments or the stability at the end of construction.

Shear Strength

When the soil is completely saturated and the embankment is constructed rapidly relative to the time of consolidation, the shear strength of soils can be represented by a horizontal envelope with an angle of internal friction ϕ equal to 0 so that the $\phi = 0$ analysis can be applied. Because the shear strength is independent of the confining pressure, an unconfined compression test can be used to determine the cohesion c that is one-half of the unconfined compressive strength. Because of sample disturbance, the unconfined compression test generally underestimates the shear strength. A more representative shear strength may be obtained from an unconsolidated, undrained triaxial test using a confining pressure approximately equal to the anticipated overburden pressure. One-half of the deviator stress, which causes the specimen to fail, is the cohesion of the soil.

If the soil is only partially saturated, either the construction period is long compared with the time of consolidation or the soil is granular; ϕ will no longer be 0, and the shear strength will depend on the magnitude of confining pressure. Even in this case, the $\phi = 0$ analysis can still be applied if the soil is divided into different layers and different values of c, based on the anticipated overburden pressure, are used for each layer.

Stability Chart

Figure 1 shows the stability chart for the $\phi = 0$ analysis. The chart is based on a homogeneous simple slope and a circular failure surface, as shown in the upper left corner of Figure 1. The embankment has a height H, and a side slope S:1. A ledge is located at a depth DH below the toe, where D is the depth ratio. It can be seen from the figure that, the deeper the circle is, the smaller the stability factor will be; therefore, the critical circle is always tangent to the ledge. The center of the circle is at a horizontal distance XH and a vertical distance YH from the edge of the embankment. By equating the driving moment about the center of the circle due to weight to the resisting moment due to the cohesion of the soil along the failure arc, the developed cohesion c_d is obtained. The stability factor N_s is defined as

$$N_s = \frac{\gamma H}{c_d} \tag{1}$$

where γ = unit mass of soil. A computer program was developed for the required calculations. The chart is different from Taylor's (1) in that the stability factors for

various circles are shown, and thus the application of the chart to nonhomogeneous soils is possible.

For a section of homogeneous soil with the critical circle passing below the toe, it can be easily proved (1) that the center of the critical circle lies on a vertical line intersecting the slope at midheight, or X = 0.5S. This type of failure surface is called a midpoint circle, the results of which are shown by the solid curves in Figure 1. If the depth ratio D is small, the failure surface may intersect the slope at or above the toe. This type of failure surface is called a toe or slope circle, the results of which are shown by the dashed curves. For D = 0 and S < 2.5, the value of X for the center of the critical circle may be different from 0.5S, as shown in the figure.

Nonhomogeneous Slopes

For illustration of the application of the chart to nonhomogeneous slopes, consider the embankment shown in Figure 2. The embankment is 20 ft (6.1 m) high and has a side slope of 3:1 and a cohesion of 1,500 lb/ft^2 (71.9 kPa). The foundation consists of one 40-ft-thick (12.2-m) soil layer having a cohesion of 800 lb/ft^2 (38.3 kPa), and one 20-ft-thick (6.1-m) soil layer having a cohesion of 100 lb/ft^2 (4.8 kPa), which is underlaid by a ledge. The assumption of a cohesion as low as 100 lb/ft^2 (4.8 kPa) is not realistic but is used merely to indicate the contrast in shear strength among different layers. Although the unit weights for different soils are generally not the same, an average unit mass of 130 lb/ft^3 (2080 kg/m^3) is assumed. Because the weakest layer lies directly above the ledge, the critical circle will be tangent to the ledge, or D = 60/20 = 3.

If the slope is homogeneous with S = 3 and D = 3, from Figure 1 the most critical circle is a midpoint circle with a center located at YH = 2 × 20 = 40 ft (12.2 m) above the top of embankment, and a minimum stability factor of 5.7 is obtained. The developed cohesion c_d, or the cohesion that is actually mobilized, can be determined by

$$c_d = \frac{\gamma H}{N_s} = \frac{130 \times 20}{5.7} = 456 \text{ lb/ft}^2 \text{ (21.8 kPa)} \qquad (2)$$

Because the slope is not homogeneous, the center of the most critical circle may be different from that of a homogeneous slope. However, unless D and S are small, the difference between the two centers is generally small; therefore, the critical center for homogeneous slopes can be used for nonhomogeneous slopes as well.

In Figure 2, the circle with the center at 40 ft (12.2 m) above the top of embankment is the critical circle based on a homogeneous slope. The average effective cohesion c_e, or the maximum cohesion that can be mobilized along the failure arc, can be determined by measuring the length of arc through each soil and by taking the weighted average.

$$c_e = \frac{24 \times 1{,}500 + 2 \times 57 \times 800 + 142 \times 100}{24 + 2 \times 57 + 142} = 505 \text{ lb/ft}^2 \text{ (24.2 kPa)} \qquad (3)$$

By definition,

$$\text{factor of safety} = \frac{c_e}{c_d} = \frac{505}{456} = 1.11 \qquad (4)$$

If a circle of larger radius with Y = 6 or YH = 6 × 20 = 120 ft (36.6 m) is used, from Figure 1, N_s = 6.05, or

Figure 1. Stability chart for $\phi = 0$ analysis.

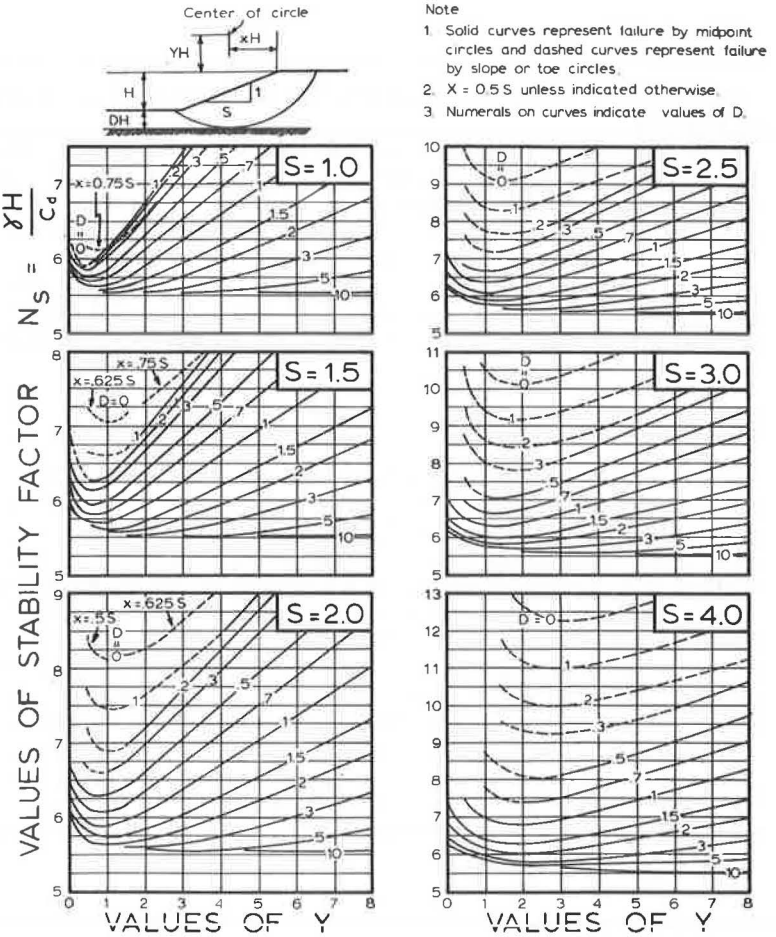

Figure 2. Failure circles in nonhomogeneous slope.

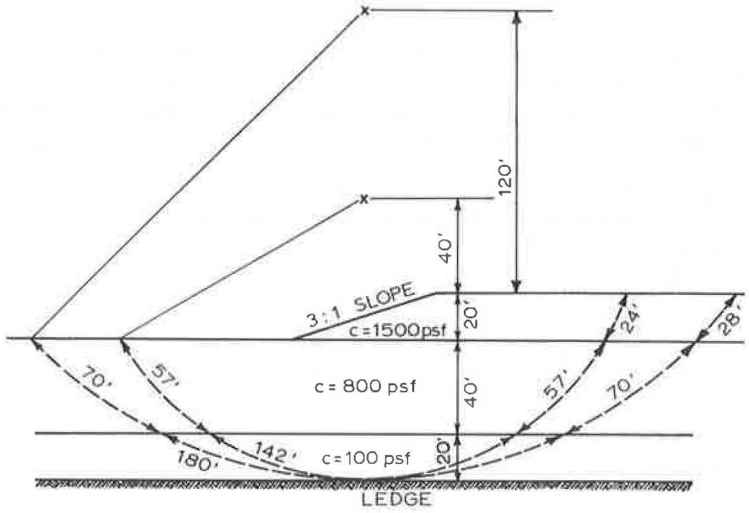

Figure 3. Nonhomogeneous slope with multiple soil layers.

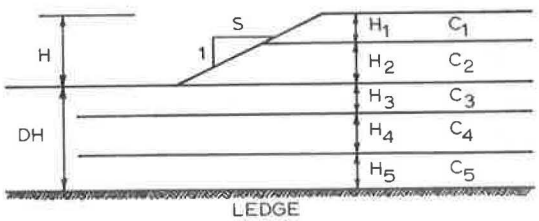

$$c_d = \frac{130 \times 20}{6.05} = 430 \text{ lb/ft}^2 \text{ (20.6 kPa)} \quad (5)$$

When the length of arc through each soil layer is measured,

$$c_e = \frac{28 \times 1{,}500 + 2 \times 70 \times 800 + 180 \times 100}{28 + 2 \times 70 + 180} = 494 \text{ lb/ft}^2 \text{ (23.7 kPa)} \quad (6)$$

therefore,

$$\text{factor of safety} = \frac{494}{430} = 1.15 \quad (7)$$

It can be seen that the use of the critical center based on a homogeneous slope still yields a smaller factor of safety. When the critical failure surface is tangent to the bottom of a weak stratum and the center is moved upward, the decrease in effective cohesion due to a larger radius is not as significant as the decrease in developed cohesion; thus a greater factor of safety is obtained. This is especially true when D is small. If the critical center based on homogeneous slope is moved downward, the effective cohesion increases while the developed cohesion decreases, and a greater factor of safety results.

For the slope shown in Figure 2, the ICES-LEASE computer program gives a minimum factor of safety of 1.05 with the center of the most critical circle at X = 1.5 and Y = 2.

Comparison With Computer Solutions

To check the accuracy of the method for analyzing nonhomogeneous slopes, I determined the factors of safety for the slope shown in Figure 3 by the chart and compared them with those obtained from the ICES-LEASE computer program. The total unit mass of soils is assumed to be 120 lb/ft^3 (1920 kg/m^3). The chart solution was obtained by assuming that the center of the critical circle was the same as that of a homogeneous slope. Fifteen cases involving various combinations of depth ratios, slopes, and soil layers were investigated, and the results are given in Table 1. Both solutions check closely and there is no discrepancy greater than 5 percent; thus the accuracy of the chart solutions is verified.

To determine the minimum factor of safety from the chart, one can investigate one or more circles, depending on the locations of various soil layers. For example, cases 5, 6 and 7 in Table 1 have the same geometry, except that the cohesions for the last three layers are interchanged. In case 5, the most critical circle is tangent to the ledge at the bottom of layer 5; therefore, only one circle needs to be studied. In case 6, the most critical circle is tangent to the bottom of either layer 4 or 5; therefore, two circles are needed. The two circles tangent to the bottom of layers 3 and 5 should be investigated for case 7.

EFFECTIVE STRESS ANALYSIS

The effective stress analysis can be used to predict the long-term stability of embankments. After a long time, the pore pressure becomes stabilized, and the effective stress can be estimated and used for the analysis.

Shear Strength

In effective stress analysis, the shear strength of soils is expressed by Coulomb's law

$$s = \bar{c} + (\sigma - u) \tan \bar{\phi} \quad (8)$$

in which s = shear strength, $\bar{c}$ = effective cohesion, $\bar{\phi}$ = effective friction angle, σ = total normal stress, and u = pore pressure. Because the effective strength parameters $\bar{c}$ and $\bar{\phi}$ must be available before an analysis can be made, the effective stress analysis is also called the $\bar{c}$, $\bar{\phi}$ analysis.

The effective strength parameters can be determined from slow types of triaxial tests or, more conveniently, from triaxial tests with pore pressure measurements. Approximate correlations between strength parameters and the classification or index properties of soils can be found in the literature (8).

Stability Chart

Figure 4 shows the stability chart for the $\bar{c}$, $\bar{\phi}$ analysis. Two extreme cases are presented: one for zero pore pressure as indicated by the solid curves and one for a pore pressure ratio of 0.5 as indicated by the dashed curves. The pore pressure ratio is defined as the ratio between the pore pressure and the total overburden pressure. A pore pressure ratio of 0.5 indicates that the pore pressure at any point on the failure surface at a distance h below the surface of the slope is equal to 0.5 γh, where γ is the total unit mass of soil. If a soil mass is 125 lb/ft^3 (2000 kg/m^3), 0.5 γ is equal to the unit mass of water γ_w; therefore, the pore pressure can be written as γ_wh. This is similar to the case of rapid drawdown when the phreatic surface coincides with the surface of the slope. This case is of practical importance for the design of earth dams and embankments subjected to flooding.

For intermediate cases, such as those involving steady-state seepage, the pore pressure ratio will be between 0 and 0.5, and its value can be roughly estimated from the location of the phreatic line, described later. Bishop and Morgenstern (2) have indicated that a straight-line relationship exists between the factor of safety and the pore pressure ratio; therefore, the factor of safety for pore pressure ratios other than 0 and 0.5 can be obtained by direct interpolation.

The factor of safety shown in Figure 4 is based on the analysis of a homogeneous slope by the simplified Bishop method (9). Part of the data were obtained from the charts and tables by Bishop and Morgenstern (2), and the remaining from the ICES-LEASE computer program. The slope and the failure surfaces are shown in the upper left corner of Figure 4. In contrast to the $\phi = 0$ analysis, which involves deep circles, the critical circle determined by the effective stress analysis is quite shallow. The chart is different from Bishop and Morgenstern's in that the ledge is assumed to be at a depth greater than 0.5 H from the toe; therefore, its presence has no effect on the factor of safety. If the ledge is located at or close to the toe, a slope circle will result, and the factor of safety may be slightly greater. Therefore, the use of the chart is on the safe side.

The major advantage of the chart shown in Figure 4 is its simplicity. For example, the factor of safety for a 3:1 slope with H = 20 ft (6.1 m), γ = 120 lb/ft^3 (1920 kg/m^3), $\bar{c}$ = 150 lb/ft^2 (7.2 kPa), $100\,\bar{c}/(\gamma H) = 6.25$, $\bar{\phi}$ = 30 deg, and a pore pressure ratio of 0.5 can be read directly from Figure 4 as 1.55. If the embankment is directly placed on a ledge, the factor of safety obtained from the Bishop and Morgenstern chart is 1.64, which is only slightly greater than the 1.55 obtained from the chart.

The chart also clearly shows the effect of friction angle, coehesion, and embankment height on the factor of safety. Note that when $\phi = 0$, the factor of safety is directly proportional to effective cohesion but inversely proportional to height; however, when $\phi \neq 0$, the effect of cohesion and height is greatly reduced. The curves for zero pore

Table 1. Chart versus computer solutions for various depth ratios, slopes, and soil layers.

Case Number	Depth Ratio	Slope	Thickness (ft)					Cohesion (lb/ft²)					Factor of Safety	
			H_1	H_2	H_3	H_4	H_5	C_1	C_2	C_3	C_4	C_5	By Chart	By Computer
1	0.250	1.5	10.0	10.0	5.0	0	0	1,500	750	75	0	0	1.19	1.22
2	0.250	3.0	20.0	0	5.0	0	0	1,000	0	100	0	0	1.62	1.53
3	0.875	1.5	2.5	17.5	5.0	7.5	5.0	1,800	1,200	300	150	600	1.19	1.15
4	0.875	1.5	2.5	17.5	5.0	7.5	5.0	1,800	1,200	150	600	300	1.32	1.32
5	1.000	2.0	2.5	17.5	2.5	7.5	10.0	1,800	1,200	600	300	150	1.01	0.99
6	1.000	2.0	2.5	17.5	2.5	7.5	10.0	1,800	1,200	300	150	600	1.27	1.24
7	1.000	2.0	2.5	17.5	2.5	7.5	10.0	1,800	1,200	150	600	300	1.35	1.37
8	1.000	2.5	15.0	0	7.5	7.5	0	1,000	0	400	100	0	1.14	1.15
9	1.000	2.5	2.5	17.5	2.5	7.5	10.0	1,200	800	100	400	200	0.91	0.89
10	1.000	4.0	5.0	10.0	2.5	12.5	0	1,000	500	100	300	0	1.34	1.29
11	1.500	3.0	2.5	17.5	5.0	5.0	20.0	1,200	800	200	100	400	0.97	0.96
12	1.500	3.0	2.5	17.5	5.0	5.0	20.0	1,200	800	400	200	100	0.61	0.58
13	1.500	4.0	2.5	17.5	5.0	5.0	20.0	1,800	1,200	150	600	300	1.16	1.13
14	1.500	4.0	2.5	17.5	5.0	5.0	20.0	1,800	1,200	300	150	600	1.63	1.64
15	5.000	1.0	10.0	0	50.0	0	0	1,500	0	150	0	0	1.00	0.96

Note: Different layers of soils are shown in Figure 3. 1 ft = 0.3 m, 1 lb/ft² = 47.9 Pa.

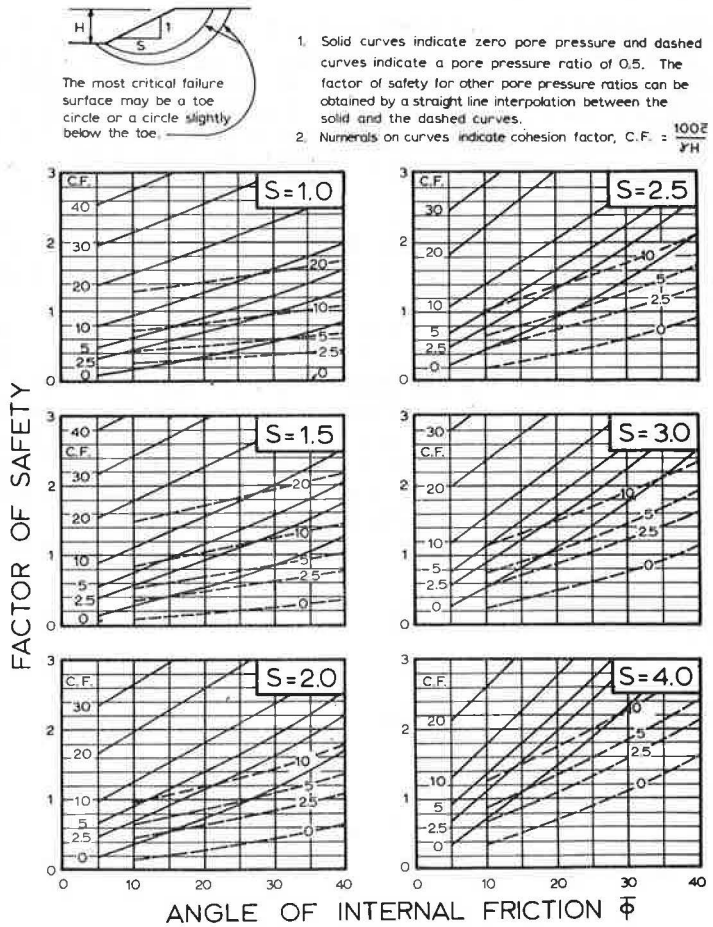

Figure 4. Stability chart for $\bar{c}$, $\bar{\phi}$ analysis.

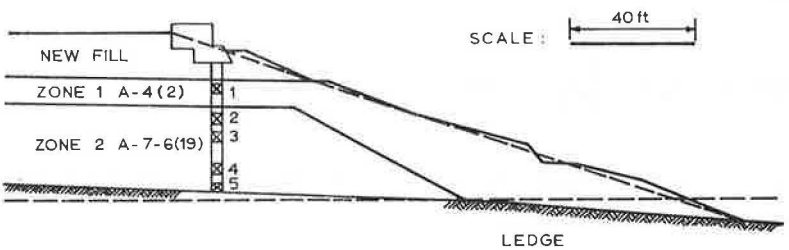

Figure 5. Proposed fill on south bank of Cumberland River.

pressure can also be used for total stress analysis when $\phi \neq$ zero.

PRACTICAL APPLICATIONS

The two charts shown in Figures 1 and 4 can be used by practicing engineers for the design and analysis of earth embankments, and I have applied the charts in my consulting practice and found them useful. They can be used to determine the factor of safety of a proposed slope or to check the reasonableness of a computer solution. Described below are two of the many actual cases in which these charts have been applied. These two cases are more complex than the simple slopes shown in Figure 3 and therefore may demonstrate the wide applicability of the charts.

South Bank of Cumberland River

Figure 5 shows a proposed fill on the south bank of the Cumberland River along Ky-225 in Knox County. The new fill will be placed on an existing embankment that consists of two zones. Shelby tube samples (Table 2) were taken from various depths, as indicated by the cross marks in Figure 5. The unit mass, moisture content, and unconfined compressive strength of the soils were determined, and the unconfined compressive strength of the fill material is assumed to be 3,000 lb/ft^2 (143.7 kPa). The effective strength parameters of the fill material (Table 3) and the materials in zones 1 and 2 (Figure 5) were determined by triaxial tests with pore pressure measurements. The fill is subjected to rapid drawdown with the initial water table 2 ft (0.6 m) below the top of the fill. The problem is to determine the factor of safety for both short-term and long-term stability.

In Figure 5, the surface of the slope is irregular, and the ledge is not horizontal. However, they can be approximated by a uniform slope of 3:1 and a horizontal ledge, as indicated by the dashed lines. In the total stress analysis, the cross section is divided into various zones, each with a different value of cohesion as shown in Figure 6. From Figure 1, the horizontal and vertical distances from the critical center to the edge of embankment for H = 54 ft (16.5 m), S = 3, and D = 0 are XH = 0.5 × 3 × 54 = 81 ft (24.7 m) and YH = 2 × 54 = 108 ft (32.9 m) respectively. The stability factor is 10.1. If the average unit mass γ is assumed to be 125 lb/ft^3 (2000 kg/m^3),

$$c_d = \frac{125 \times 54}{10.1} = 668 \text{ lb/ft}^2 \text{ (32.0 kPa)} \tag{9}$$

The effective cohesion based on the failure circle in Figure 6 is

$$c_d = \frac{21 \times 1{,}500 + 16 \times 740 + 32 \times 790 + 29 \times 420 + 54 \times 150 + 44 \times 740}{21 + 16 + 32 + 29 + 54 + 44}$$

$$= 620 \text{ lb/ft}^2 \text{ (29.7 kPa)} \tag{10}$$

Therefore,

$$\text{factor of safety} = \frac{620}{668} = 0.93 \tag{11}$$

The factor of safety obtained by the ICES-LEASE computer program using the

Table 2. Data from Shelby tube samples of fill from south bank of Cumberland River.

Location of Samples	Total Unit Mass (lb/ft³)	Moisture Content (percent)	Unconfined Compressive Strength (lb/ft²)	Cohesion Used (lb/ft²)
1	116.9	24.6	1,480	740
2	129.0	20.3	1,520	790
3	123.0	23.0	1,660	790
4	120.4	28.4	840	420
5	126.6	27.6	300	150

Note: 1 lb/ft³ = 16.01 kg/m³. 1 lb/ft² = 47.9 Pa.

Table 3. Effective strength parameters of fill from south bank of Cumberland River.

Zone	$\bar{c}$ (lb/ft²)	$\bar{\phi}$ (deg)	γ (lb/ft³)
Fill	200	30	128
1	167	30	120
2	387	27	125
Average	251	29	124

Note: 1 lb/ft² = 47.9 Pa, 1 lb/ft³ = 16.01 kg/m³.

Figure 6. Total stress analysis of south bank of Cumberland River.

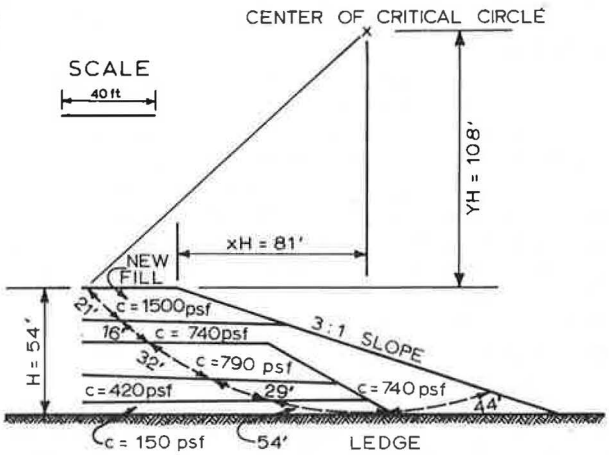

Figure 7. Effective stress analysis of south bank of Cumberland River.

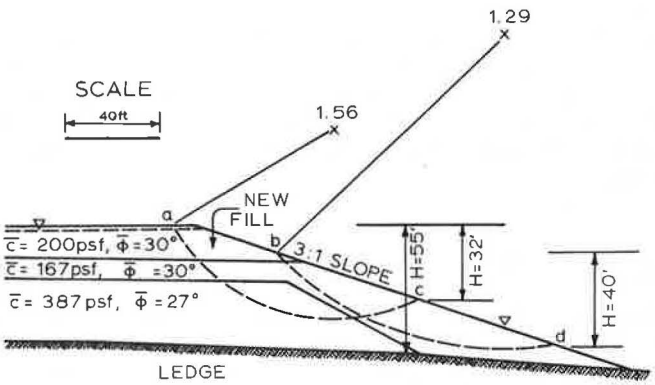

Figure 8. Cross section of Springfield Dam.

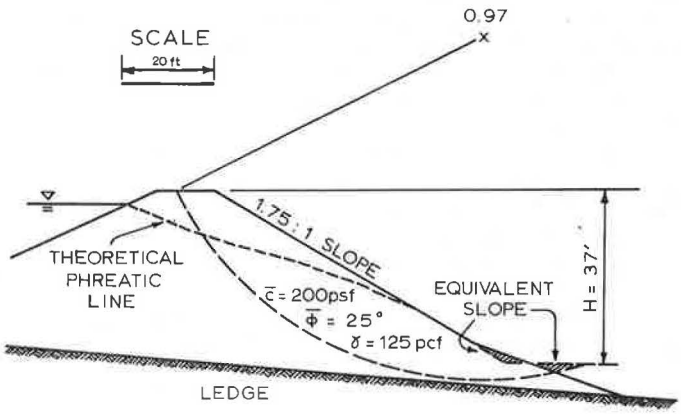

sloping ledge and the actual unit masses of soils is 0.86. Both values check closely and indicate that the embankment may fail during or immediately after construction.

In the effective stress analysis for long-term stability, a homogeneous slope must be assumed. Because the effective strength parameters and unit weights of the three soils are not too different, average values of $\bar{c}$ = 251 lb/ft^2 (12.0 kPa), $\bar{\phi}$ = 29 deg, and γ = 124 lb/ft^3 (198 kg/m^3) may be used. The total height of the embankment measured from the ledge at the middle of the slope, as shown in Figure 7, is 55 ft (16.8 m). Although the water table before drawdown is 2 ft (0.6 m) below the top of the fill, it is assumed to be at the top of the fill; therefore, a pore pressure ratio of 0.5 can be applied. With S = 3, $\bar{\phi}$ = 29 deg, and 100 $\bar{c}/\gamma H$ = 3.68, from Figure 4, a factor of safety of 1.30 is obtained. The minimum factor of safety obtained from the ICES-LEASE computer program is 1.29. The close agreement between the chart and the computer solutions is only coincidental. The computer solution shows that the most critical circle lies entirely in zone 1 and does not cut through all three materials as assumed in the chart solution, because the material with an effective cohesion of 387 lb/ft^2 (18.5 kPa) is too strong for the critical circle to pass through. Unless the materials in the embankment are quite uniform, the use of average strength parameters involves a high degree of risk and should proceed with caution.

Figure 7 shows the results of effective stress analysis by the ICES-LEASE computer program. The minimum factor of safety is 1.29, and the critical circle lies mostly in the existing slope. If the failure surface cuts through the new fill, a larger factor of safety, such as the 1.56 shown, is obtained. The factor of safety decreases as the circle moves to the right until it reaches a minimum value of 1.29. The factor of safety for the two circles shown in Figure 7 can be checked by the stability chart.

For the right circle, the height of slope may be taken as the vertical distance between points b and d where the failure circle and the slope intersect, or H = 40 ft (12.2 m). Note that any error in estimating the value of H will have a small effect on the factor of safety. For all practical purposes, the failure circle lies only in zone 1 with $\bar{c}$ = 167 lb/ft^2 (8.0 kPa) and γ = 120 lb/ft^3 (1920 kg/m^3), or 100 $\bar{c}/(\gamma H)$ = 3.48. For S = 3, $\bar{\phi}$ = 30 deg, 100 $\bar{c}/(\gamma H)$ = 3.48, and pore pressure ratio of 0.5, from Figure 4 the factor of safety is 1.30, which checks with the computer solution of 1.29.

For the left circle, the height of slope may be taken as the vertical distance between points a and c, or H = 32 ft (9.8 m). Because the failure circle cuts through all three soils, average values of $\bar{c}$, $\bar{\phi}$, and γ are used. The factor of safety determined from the chart is 1.55, which checks with the 1.56 determined from the ICES-LEASE computer program.

Springfield Dam

The Springfield Dam, which provides water supply to Springfield, Kentucky, is located in Washington County. The original dam was constructed long ago and was raised about 4 ft (1.2 m) in 1947 by placing a new, rolled earth fill on the top and along the downstream slope of the original earth dam. Recently failures took place at the downstream slope when the surface slid slightly below the bottom of the new fill. The cross section of the dam, at which failure occurred, is shown in Figure 8. Since failure occurred long after construction, an effective stress analysis with steady-state seepage was made by using the ICES-LEASE computer program. The phreatic line, or the line of seepage, was determined theoretically (10) and is shown in Figure 8. When $\bar{c}$ = 200 lb/ft^2 (9.6 kPa), $\bar{\phi}$ = 25 deg, and γ = 125 lb/ft^3 (2000 kg/m^3), a minimum factor of safety of 0.97 was obtained. These values of $\bar{c}$ and $\bar{\phi}$, which are typical for the type of soils used in the dam and which result in a factor of safety slightly smaller than 1, can be reasonably taken as the shear strength of soil at the time of failure and, therefore, used for the redesign of the dam.

The factor of safety obtained by the computer can be checked by the stability chart. An approximate method for determining the pore pressure ratio under steady-state seepage is to estimate the percentage of area below the phreatic line with respect to the total area of the sliding mass. If the phreatic line is on the top and along the surface

of the slope, as in the case of rapid drawdown, the area below the phreatic line is 100 percent; therefore, the dashed curves shown in Figure 4 should be used. If there is no seepage and no pore pressure, the area below the phreatic line is 0 percent; therefore, the solid curves shown in Figure 4 should be used. For the case shown in Figure 8, the area below the phreatic line is about 75 percent. Therefore, 75 percent of the value obtained from the dashed curves and 25 percent of that from the solid curves should be used to determine the factor of safety.

Although the downstream slope at the bottom of the embankment is different from that at the top, an equivalent slope with a height of 37 ft (11.3 m) can be assumed. If H = 37 ft (11.3 m), $\bar{c}$ = 200 lb/ft^2 (9.6 kPa), and γ = 125 lb/ft^3 (2000 kg/m^3), then $100\ \bar{c}/(\gamma H) = 4.32$. From Figure 4, the factor of safety for S = 1.5 and ϕ = 25 deg is 0.7 from the dashed curves, and 1.3 from the solid curves with a composite value of $0.75 \times 0.7 + 0.25 \times 1.3 = 0.85$. Similarly, the factor of safety for S = 2.0 is $0.75 \times 0.9 + 0.25 \times 1.6 = 1.07$. The factor of safety for S = 1.75 is 0.5 (0.85 + 1.07) = 0.96, which checks with the 0.97 obtained from the computer.

SUMMARY AND CONCLUSIONS

Two simple charts are presented for the stability analysis of earth embankments. The chart for the $\phi = 0$ analysis can be used to evaluate the short-term stability of embankments, and that for the $\bar{c}$, $\bar{\phi}$ analysis can be used to evaluate long-term stability. Although both charts are based on a homogeneous slope, a method was developed so that the chart for the $\phi = 0$ analysis can be applied to nonhomogeneous slopes as well.

In short-term stability analysis, the slope is divided into layers or zones, the cohesion of which may be determined from unconfined compression or unconsolidated, undrained triaxial tests. For a homogeneous slope, the location of the most critical circle and its stability factor can be determined from the chart, and in most cases this circle can also be used to compute the factor of safety for a nonhomogeneous slope. If the geometry of the slope is such that the critical circle for a homogeneous slope is no longer the same as that for a nonhomogeneous slope, the chart can be used to determine the factors of safety for other circles, and a minimum factor of safety can be obtained.

In long-term stability analysis, the effective strength parameters $\bar{c}$ and $\bar{\phi}$ of the various soil layers must be determined, and the average values, which represent the combined effect of all layers, must be assumed. The chart, which can be applied to determine the factor of safety for a homogeneous slope subjected to rapid drawdown or steady-state seepage, is based on the assumption that no ledge exists close to the surface. If a ledge is located at or close to the toe, the factor of safety may be slightly greater, and the use of the chart is on the safe side.

Examples demonstrate the application of these charts to the stability analysis of earth embankments. The charts can be used to determine the factor of safety of a proposed slope or to check the reasonableness of a computer solution. The solutions obtained from the charts are compared with those from the ICES-LEASE computer program and are found to be in good agreement. Although this paper is concerned primarily with earth embankments, the charts developed can be used for the analysis of cut slopes as well.

It should be emphasized that the greatest uncertainty in stability problems arises in the selection of shear strength. The error associated with the use of stability charts is usually small compared with that arising from the selection of strength parameters. Therefore, careful judgment in the selection of strength parameters is needed in the stability analysis of earth slopes.

ACKNOWLEDGMENTS

Data for the south bank of the Cumberland River were provided by the Bureau of Highways, Kentucky Department of Transportation, and those for the Springfield Dam by Howard K. Bell Consulting Engineers, Lexington, Kentucky. The stability analyses

were made by Stokley and Associates, to whom I served as a consultant, and their assistance in making the publication of this paper possible is gratefully acknowledged. The chart and computer solutions given in Table 1 were obtained by my students at the University of Kentucky as a homework exercise for an undergraduate course in foundation engineering. The support given by the University of Kentucky Computing Center for the use of an IBM 360 computer and the ICES-LEASE program is appreciated.

REFERENCES

1. D. W. Taylor. Stability of Earth Slopes. Journal of Boston Society of Civil Engineers, Vol. 24, 1937, pp. 197-246.
2. A. W. Bishop and N. Morgenstern. Stability Coefficients for Earth Slopes. Geotechnique, Vol. 10, No. 4, 1960, pp. 129-150.
3. N. Morgenstern. Stability Charts for Earth Slopes During Rapid Drawdown. Geotechnique, Vol. 13, No. 2, 1963, pp. 121-131.
4. E. Spencer. A Method of Analysis of the Stability of Embankments Assuming Parallel Inter-Slice Forces. Geotechnique, Vol. 17, No. 1, 1967, pp. 11-26.
5. J. H. Hunter and R. L. Schuster. Stability of Simple Cuttings in Normally Consolidated Clays. Geotechnique, Vol. 18, No. 3, 1968, pp. 372-378.
6. J. H. Hunter and R. L. Schuster. Chart Solutions for Analysis of Earth Slopes. Highway Research Record 345, 1971, pp. 77-89.
7. W. A. Bailey and J. T. Christian. ICES-LEASE-I, A Problem Oriented Language for Slope Stability Analysis, User's Manual. M.I.T., Soil Mechanics Publication No. 235, April 1969.
8. Design Manual, Soil Mechanics, Foundations, and Earth Structures. Department of Navy, NAVFAC DM-7, March 1971, p. 7-3-17 and p. 7-9-2.
9. A. W. Bishop. The Use of the Slip Circle in the Stability Analysis of Slopes. Geotechnique, Vol. 5, No. 1, 1955, pp. 7-17.
10. D. W. Taylor. Fundamentals of Soil Mechanics. John Wiley and Sons, 1948, pp. 181-185.

DISCUSSION

H. Y. Fang, N. Snitbhan, and W. F. Chen, Fritz Engineering Laboratory, Lehigh University

Huang has shown useful design charts for stability analyses of earth embankments. The solutions were obtained from the limit equilibrium approach, an extension of Taylor's work. Two cases have been studied: short-term stability based on the $\phi = 0$ analysis for a nonhomogeneous soil and a long-term stability for a homogeneous soil.

It has been pointed out previously (11, 14, 15, 17) that the limit equilibrium methods inherit many weaknesses. The soil's stress-strain relationship is totally neglected, and arbitrary assumptions must be made regarding the shape of the slip surface and a direct or an indirect pattern of the normal stress distribution along such a surface. Since Huang's results were based on these assumptions, there is no assurance that the minimum solutions have been achieved. A simple example shows the comparisons of Huang's and our results using the limit equilibrium and limit analysis methods respectively for $\phi = 0$ and $\beta = 45$ deg (S = 1.0):

1. Case 1. Slip surface passing through toe. Huang's limit equilibrium solution, $N_s = 6.12$ (D = 0); and our limit analysis solution, $N_s = 5.86$.
2. Case 2. Slip surface passing below toe. Huang's limit equilibrium solution,

N_s = 5.83 (D = 0.3); and our limit analysis solution, N_s = 5.53.

A complete solution derived from the limit analysis method and from the design charts for an anisotropic, nonhomogeneous slope (ϕ = constant c increasing linearly with depth) can be found (13, 18). Two typical examples, however, are presented to illustrate the purpose of the stability analysis of a slope on nonhomogeneous soil.

Example 1

Given a homogeneous slope, where β = 30 deg, φ = 0 deg, γ = 120 lb/ft^3 (1920 kg/cm^3), and c = 550 lb/ft^2 (26 400 kPa), find the critical height H_c. From Figure 9,

$$N_{so} = \frac{\gamma H_c}{c} = 5.5 \text{ (interpolated)} \tag{12}$$

Therefore,

$$H_c = \frac{5.5 \times 550}{120} = 25.3 \text{ ft (7.7 m)} \tag{13}$$

Example 2

Given a layered slope as shown in Figure 10, where n = -0.5, β = 30 deg, ϕ = 0 deg, γ = 120 lb/ft^3 (1920 kg/cm^3), and c = 550 lb/ft^3 (26 400 kPa), find the critical height H_c. From Figure 10,

$$\frac{N_{sn}}{N_{so}} = 0.72 \tag{14}$$

Therefore,

$$H_c = 0.72 \times 25.3 = 18.2 \text{ ft (5.5 m)} \tag{15}$$

REFERENCES

11. W. F. Chen, M. W. Giger, and H. Y. Fang. On the Limit Analysis of Stability of Slopes. Soils and Foundations, Vol. 9, No. 4, Dec. 1969, pp. 23-32.
12. W. F. Chen and M. W. Giger. Limit Analysis of Stability of Slopes. Journal of Soil Mechanics and Foundations Division, ASCE, Vol. 97, No. SM1, Jan. 1971, pp. 19-26.
13. W. F. Chen, N. Snitbhan, and H. Y. Fang. Stability of Slope in Anisotropic Nonhomogeneous Soils. Canadian Geotechnical Journal, Vol. 12, No. 1, Feb. 1975.
14. W. F. Chen. Limit Analysis and Soil Plasticity. Elsevier Scientific Publishing Co., Amsterdam, Netherlands, 1975.
15. H. Y. Fang and T. J. Hirst. Application of Plasticity Theory to Slope Stability Problems. Highway Research Record 323, 1970, pp. 26-38.

Figure 9. Stability factor versus slope for isotropic-homogeneous soils by limit analysis method.

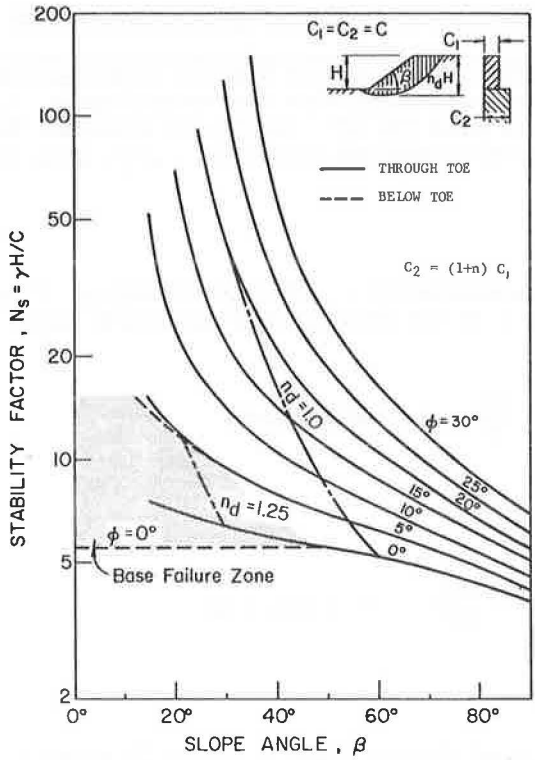

Figure 10. Effect of variation of cohesion with depth on stability factor for isotropic soil by limit analysis method.

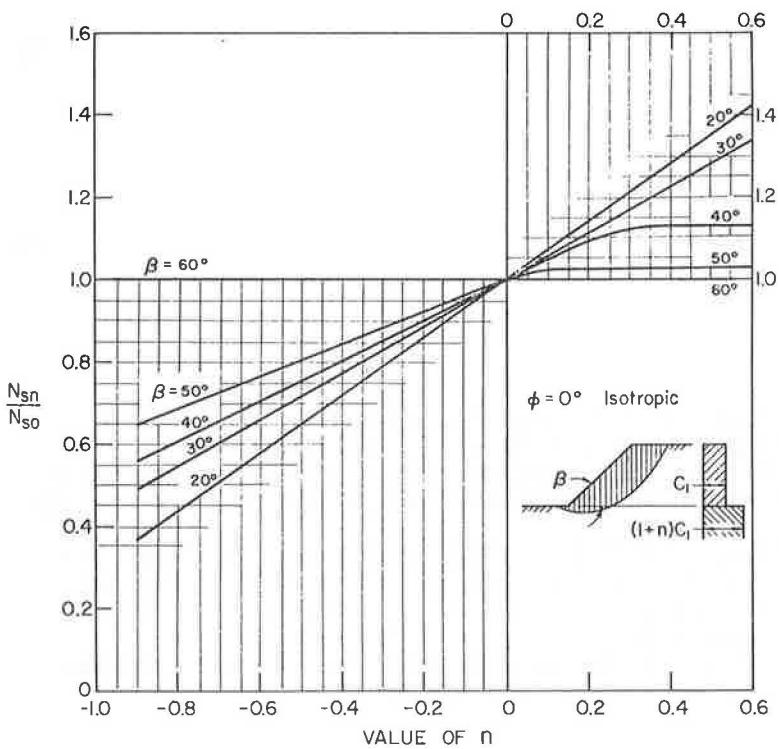

16. H. Y. Fang, W. F. Chen, H. L. Davidson, and J. Rosenfarb. Bibliography on Soil Plasticity. Envo Publishing Co., 1974.
17. H. Y. Fang. Stability of Earth Slopes. In Foundation Engineering Handbook, Van Nostrand Reinhold Co., 1975, pp. 354-371.
18. N. Snitbhan, W. F. Chen, and H. Y. Fang. Slope Stability Analysis of Layered Soils. Proc., 4th Southeast Asian Conference on Soil Engineering, Kuala Lumpur, Malaysia, April 1975.

AUTHOR'S CLOSURE

I appreciate the discussion by Fang, Snitbhan, and Chen. The additional charts they presented form a pertinent supplement to the original paper. Although they mentioned that these charts were obtained from the limit analysis method, a recent communication with them indicated that in many cases the limit analysis method they used was actually the same as the limit equilibrium method used by me; in other cases the results might be quite different. For the case of a $\phi = 0$ soil and a circular failure surface, as they cited in their examples 1 and 2, both methods should yield identical results. Therefore, the difference in stability factor between the two methods is due to the difference in the numerical technique used. However, the stability factors I used of 6.12 and 5.83 check more closely with those of 6.05 and 5.85 obtained from Taylor's stability chart (19).

REFERENCE

19. Taylor, D. W. Fundamentals of Soil Mechanics. John Wiley and Sons, 1948, p. 461.

ROCK EVALUATION FOR ENGINEERED FACILITIES

D. J. Hagerty, University of Louisville; and
R. C. Deen, M. W. Palmer, and C. D. Tockstein,
Division of Research, Kentucky Department of Transportation

An engineering classification system was designed for intact rock samples based on simple index tests that could be used to categorize Kentucky surface and near-surface rock types and to assist Kentucky Department of Transportation personnel in planning for transportation facilities. While the literature survey was being conducted, several facts became apparent: (a) A large number of geologic and technical and general and specific rock classification systems already existed; (b) an equally large number of index tests had been devised; and (c) there was a lack of communication among geologists and civil and mining engineers involved in specialized areas of rock-related work and, to some extent, among individuals within each field. It was evident from a careful study of existing classification systems and index testing procedures that developing yet another specialized classification system with associated index tests would not be a significant contribution. It was decided, therefore, to concentrate on development of an overall rock evaluation schema that, although useful for a specific purpose, would avoid the undesirable disparate characteristics of narrowness or overgeneralization prevalent in many classification systems and that would be developed so that accumulated information could be systematically stored for easy access and use. It was apparent that full development and implementation of a program of this nature would require further studies and cooperation of many individuals and organizations. Such a program, properly developed and used, would substantially contribute to an advancement, and a delineation of the schema and guidelines for its implementation would be a worthy goal.

•THE need for comprehensive information on the characteristics and behavior of earth materials has been recognized for many years, perhaps for as long as significant construction has taken place in and on the surface of the earth. Recently, however, the magnitude and complexity of engineered construction have greatly increased and have resulted in a corresponding increase in the need for information on the engineering properties of soil and rock materials. Direct testing of soil and rock can be used to furnish necessary information. However, both field and laboratory testing can be extremely expensive, particularly when testing must include applications of stress to large masses of earth material. For this reason, significant technical and economic advantages can be realized through the development of indirect or shortcut methods for obtaining indications of the properties and characteristics of geologic materials.

Some years ago, the value of topographic maps, aerial photographs, pedologic descriptions, and geologic surveys in characterizing soil materials was realized. To make this information useful for engineering studies, a serious effort was initiated to obtain data on the engineering properties of various soil groups and associations based on geologic and pedologic surveys. The correlation of performance data with information on areal distribution and location based on the surveys has proved extremely valuable in the planning and construction of facilities in and on soil.

Publication of this paper sponsored by Committee on Exploration and Classification of Earth Materials.

Recently, the size and importance of structures and facilities designed by engineers and architects have greatly increased. This has produced an increased interest in the rock materials underlying surficial soil layers. A clear need has arisen for a program to provide an engineering evaluation of rock materials for the purposes of location, design, construction, and maintenance of engineered facilities. However, a serious gap exists in the association of engineering characteristics with rock units identified from geologic classifications. Therefore, there is a need for the development of a comprehensive evaluation program that permits use of existing data and that helps in the procurement of necessary information on engineering characteristics of rock.

SCOPE OF STUDY

The initial work plan included development of a classification system based on index tests. An investigation of previous works in classification of rock on the basis of index tests showed that a variety of classification systems using many different index tests had been developed. However, this survey showed that no general applicable system had been developed and that little communication had been established between field investigators, facility designers, and those in charge of construction and maintenance of facilities. Therefore, the initial work plan was modified to include the development of a comprehensive methodology for evaluation of rock. The development of such an evaluation schema was to include the establishment of an information bank to provide access to collected data by any interested individual. A survey of the categories of information on geologic materials, particularly rock strata, was undertaken. On the basis of this investigation of existing data, a method was devised to collect, categorize, and present more extensive data on rock materials. The general schema for the evaluation program was then developed. Currently, research is continuing to test and verify the validity of the evaluation program that has been developed. A final step in this effort will be a full implementation of the rock evaluation program for project planning in Kentucky.

GEOLOGIC INFORMATION

Any study of rock materials must rely at least in part on a background of geologic information. For several hundred years, geologists have investigated rocks of the earth surface, attempting to organize and codify rock units so that their origin, genesis, and transformation can be properly understood. This work is of tremendous significance for engineering studies of rock materials. Earth materials of concern to the engineer exist in a geologic environment. These materials possess physical characteristics that are a function of their mode of origin and the subsequent geologic processes that have acted on them. These events in geologic history lead to a particular lithology, to a particular set of geologic structures, and to a particular in situ state of stress. In the planning, design, construction, and maintenance of engineered facilities, geologic structures, distribution of rock types, and variations in existing states of stress in rock materials have significant influence. A familiarity with local geologic conditions and information is valuable because results of past studies and investigations can be incorporated into an information system. This local geologic information can be used to ensure that tests selected for classification purposes are compatible with the rocks encountered in a study area. Geologic structures and materials that have exhibited unfavorable characteristics or that are potential sources of trouble can be quickly located. Moreover, knowledge of in situ stresses can be extremely useful in design, and a knowledge of existing geology in an area under study can provide assistance in the planning and conduct of a testing program for a particular project at a particular site.

In the development of the rock evaluation program for Kentucky, the geology of the state was reviewed, and existing geologic information was organized and codified to provide easy access for engineers and technicians not well versed in the topic. We recommend that such an organization of geologic information be carried out as a primary step in developing any rock evaluation program in other geologic areas.

ROCK CLASSIFICATION

The organization of geologic information as described above illustrates the basic purpose of any rock classification system: the transfer of information on rock properties from laboratory or field investigators to design engineers and contractors. The optimum means for such transfer of information would be the conduct of tests on rock in its native environment to simulate any proposed construction activity. Behavior of the rock under simulated construction conditions could be monitored, and predictions concerning behavior during construction and subsequent operation of the prototype facility could be made. However, the expense of large-scale testing of in situ rock is such that this approach is not economically feasible. For this reason, inexpensive indirect tests are desirable. If such tests can be developed and used to indicate indirectly the behavior of rock materials under actual construction and operating conditions, great economies can be realized not only in exploration and testing but also in design and construction. When index testing of samples of material taken from a particular site has been used and when performance has been predicted on the basis of test results and a knowledge of differences between the laboratory test conditions and actual field conditions associated with the proposed facility, considerable success has been attained in the investigation of soil materials, and, to a lesser extent, in studies of rock materials.

The primary difficulty in using index tests for rock characterization is that large samples would be required to test a representative mass of material. Discontinuities located at significant spacings and changes in characteristics of material over long distances would require testing of large specimens, and this cannot be done economically. Therefore, evaluation of rock properties on the basis of index tests must always be considered as a superficial investigation limited by physical and mathematical continuity. Large-scale rock discontinuities and structural features cannot be preserved in laboratory specimens. These discontinuities and inhomogeneities greatly affect rock deformation and failure in the field. A significant degree of uncertainty will always exist in any prediction of field behavior based on index test results. Nevertheless, index tests can serve as useful indicators of rock behavior, especially in the location and preliminary planning stages. For this reason, we have given considerable attention to selecting index properties and to using such properties in the classification of rock materials. Index tests must be characterized by simplicity, economy, and ease of performance. Additionally, index test results must be reproducible, within reasonable limits, by various practitioners in various locations who use standardized equipment and procedures. Most importantly, the test property must be an index of a material or mechanical property that the design engineer can use effectively.

Many geologic classification systems for rock have been proposed. In general, these systems emphasize properties and characteristics of intact material and neglect discontinuities and possible sources of weakness in rock masses that are of critical importance in engineering activities. The most widespread geologic classification of rock has been based on genesis, and rock materials have been divided into igneous, sedimentary, and metamorphic categories. Within these categories, various subclasses have been developed based on petrographic studies that include characterization of the texture and mineralogy of the rock. In addition to genetic and petrographic classifications, geologists have developed chemical classification systems for rock material that are of limited applicability in engineering studies. Basic genetic classifications have been useful when they could be correlated with the engineering properties of the rock materials; however, genetic classifications are not sufficiently specific and quantitative for engineering applications.

Physiographers and geomorphologists have developed systems for classifications of landforms that have proved to be useful as indicators of properties and structures in underlying bedrock. Physiographic classification systems of surficial terrain have proved useful in the location, planning, design, and construction of transportation facilities. The general qualitative character of most geological classification systems has been modified to yield a quantitative methodology of terrain description in the pattern-unit-component-evaluation (PUCE) system developed in Australia. The PUCE system appears to be a useful transitional step between purely qualitative geologic

classifications and quantitative engineering classification systems for rock.

A number of engineering classification systems have been developed for rock materials. Some of these systems are based on inherent rock characteristics, others are based on a particular purpose or use for the rock, and some are based on a combination of inherent characteristics and intended uses. A review of existing classification systems indicated that strength, lithology, anisotropy, and durability can be used to characterize the properties of an intact sample. These characteristics are shown in the form of a classification system in Table 1.

A variety of tests have been proposed as indicators of rock strength. Uniaxial compressive tests have been used in rock classification systems, and hardness tests and various penetration tests have been used as indicators of rock strength. Compressive strength tests require machined specimens and thus are somewhat costly in terms of sample preparation. Hardness tests appear to be subject to variations in testing techniques. The point-load strength index has been selected as a measure of tensile strength; empirical results show excellent correlation between this index and the unconfined compression strength of rock materials.

The lithology of rock materials does not have a direct bearing on mechanical properties, but traditional geologic rock names based on the texture, mineral content, structure, particle size, and cementing matrix yield significant information on the relation between an intact sample and the rock mass from which the sample was taken. Knowledge of rock lithology can provide an intuitive feeling for the character of the rock mass and can suggest mass effects that may be common to certain groups of rocks.

Almost all rock materials show directional differences in their responses to applied stresses and environmental conditions. For this reason, anisotropy of an intact specimen is of significant interest. We have selected point-load test results to define the strength anisotropy index as the ratio between maximum and minimum strength values. In general, this ratio is established by performing the point-load test on specimens oriented so that the load first is applied parallel to the planes of weakness in the specimen and then is applied perpendicularly to those planes.

Behavior of rock materials under long-term changes in environmental conditions can be of significant importance to engineering projects. Durability tests have been used to characterize earth materials as soil or rock and to indicate susceptibility of rock material to alteration in a weathering environment. A large number of durability tests have been suggested by other investigators; swell tests and slake-durability tests have been commonly used. The most successful classification scheme for transitional materials with characteristics intermediate between those of true soils and true rock appears to be that developed by Gamble (14). We have modified this work to yield the system shown in Figure 1. This classification system uses values of plasticity index and two-cycle slaking durability. All samples with a low plasticity index and durability values greater than 95 percent can be considered rock materials.

Intact sample testing and classification may be sufficient for preliminary planning and location studies, but the design of facilities will require more comprehensive and direct testing of rock materials and will necessitate examination of in situ conditions. To satisfy this need, some sort of in situ classification system is required. Many classification systems have been developed by previous investigators, and relatively few are generally applicable in situ classification systems, which for the most part, have been evaluation schemes used at particular sites for specific purposes (e.g., for tunneling or blasting requirements).

It appears that the greatest success has been attained by combining tests on intact samples with an analysis of field conditions that tend to govern the behavior of rock materials. Upper limits for strength and deformation resistance may be established on the basis of laboratory tests on intact samples, and these values may be reduced (adjusted) on the basis of field tests that show the influence of discontinuities and weathered zones. Rock models have been prepared to allow an assessment of rock behavior under conditions associated with construction and operation of a proposed facility. The basis of these modeling studies has been, in most cases, a comprehensive survey of discontinuities present at the proposed site of a facility. Since joints are the most widespread discontinuities in rock, in situ classification systems often

Table 1. Proposed intact sample classification system.

Class Number	Tensile Strength		Anisotropy		Durability		Lithology	
	Description	Point-Load Index[a] (MPa)	Description	Strength-Anisotropy Index[b]	Description	Slake-Durability Index[c] (percent)	Description	Symbol[d]
1	Very strong	>10	Isotropic	1.0 to 1.2	Very durable	>50	Sandstone	SS
2	Strong	3 to 10	Slightly anisotropic	1.2 to 1.5	Durable	25 to 50	Shale	SH
3	Moderately strong	1 to 3	Moderately anisotropic	1.5 to 5.0	Moderately alterable	10 to 25	Limestone	LS
4	Weak	0.3 to 1	Anisotropic	5 to 20	Alterable	5 to 10		
5	Very weak	<0.3	Very anisotropic	>20	Highly alterable	<5		

Note: 1 in. = 25.4 mm. 1 psi = 6895 Pa.

[a]Force at failure/square of distance between loaded points in test method (10).
[b]Maximum strength/minimum strength.
[c]Percentage retained on 2-mm screen after slaking in a test (13).
[d]1-LS-2-1 indicates a very strong, slightly anisotropic, very durable limestone.

Figure 1. Durability-plasticity classification for shales and other argillaceous rocks.

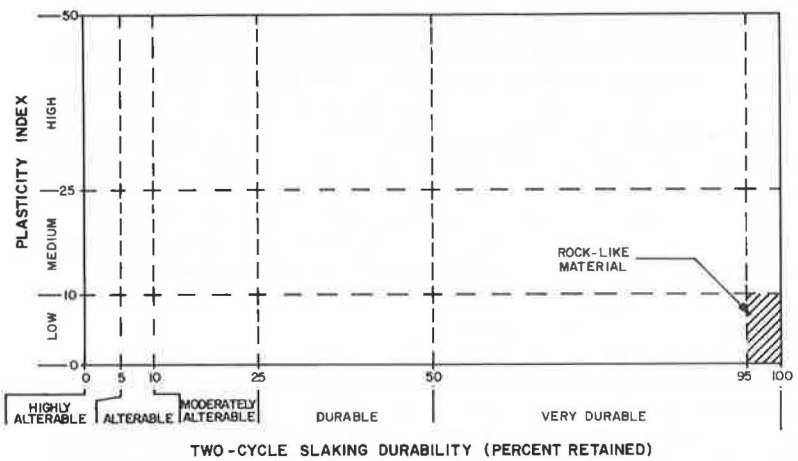

Table 2. Proposed in situ rock classification system.

Class Number	Strength and Deformability—Rock Quality (Continuity)									Intact-in Situ Reducti Factor[a]	
	Bedding Thickness		Joint Spacing		Joint Frequency		Joint Infiltration Material[a]	Gross Heterogeneity			
	Description	Size (mm)	Description	Size (mm)	Description	Joints per Meter		Description	Permeability (nm/s)	Degree of Correlation	Velo Ratio
1	Very thin	<10	Very close	<10	Very low	<0.3	Air	Very low	<1	Excellent	>0.8
2	Thin	10 to 50	Close	10 to 50	Low	0.3 to 1.0	Water	Low	1 to 10	Good	0.6 t 0.8
3	Medium	50 to 300	Moderately close	50 to 300	Medium	1 to 2	Cohesion-less soil	Medium	10 to 100	Fair	0.4 t 0.6
4	Thick	300 to 1,500	Wide	300 to 1,500	High	2 to 4	Inactive clay	High	100 to 1,000	Poor	0.2 t 0.4
5	Very thick	>1,500	Very wide	>1,500	Very high	>4	Active clay	Very high	>1,000	Very poor	<0.2

Note: For lithology description and symbol see Table 1. 1 ft = 0.3 m. 1 in. = 25.4 mm.

[a]Subject to modification with further testing. [b]In situ sonic velocity/intact specimen sonic velocity.

include a comprehensive joint survey program. On the basis of a review of existing in situ classification systems, we have developed a classification system (Table 2). This system is designed to incorporate the effects of discontinuities and mass anisotropy on the characteristics and behavior of the rock. The presence of faults and shear zones has been taken into account by considering these discontinuities and joints in the same way.

PROPOSED ROCK EVALUATION SYSTEM

After the classification systems for intact samples and for in situ conditions were developed, the next step was to create a method for exchange of information in the evaluation system. Results of classification programs would be essentially useless if there were no means to make such information readily available in understandable form to engineers and other investigators involved in design and construction activities. Therefore, a system has been developed to provide engineers with a means to obtain information for site selection, facility design, and construction and maintenance planning. The proposed system consists of two phases: an acquisition segment for the collection and collation of data and an application segment in which collected data can be used in classification programs and can be analyzed with regard to the use of rock materials in various circumstances.

The first segment of the program consists of data acquisition. The central feature of this segment is the data bank in which information from field and laboratory testing and from case histories will be stored. The attributes of the data bank are shown in Figure 2. Information storage is to be accomplished under three categories. Category 1 contains information pertinent to the location, identification, and natural environment from which the data (sample or case history information) originated. Category 2 is provided for storage of results of visual observations, index tests, and detailed tests of rock mechanical properties. Category 3 is for the storage of information from case histories and performance reports from contemporary construction and also from completed facilities.

Procurement of data for insertion under categories 1 and 2 of the data bank will involve both laboratory and field testing techniques. Samples should be selected on the basis of geologic considerations and current availability. Samples should be tested at the site immediately after removal from a core barrel or similar device if at all possible. Since this is not practical in all situations, samples can be returned at their natural moisture content and in an undisturbed condition to a laboratory for further testing. The testing sequence in the laboratory should begin with a swell test and a slake-durability test to provide immediate differentiation between soil and rock materials. The remainder of the information for storage in category 2 of the data bank can be obtained through index testing and refined laboratory or large-scale in situ tests.

Case history information for inclusion in the data storage system generally cannot be easily quantified. However, a concise version of empirical information can be placed in a coded reference file. The code and identification of site or formation investigated can be entered in the data bank so that when a search is made the existence of this information will be made known to the investigator, who can then conduct further searches for the detailed information on previous experience at a given site or in a particular formation.

The data bank will consist of a system of computer files arranged according to categories 1, 2, and 3. Computer programming will be used to facilitate storage, retrieval, and use of acquired information. A sample showing the methodology for storage and retrieval of category 1 information is shown in Figure 3. The same methodology has been followed for category 2 and category 3 data.[1]

[1] Illustrations of the transfer of information to positions on a computer data card are available in Xerox form at cost of reproduction and handling from the Transportation Research Board. When ordering, refer to XS-58, Transportation Research Record 548.

Figure 2. Data bank attributes.

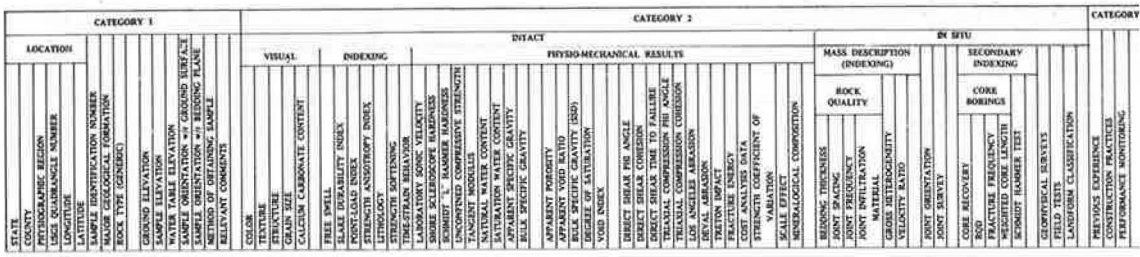

Figure 3. Portion of coding instructions for category 1 file subsystem.

CATEGORY 1, IDENTIFICATION DATA SUBFILE
(Data Card No. 1)

ATTRIBUTE	ATTRIBUTE CODE	LOCATION (COLUMN)	FORMAT	INSTRUCTIONS AND REMARKS
State	ST	1 - 2	I2	List the names of the states alphabetically and assign numbers sequentially from 01 through 50. Code number for Kentucky would be 17.
County	CO	3 - 5	I3	List the names of the counties within a state and assign numbers sequentially from 001.
Physiographic Region	PR	6 - 7	I2	Physiographic region from which the sample was obtained 01 Purchase 02 Western Coal Field 03 Western Pennyroyal 04 Eastern Pennyroyal 05 Knobs 06 Outer Bluegrass 07 Inner Bluegrass 08 Eastern Coal Field
USGS Map	MN	8 - 11	I4	USGS number of geologic quadrangle map which encompasses the sample site. Examples No. Map Name 0246 Kirsey 0763 Lovelaceville 1025 Addyston 0000 Crofton (map not published)
Longitude	LONG	12 - 15	I4	Longitude of the sample site will be described in terms of degrees and minutes. Seconds of longitude will be rounded to the nearest minute. Examples 82° 34' 17" = 8234 86° 06' 47" = 8607 89° 15' 15" = 8915
Latitude	LAT	16 - 19	I4	Latitude of the sample site will be described in the same manner as longitude.
Sample Identification No.	ID	20 - 24	A5	Columns 20-21 - Last two digits of the year in which the sample was obtained. Column 22 - Month in which sample was obtained: 1 - January 2 - February • • • 9 - September 0 - October N - November D - December Columns 23-24 - Specimen number.
Geological Formation	GF	25 - 27	I3	Major geological formation from which the sample was obtained
				Ground elevation at sample site to nearest tenth of a meter.
		- 36	F4.1	Elevation from which sample was taken to nearest tenth of a meter.
Elevation	WTE	37 - 40	F4.1	Elevation of water table to nearest tenth of a meter.
Sample Orientation	SOG	41 - 42	F2.0	00 to 90 indicates the angle between the sample axis and the ground surface to the nearest degree.
Sample Orientation	SOB	43 - 44	F2.0	00 to 90 indicates the angle between the sample axis and the major bedding plane to the nearest degree.
Method of Obtaining Sample	MOS	45	I1	1 - NX core 2 - block sample 3 - quarry sawn 4 - hand tools 9 - other (may be further delineated at a future time)
Relevant Comments	RC	46	I1	0 - no comments 1 - relevant comments available
	FREE1	47 - 48	I2	Blank (may be designated at a later time)

Use of the information stored in the data bank can be accomplished through the development of specific classification and application programs. However, a generalized classification can be obtained by using the systems given in Tables 1 and 2. For specific purposes, such as the analysis of rock formations for suitability in tunneling operations, a more detailed classification system could be developed. Acquired information can be used in the classification of rock materials and could be further used through the development of a series of use tables. In such a table, a number of uses (e.g., aggregate and rock fill) for rock materials are shown. The four indexes used for classification of rock materials can be quantified in terms of acceptable values for the rock material for use in any one of the ways given in the table. If a rock is to be used as aggregate in a highway construction project, acceptable values of the point-load index, lithology, strength anisotropy index, and slake-durability index can be developed. Then, any rock available for use in a particular project as aggregate can be tested, and the test values obtained for that rock can be compared with the ranges of acceptable values given in the table. In this way, the acceptability of various rock units for use in different ways can be quantitatively evaluated. Use tables can be developed for particular applications. For example, Franklin developed a diagram in the form of a use table that showed the ease of excavation of rock by blasting, ripping, and digging. The diagram was based on ranges of point-load index and fraction frequency. Use tables represent quantitative criteria developed from behavioral models of rock masses.

Use tables and the classification system can be combined in the application segment of the rock evaluation program. A user can request information from the data bank through a selected classification system and use table. The information retrieved from the data bank can be processed in the classification system, and a particular site or a particular rock unit can be evaluated for specific uses. The user must then evaluate the data obtained from the data bank. In general, the user must decide whether or not sufficient data have been obtained for the evaluation of a particular site as the location of a proposed facility. If sufficient data have been obtained, they will allow the user to decide whether or not the particular site under investigation is suitable for the proposed activity. If the site is not suitable, it can be abandoned. If the site is suitable, the user can then indicate that design and construction operations are appropriate at this site. If the user decides that insufficient data are available on the characteristics of the rock units at a particular site or under a particular stress environment, he or she may then specify the performance of additional tests to furnish required information. On the basis of these additional tests, the user may decide that the site is unsuitable for the planned activity or may elect to proceed with design and construction. During construction phases, performance of the rock units at a particular site should be monitored and evaluated. This information can then be returned to the data bank as case history information. After construction is completed, performance of the engineered facility and the rock units adjacent to that facility should be monitored. This performance monitoring also furnishes data that will be valuable in the location, design, and construction of other facilities. For this reason, performance monitoring data should be returned to the data bank as case history information. Ideally, the proposed rock evaluation program will be a self-sustaining, ever-expanding source of valuable information concerning the engineering properties and behavior of rock materials.

SUMMARY

Rock engineering includes a number of significant major operations: engineering analysis and interpretation of geologic information, prediction or determination of engineering properties of rock masses for use in analysis and design, and implementation of completed designs through construction activities in or on rock. Individuals drawn from various professions and disciplines are involved in these facets of rock engineering. To facilitate communication among these individuals and to assist in all facets of rock engineering, a rock evaluation program has been proposed.

This evaluation program is especially useful for the planning, design, and construction of transportation facilities in and on rock. Data on engineering characteristics of

rock units are used in a classification program. The classification program includes characterization of rock units based on tests on intact samples and on evaluation of in situ rock properties. Classifications can be modified for particular types of projects, and use tables can be developed for the evaluation of rock units for use in specific purposes. A computerized system for the storage and retrieval of information has been developed. Data for inclusion in the information bank are derived from laboratory and field testing and from monitoring rock behavior during construction and subsequent operations of completed facilities. Current study efforts are directed toward verifying and improving the methodology set forth in this preliminary development of the rock evaluation program. It is hoped that development of this program will be significantly helpful to individuals engaged in rock engineering and, in particular, to individuals concerned with the planning, design, construction, and maintenance of transportation facilities in and on rock.

REFERENCES

1. G. D. Aitchison and K. Grant. The P.U.C.E. Programme of Terrain Description, Evaluation and Interpretation for Engineering Purposes. Proc., 4th Regional Conference for Africa on Soil Mechanics and Foundation Engineering, Cape Town, South Africa, Vol. 1, Dec. 1967.
2. D. J. Belcher, L. E. Gregg, and K. B. Woods. The Formation, Distribution and Engineering Characteristics of Soils. HRB Bulletin 10, Engineering Experiment Station, Purdue Univ., Jan. 1943.
3. E. Broach and J. A. Franklin. The Point-Load Strength Test. International Journal of Rock Mechanics and Mining Sciences, Pergamon Press, Great Britain, Vol. 9, 1972.
4. D. F. Coates. Classification of Rocks for Rock Mechanics. International Journal of Rock Mechanics and Mining Sciences, Pergamon Press, Great Britain, Vol. 1, 1964.
5. R. F. Coon. Correlation of Engineering Behavior With the Classification of In-Situ Rock. Univ. of Illinois, Urbana, PhD thesis, 1968.
6. G. I. Cottiss, R. W. Dowell, and F. A. Franklin. A Rock Classification System Applied in Civil Engineering. Civil Engineering and Public Works Review, June 1971.
7. R. C. Deen. An Engineering Soil Survey of Fayette County, Kentucky. HRB Bulletin 213, 1959, pp. 12-27.
8. D. U. Deere. Technical Description of Rock Cores for Engineering Purposes. Rock Mechanics and Engineering Geology, International Society of Rock Mechanics, Vol. 1, No. 1, 1964.
9. N. Duncan. Engineering Geology and Rock Mechanics. International Textbook Co., London, 1969.
10. J. A. Franklin. Observations and Tests for Engineering Description and Mapping of Rocks. Proc., 2nd Congress of the International Society of Rock Mechanics, Belgrade, Vol. 1, Theme 1, No. 3, 1970.
11. J. A. Franklin. Suggested Methods for Determining Water Content, Porosity, Density, Absorption and Related Properties and Swelling and Slake-Durability Index Properties. International Society for Rock Mechanics, Commission on Standardization of Laboratory and Field Tests, and Committee on Laboratory Tests, Document 2, Nov. 1972.
12. J. A. Franklin, E. Broach, and G. Walton. Logging the Mechanical Character of Rock. Trans., Institute of Mining and Metallurgy, Vol. 80, 1971.
13. J. A. Franklin and R. Chandra. The Slake-Durability Test. International Journal of Rock Mechanics and Mining Science, Pergamon Press, Great Britain, Vol. 9, 1972.
14. J. C. Gamble. Durability-Plasticity Classification of Shales and Other Argillaceous Rocks. Univ. of Illinois, Urbana, PhD thesis, 1971.

15. R. Jovanovic. Anisotropy of Rocks as an Element—Principle for Rock Classification in Engineering-Geological Sense. Proc., 2nd Congress of the International Society for Rock Mechanics, Belgrade, Vol. 1, Theme 1, No. 37, 1970.
16. B. K. McMahon. Indices Related to the Mechanical Properties of Jointed Rock. Proc., 9th Symposium on Rock Mechanics, American Institute of Mining, Metallurgical, and Petroleum Engineers, Inc., New York, 1968.
17. R. P. Miller and D. U. Deere. Engineering Classification and Index Properties for Intact Rock. Air Force Weapons Laboratory, Rept. AFWL-TR-65-116, 1966.
18. N. R. Morgenstern. Ultimate Behavior of Rock Structures. In Rock Mechanics in Engineering Practice (K. G. Stagg and O. C. Zienkiewicz, eds.), John Wiley and Sons, New York, 1969.
19. L. Obert and W. I. Duvall. Rock Mechanics and the Design of Structures. John Wiley and Sons, New York, 1967.
20. D. R. Reichmuth. Point Load Testing of Brittle Materials to Determine Tensile Strength and Relative Brittleness. Proc., 9th Symposium on Rock Mechanics, American Institute of Mining, Metallurgical, and Petroleum Engineers, Inc., New York, 1968.
21. C. D. Tockstein and M. W. Palmer. A Rock Evaluation Schema for Transportation Planning in Kentucky. Division of Research, Kentucky Bureau of Highways, 1974.
22. L. B. Underwood. Classification and Identification of Shales. Journal of Soil Mechanics and Foundations Division, ASCE, Vol. 93, No. SM6, Nov. 1967.
23. Tunneling in Rock. In Developments in Geotechnical Engineering (E. E. Wahlstrom, ed.), Elsevier Scientific Publishing Co., Amsterdam, Vol. 3, 1973.

PRELOADING BY VACUUM: CURRENT PROSPECTS

Robert D. Holtz, Purdue University; and
Oleg Wager, Swedish Geotechnical Institute, Stockholm

The concept of using atmospheric pressure to apply a precompression load for accelerating the consolidation of foundations for embankments constructed on soft clay soils was first described by Kjellman in 1952. The method, although theoretically sound, was impractical then because the plastic sheets that covered the sand filter deteriorated rapidly in field use, and consequently the vacuum could not be easily maintained. Recently, new plastic and fabric materials have been developed that promise to make the Kjellman vacuum preloading method practical. The materials are cheap, strong, and resistant to deterioration by sunlight and weather. Practical applications and several specific advantages of the vacuum method are described, and factors affecting the costs of highway and other preloading construction are given. Depending on the relative costs of the fill materials and the plastic membranes, the vacuum method can be significantly cheaper than conventional preloading using sand or gravel surcharge fills.

•IN 1952, Walter Kjellman (1), then director of the Swedish Geotechnical Institute, described a new method for using atmospheric pressure to apply temporary surcharge loadings for precompressing clays under highways and buildings. In the method, a plastic or rubber membrane is placed over a sand or gravel filter layer and sealed to the clay below the ground water table. Then a vacuum pump is connected, and the air is pumped out of the porous filter (Figure 1). The vacuum is maintained at the desired preload pressure, and a pressure difference of 0.6 or 0.7 atm (60 to 70 kPa), which is equivalent to about 16 ft (5 m) of sand fill at typical unit weights, is practical. Kjellman (2) intended the method to be used in conjunction with his paper drain wicks for accelerating the consolidation of clay soils, but it could be used with any type of deep drainage or simply to apply a surcharge without deep drainage.

The Kjellman method was tried at four test sites in Sweden in the late 1940s. At two of the sites, Kjellman paper drains were installed to a 16-ft (5-m) depth before a 0.9-ft-thick (0.3-m) sand fill was placed as the filter layer. At three sites, the membrane used was a 0.01-in.-thick (0.3-mm) polyvinyl chloride (PVC) plastic sheet, which unfortunately became brittle and developed leaks after just about 1 month. Apparently the deterioration of the plastic was caused by sunlight. A fourth test was tried using strips of rubberized fabric pasted together at the joints, and, although this material resisted deterioration better than PVC, it was not entirely satisfactory because of problems of sealing the joints and its high cost. No further tests were tried then, and as far as is known the method was never applied on actual construction projects in Sweden or anywhere else.

RECENT DEVELOPMENTS

During the past few years, skyrocketing construction costs have forced highway engineers to consider alternative solutions to many geotechnical problems that previously

Publication of this paper sponsored by Committee on Embankments and Earth Slopes.

were rather easily solved by conventional means. For example, in the case of preloading and surcharge fills, the cost of fill materials increases about 10 percent per year or more because of increasing transportation costs, increasing cost of placing and then removing the surcharge materials, and, in some cases, the depletion or absence due to geologic factors of sand and gravel resources located near population centers. These developments and the fact that the most economic application of the precompression method is at sites where subsurface conditions are particularly poor and where the loadings are relatively light but cover large areas make the vacuum method increasingly attractive and economic.

In addition, since Kjellman's early experiments, significant advances have been made in the development of plastic materials and man-made fibers. Available today are vinyl and other types of plastic sheets that are often reinforced with woven polyamide (nylon) and other fabrics. These materials make an excellent air-tight membrane that is both strong, tough, and resistant to weathering and deterioration by sunlight and ideally suited for the vacuum preloading process. These materials are used for air-supported structures (e.g., warehouses and indoor sports halls), temporary environmental protection, reservoir liners, and the like. They are supplied in lightweight rolls that are easily handled in the field. Depending on the material, joints can readily be made by field welding by a hot air or a radio-frequency gun, field sewing, or special adhesive tapes. Costs, which depend on the thickness, strength, and weather resistance of the material, vary from 3.5 to about 25 cents/ft^2 ($0.38 to $2.70/m^2).

PRACTICAL APPLICATIONS

The geology and geotechnical properties at a given site must be suitable for using the precompression method, and the design and economics would govern whether or not the method would be used with deep drainage. Precompression theory and design, which are independent of how the preload is actually applied, have been covered in an excellent article by Johnson (3) and need no elaboration here. This section will describe some of the practical considerations associated with the application of the vacuum surcharge method itself using the new membrane materials.

Kjellman's sketch (Figure 1) showing the principal features is still applicable today. The filter layer should be a coarse sand or sand-gravel mixture about 12 to 20 in. thick (30 to 50 cm), and the membrane would be placed over it in sections, the joints welded, and the entire membrane sealed around the edges. If there is no dry crust and if the water table is close to the ground surface, then sealing can be made by simply piling some soil on the membrane around its periphery (Figure 2). If the dry crust is not too thick and the water table is high, a shallow ditch can be dug around the area, the membrane placed over the filter and down into the ditch, and then the ditch backfilled over the membrane (Figure 3).

Selection of the vacuum pump must consider the size of the area to be preloaded, the thickness of the filter, the desired magnitude of the preload, length of time it is to be applied, and presence of water. The size of the pump required is surprisingly small. For example, at two recent demonstrations of the method in Sweden, areas about 26 ft (8 m) square were effectively surcharged with about 0.8 atm (80 kPa) by a small pump driven by a ¼-hp (0.18-kW) motor. For larger areas, vacuum pumps with a 20-in.-thick (50-cm) filter are available that can easily maintain a vacuum of 0.6 to 0.7 atm (60 to 70 kPa) continuously for an area of 5,000 yd^2 (6000 m^2) [for example, a highway section 100 by 660 ft (30 by 200 m)]. To protect the pump, the vacuum line should be brought into a tank so that any water that collected could be periodically drawn off. To reduce pumping costs a vacuum switch could be connected to the pumps so that they would turn on when the vacuum reached, say, 0.6 atm (60 kPa) and would turn off at 0.8 atm (80 kPa).

Application of the preload in steps is generally unnecessary with the vacuum method because with typical preloads the chance of a bearing capacity failure of the surcharged area, or even a local slide, is greatly reduced. This is because there are no large shearing stresses on the base of the embankment that would occur with a granular fill

Figure 1. Principle of Kjellman's Swedish vacuum method.

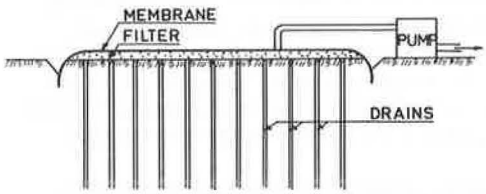

Figure 2. Kjellman method used where there is no dry crust and high water table.

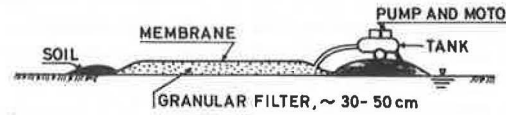

Figure 3. Kjellman method used where there is a thin, dry crust and high water table.

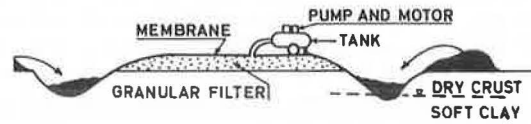

and that contribute to local instability. The presence of the vacuum at the surface of the clay also increases the efficiency of the surcharge because it provides an additional gradient over and above that caused by the increase in total stress due to the atmospheric pressure acting on the filter layer. With these two advantages of the vacuum method, it may be possible to greatly decrease the time required for preloading and at the same time avoid the expensive instrumentation, careful inspection, and delays that are often necessary with stage construction of large surcharge fills on weak foundations. An additional factor in favor of the vacuum method is that the time required for removal of the surcharge is negligible in comparison with the time required to remove and dispose of large masses of sand fill.

Another practical consideration is that the cost of the membrane material is usually so cheap that it probably is not worth the cost to remove it. In this case, it is suggested that initially the filter layer can be a minimum thickness, say 1 ft (0.3 cm), and, after preloading is complete, additional fill can be placed directly on the membrane to bring the embankment up to desired grade. The advantage of this is that, for very soft ground, the final height of the fill can be constructed after the soft soils are stabilized; of course the rest of the embankment need not be pervious material but can just as well be compacted earth fill. Depending on moisture considerations, such as frost action and swelling, an impervious membrane may be desirable in the fill; otherwise the membrane may be easily punctured with a harrow or other tool that is pulled behind a tractor. In addition, the membrane left in the fill can provide some reinforcement to the embankment, which is an added factor of safety.

COSTS

The many factors that enter into the design of preloading systems make cost comparisons between conventional surcharge fills and new techniques such as the vacuum method difficult. Cost of delays, cost and availability of suitable materials for the fill, and potential instability of the fill are but a few of the more important factors that must be considered in the design (3). Since the vacuum method has yet to be applied in any full-scale field situation, it is difficult to accurately estimate special costs associated directly with the method, for example, the cost of placement and sealing the joints and pumping costs. These costs must include a realistic consideration of any labor cost arising from operating union contracts and other labor regulations. In any event, as the cost of the surcharge materials increases relative to the cost of the membrane, the more economical the vacuum method becomes. For typical highway preloading situations, the difference can be 50 percent or more.

For the case of preloading large rectangular areas, water as an alternative surcharge

method can be competitive but would generally be impractical for ordinary highway construction. Cost estimates were made for the project described by Tozzoli and York (4), and the vacuum method probably would have been somewhat cheaper than the water method. Certain problems experienced with the water method probably would not have occurred with the vacuum method, for example, wave erosion of the retention dikes and damage of the PVC liner by birds (some materials described earlier are strong enough to resist tearing by birds). In addition, the surcharge could have been instantly removed, but about 3 months were required to pump the water from the preloading ponds. Additional advantages of the vacuum method for this project include the elimination of the problem of low stability of the retention dikes and an increased consolidation gradient so that the time required for preloading with the vacuum method would have been significantly less.

PROSPECTS

The use of the Kjellman vacuum method for preloading highway and other fills is currently feasible, practical, and probably quite economic, especially as the cost of conventional surcharge materials increases. For typical highway preloading projects the cost difference could be 50 percent or more, depending on the cost of surcharge materials. Other advantages of the method include immediate rather than stage construction; instantaneous removal of the surcharge; avoidance of failures due to the reduction of the shearing stresses under the embankment; an increased gradient and consolidation rate; some additional reinforcement in the embankment; and, if desired, a free moisture barrier in the embankment.

ACKNOWLEDGMENTS

We wish to thank G. A. Leonards and C. W. Lovell, Jr., who provided several helpful comments, and Janice Wait, who typed the manuscript.

REFERENCES

1. W. Kjellman. Consolidation of Clay Soil by Means of Atmospheric Pressure. Proc., Conference on Soil Stabilization, M.I.T., 1952, pp. 258-263.
2. W. Kjellman. Accelerating Consolidation of Fine-Grained Soils by Means of Cardboard Wicks. Proc., 2nd International Conference on Soil Mechanics and Foundation Engineering, Rotterdam, Vol. 2, Subsection 9d1, 1948, pp. 302-305.
3. S. Johnson. Precompression for Improving Foundation Soils. Journal, Soil Mechanics and Foundations Division, ASCE, Vol. 96, No. SM1, 1970.
4. A. J. Tozzoli and D. L. York. Water Used to Preload Unstable Subsoils. Civil Engineering, Vol. 43, No. 8, 1973, pp. 56-59.

CONSOLIDATION OF RANDOMLY HETEROGENEOUS CLAY STRATA

Eduardo E. Alonso, Escuela Técnica Superior de Ingenieros de Caminos, Canales y Puertos, Universidad Politécnica de Barcelona, Spain; and Raymond J. Krizek, Technological Institute, Northwestern University

A simulation procedure is used to analyze the influence of a randomly varying coefficient of permeability on the one-dimensional consolidation settlement of clay layers. The method of analysis involves (a) simulating of soil profile when the basic characteristics of the homogeneous random function describing the soil permeability are known, (b) making the governing field equation discrete by means of an implicit finite difference scheme, and (c) statistically analyzing the resulting sample population when the simulation has been performed a sufficient number of times. When compared with results determined by the classical deterministic approach, the application of this analysis to a specific case shows significant differences and allows the use of standard procedures in significance testing, rather than the single estimate provided by the deterministic case, to make decisions at a given significance level.

THE classical theory of consolidation incorporates two constitutive relations in its derivation: Darcy's law, which governs the flow of water through the pores of the soil, and Hooke's law, which governs the deformational behavior of the soil skeleton. In the one-dimensional situation, each of these relations involves one material parameter, the coefficient of permeability k_x in the case of flow and the coefficient of volume change m_x in the case of deformation; both are usually assumed to be constant. However, Alonso and Krizek (1) have shown that the parameters defining the soil behavior vary randomly in space and are conveniently described by a random function of spatial coordinates. In this paper the process of one-dimensional consolidation of randomly heterogeneous strata subjected to a constant load is studied. Only the effect of a random variation will be considered because the effect of deterministic heterogeneity has been studied elsewhere (5). An approach of this kind will enable us to (a) conveniently describe the complexity of the heterogeneous variation in soil properties; (b) formulate the problem by considering, in an unambiguous way, the random variation of the soil; and (c) provide probabilistic answers that indicate a range of possible values with an associated confidence level, rather than a single deterministic estimate. This will be demonstrated by studying the dissipation of pore-water pressures and the increase in the degree of consolidation for a consolidating clay layer.

CONSOLIDATION EQUATION

Generally, k_x and m_x are both functions of position and the effective vertical stress within the consolidating layer. However, under the hypothesis of small strains, little error is obtained by considering k_x and m_x as functions of only the spatial coordinates. Therefore, the increment of volume change undergone by an element of soil can be explained solely in terms of the time-dependent changes in the void ratio e, and the

Publication of this paper sponsored by Committee on Mechanics of Earth Masses and Layered Systems.

continuity equation for the flow of pore water can be written as

$$\frac{\partial}{\partial x}\left[\frac{k_x(x)}{\gamma_w}\frac{\partial u_e}{\partial x}\right] = \frac{\partial e}{\partial t} \tag{1}$$

where u_e denotes the excess of pore-water pressure, and γ_w is the unit weight of water. Considering the definition of m_x, equation 1 becomes

$$\frac{1}{\gamma_w}\frac{\partial u}{\partial x}\left[k_x(x)\frac{\partial u}{\partial x}\right] = -m_x(x)\frac{\partial \bar{\sigma}}{\partial t} \tag{2}$$

where $\bar{\sigma}$ represents the effective vertical stress, which can be readily expressed in terms of the total applied stress σ, and u_e as $\bar{\sigma} = \sigma - u_e$. If time-dependent variations of the externally applied load are not considered, equation 2 may be expressed as

$$\frac{1}{\gamma_w}\frac{\partial}{\partial x}\left[k_x(x)\frac{\partial u_e}{\partial x}\right] = m_x(x)\frac{\partial u_e}{\partial t} \tag{3}$$

which, in terms of the coefficient of consolidation, $c_x(x) = k_x(x)/m_x(x)\gamma_w$, becomes

$$\frac{\partial^2 u_e}{\partial x^2} + \frac{1}{k_x(x)}\frac{dk_x(x)}{dx}\frac{\partial u_e}{\partial x} = \frac{1}{c_x(x)}\frac{\partial u_e}{\partial t} \tag{4}$$

If $k_x(x)$ and $c_x(x)$ are assumed to be random functions $K(x)$ and $C(x)$ of the space coordinate x, the differential equations given above become random differential equations for the excess pore pressure. Such equations are analytically untractable mainly because of the nonlinearity in the random component of the equation, and the only suitable approach currently seems to be the use of a simulation procedure in conjunction with some numerical technique and a digital computer. Although this approach can be costly if an extensive parameter study is undertaken, the answers for the specific cases studied here are complete in that the full probability structure of the solution, including first and second moments, is a natural output of the procedure. The first step toward the solution requires a method whereby random processes can be generated from basic characteristics.

SIMULATION OF RANDOM COEFFICIENTS

If $k_x(x)$ and $m_x(x)$ are considered to be random functions, there is usually a positive correlation between them, and any simulation procedure must account for this fact if rather conservative results are to be avoided. To simulate multivariate processes, Shinozuka (6) proposed methods that depend on a knowledge of the cross-spectra function between the two processes. This situation presents a major difficulty in this problem because no data are available to find such a cross-spectra function between the coefficient of permeability and the coefficient of compressibility. Two continuous or quasi-continuous records of soil permeability and compressibility would be required in the same location, provided both processes can be shown to be homogeneous in the stochastic sense.

However, when the type of soil does not change much with depth, the changes in permeability can be associated with similar changes in the coefficient of volume change

(5). In such cases, c_x in equation 4 can be considered constant. As a matter of fact, the condition of homogeneity of records (in the stochastic sense) is not really satisfied if rather different types of soil are included in the same record, and the homogeneity condition must be invoked to enable the randomness of soils to be analyzed in some detail. This also implies that there is no significant change of soil type within the layer undergoing consolidation, and little error is introduced by considering c_x as a constant instead of as a random function. Therefore, equation 4 reduces to

$$\frac{\partial^2 u_e}{\partial x^2} + \frac{1}{K(x)} \frac{dK(x)}{dx} \frac{\partial u_e}{\partial x} = \frac{1}{c_x} \frac{\partial u_e}{\partial t} \tag{5}$$

where c_x is now a constant and independent of position. When the following changes are made in the variables,

$$X = x/H \tag{6}$$

$$T = \frac{c_x t}{H^2} \tag{7}$$

$$u = \frac{u_e}{u_0} = \frac{u_e}{\sigma_0} \tag{8}$$

where H is half of the thickness of the layer, and u_0 is the initial constant increment of pore pressure (equal to the total applied stress σ_0), equation 5 becomes

$$\frac{\partial^2 u}{\partial X^2} + \frac{1}{K^*(X)} \frac{dK^*(X)}{dX} \frac{\partial u}{\partial X} = \frac{\partial u}{\partial T} \tag{9}$$

where $K^*(X) = K(XH)$. Equation 9 can be more conveniently expressed as

$$\frac{\partial^2 u}{\partial X^2} + \frac{d}{dX} [\ell n\ K^*(X)] \frac{\partial u}{\partial X} = \frac{\partial u}{\partial T} \tag{10}$$

which involves the random coefficient $\ell n\ K^*(X)$. If the properties of the random process defining the permeability in the soil are known, the main concern is now directed toward the simulation of $\ell n\ K^*(X)$.

A homogeneous normally distributed process Z(x) can be represented as (6)

$$Z(x) = \sigma_z \left(\frac{2}{N}\right)^{1/2} \sum_{k=1}^{N} \cos\ (\omega_k x - \varphi_k) \tag{11}$$

where σ_z is the standard deviation of the process, N is a large positive integer (to ensure normality), ω_k is a random variable that is distributed with a density function $S_z(\omega)/\sigma_z^2$ [where $S_z(\omega)$ is the two-sided power spectra of the process as a function of the frequency in terms of cycles per unit of spatial length ω], and φ_k is a random variable that is uniformly distributed in the interval 0 to 2π. This representation can be used for the permeability of the soil if the conditions of homogeneity and normality hold.

[Although more efficient techniques for the simulation of multidimensional processes have been proposed for the case in which the spectral distribution is not obtainable in closed form (7), the present problem, which involves a one-dimensional process with a simple power spectra function, can be adequately handled by equation 11 and requires relatively little computation.]

Since we are dealing with statistically homogeneous layers, the first condition is generally satisfied; however, there are important reasons why a normal representation of the coefficient of permeability is not realistic. For example, a negative permeability makes no sense physically, and its logarithm is undetermined mathematically; this gives rise to difficulties in the process of simulation. However, if permeability is thought to be governed by the pore-size distribution, a log-normal representation seems more appropriate: The most salient features of a log-normal distribution are its positive skewness and definition for positive values only. Physical substantiation for this concept is provided by the process of particle breakage, which leads to a log-normal distribution of particle sizes (3, 4). However, when the coefficient of variation of a log-normal distribution becomes small, it resembles a normal distribution.

Since the logarithm of a log-normal distribution is a normal distribution (referred to random variables), it is worthwhile to investigate the possibility of a representing $\ln K^*(X)$ in the form given in equation 11. Consider a two-dimensional random vector, $\overline{W} = (W_1, W_2)$, of two jointly distributed and correlated normal random variables and define the transformation

$$(Y_1, Y_2) = \overline{Y} = \overline{g}(\overline{W}) = [g_1(W_1, W_2), g_2(W_1, W_2)] \tag{12}$$

where

$$Y_1 = g_1(W_1, W_2) = \exp[W_1] \tag{13}$$

$$Y_2 = g_1(W_1, W_2) = \exp[W_2] \tag{14}$$

Since the transformation given in equations 13 and 14 is monotonic and one-to-one, the joint probability density function of Y_1 and Y_2 can be written as

$$f_{Y_1, Y_2}(y_1, y_2) = f_{W_1, W_2}[h_1(y_1, y_2), h_2(y_1, y_2)]\,|J| \tag{15}$$

where $\overline{h} = (h_1, h_2)$ denotes the inverse transformation of $\overline{g} = (g_1, g_2)$ and $|J|$ is the Jacobian of the $\overline{h}$ transformation:

$$|J| = \begin{vmatrix} \dfrac{\partial h_1}{\partial y_1} & \dfrac{\partial h_1}{\partial y_2} \\ \dfrac{\partial h_2}{\partial y_1} & \dfrac{\partial h_2}{\partial y_2} \end{vmatrix} = \frac{1}{y_1 y_2} \tag{16}$$

However, since W_1 and W_2 are jointly correlated and normally distributed, we can write

$$f_{W_1, W_2}(w_1, w_2) = \frac{1}{2\pi\sigma_1\sigma_2\sqrt{1-\rho_{12}^2}} \exp\left\{-\frac{1}{2(1-\rho_{12}^2)}\left[\left(\frac{w_1-\mu_1}{\sigma_1}\right)^2 - 2\rho_{12}\left(\frac{w_1-\mu_1}{\sigma_1}\right)\left(\frac{w_2-\mu_2}{\sigma_2}\right) + \left(\frac{w_2-\mu_2}{\sigma_2}\right)^2\right]\right\} \tag{17}$$

where ρ_{12} is the correlation coefficient between W_1 and W_2 and is defined by

$$\rho_{12} = \frac{C_{12}}{\sigma_1\sigma_2} = \frac{1}{\sigma_1\sigma_2} E[(W_1 - \mu_1)(W_2 - \mu_2)] \tag{18}$$

where C_{12} is the covariance between W_1 and W_2. Consider now that W_1 and W_2 are two specific random variables, which are defined at points x_1 and x_2 from a normal stationary random process $W(x)$. Since $W(x)$ is assumed to be stationary, the mean and variance of the process are constant along x, and the probability density function of the random vector $\overline{Y}$, given by equation 15, can be written as

$$f_{Y_1, Y_2}(y_1, y_2) = \frac{1}{y_1 y_2 2\pi\sigma^2\sqrt{1-\rho^2}} \exp\left\{-\frac{1}{2\sigma^2(1-\rho^2)}[(\ell n\, y_1 - \mu)^2 - 2\rho(\ell n\, y_1 - \mu)(\ell n\, y_2 - \mu) + (\ell n\, y_2 - \mu)^2]\right\} \tag{19}$$

where ρ, σ^2, and μ represent the correlation coefficient, variance, and mean of the process W respectively.

Assume now that the transformation $\overline{g}$ is defined in a continuous manner for the entire process $W(x)$, and thus a new process $Y(x)$ is originated by the relationship

$$W(x) = \ell n\, Y(x) \tag{20}$$

Then, the autocorrelation function of $Y(x)$, defined as the expected value of the product Y_1Y_2 of two random variables of the process $\overline{Y}(x)$ for any two points 1 and 2, becomes

$$R_Y(1, 2) = E[Y_1Y_2] = \int_0^\infty \int_0^\infty y_1 y_2 f_{Y_1, Y_2}(y_1, y_2)\, dy_1 dy_2 \tag{21}$$

Using equation 19 with equation 21, we get

$$E[Y_1Y_2] = \int_0^\infty \int_0^\infty \frac{dy_1 dy_2}{2\pi\sigma^2\sqrt{1-\rho^2}} \exp\left\{-\frac{1}{2\sigma^2(1-\rho^2)}[(\ell n\, y_1 - \mu)^2 - 2\rho(\ell n\, y_1 - \mu)(\ell n\, y_2 - \mu) + (\ell n\, y_2 - \mu)^2]\right\} \tag{22}$$

Note that, if $W(x)$ is a homogeneous process, ρ is only a function of the distance between

points 1 and 2. Calling this distance τ, using the subscript W for the parameters of the process W(x), and introducing in equation 22 the change of coordinates $v_1 = \ell n\, y_1 - \mu$ and $v_2 = \ell n\, y_2 - \mu$, we are able to write equation 22 as

$$R_Y(\tau) = \frac{\exp(2\mu_W)}{2\pi\sigma_W^2\sqrt{1-\rho_W^2}} \int_{-\infty}^{\infty} \int_{-\infty}^{\infty} \exp\left\{\frac{1}{2\sigma_W^2(1-\rho_W^2)}[v_1^2 - 2\rho_W v_1 v_2 + v_2^2]\right\}$$

$$\exp(v_1 + v_2)dv_1 dv_2 \tag{23}$$

which can be further reduced to

$$R_Y(\tau) = \beta\exp(2\mu_W) \int_{-\infty}^{\infty} \exp(-\alpha v_1^2 + v_2)dv_1$$

$$\left\{\int_{-\infty}^{\infty} \exp[-\alpha v_2^2 + v_2(2\alpha_W v_1 + 1)]dv_2\right\} \tag{24}$$

where

$$\alpha = \tfrac{1}{2}\sigma_W^2(1 - \rho_W^2) \tag{25}$$

and

$$\beta = \tfrac{1}{2}\pi\sigma_W^2\sqrt{1 - \rho_W^2} \tag{26}$$

On integration in v_2, equation 24 transforms to

$$R_Y(\tau) = \sqrt{\frac{\pi}{a}}\,\beta\exp(2\mu_W) \int_{-\infty}^{\infty} \exp\left[-\alpha(1 - \rho_W^2)v_1^2 - (-1 - \rho_W)v_1 + \frac{1}{4\alpha}\right]dv_1 \tag{27}$$

and finally transforms to

$$R_Y(\tau) = \exp[2\mu_W + \sigma_W^2(1 + \rho_W)] \tag{28}$$

In terms of the autocovariance functions $C_Y(\tau)$ and $C_W(\tau)$ of processes Y and W, equation 28 becomes

$$C_Y(\tau) + \mu_Y^2 = \exp[2\mu_W + \sigma_W^2 + C_W(\tau)] \tag{29}$$

where μ_Y designates the mean of the Y process. Note, however, that, if Y(x) has a log-normal distribution and at every point $W = \ell n\, Y$, the mean and variance of W can be expressed as

$$\mu_W = \ell n\, \mu \left(\frac{1}{\sqrt{Y}}\right)^2_W \tag{30}$$

and

$$\sigma^2_W = \ell n\, (V^2_Y + 1) \tag{31}$$

where V_Y represents the coefficient of variation of Y. If Equations 30 and 31 are introduced into equation 29, we get

$$C_W(\tau) = \ell n \left[\frac{C_Y(\tau)}{\mu^2_Y} + 1\right] \tag{32}$$

Note in all these derivations that the process Y can be identified with the soil permeability $K^*(X)$, and W with its natural logarithm. Therefore, if $K^*(X)$ is a homogeneous log normally distributed process, its logarithm is also homogeneous. Note in Equation 32 that $C_W(\tau)$ depends only on the shift τ, and it is normally distributed. This allows us to perform the simulation of $\ell n\ K^*(X)$ according to equation 11. The following successive steps are required:

1. Analyze the record of soil permeability and find its autocovariance function $C_Y(\tau)$;
2. Use equation 32 to derive $C_W(\tau)$, the autocovariance function of $\ell n\ K^*(X)$;
3. Obtain the power spectra density function of $\ell n\ K^*(X)$ by use of a numerical procedure and the Fourier transform of $C_w(\tau)$; and
4. Apply equation 11 to the process $\ell n\ K^*(X)$, whereby the standard deviation σ_z is given by equation 31 and the frequencies W_K are distributed in accordance with the unit two-sided power spectra function derived in step 3.

As shown in equation 6, the spatial coordinate X is actually dimensionless; therefore, if we denote the dimensionless frequency $\omega_k H$ by F_k, equation 11 can be written as

$$\ell n\,[K^*(X)] = \sigma_{\ell n\ K^*(X)} \left(\frac{2}{N}\right)^{1/2} \sum_{k=1}^{N} \cos(F_k X - \varphi_k) \tag{33}$$

where the frequencies F_k are distributed in accordance with the density function $S_{\ell n\ K^*}(F)/\sigma^2_{\ell n\ K^*}$ (see Appendix), where H is the characteristic length of the problem (half the thickness of the consolidating layer in this case).

METHOD OF SOLUTION

A finite difference technique has been used to solve the differential equation for each realization of the random process, $\ell n\ K^*(X)$. Since implicit schemes generally allow larger spacings in the time domain than explicit schemes without sacrificing convergence and since a simulation procedure requires a large number of computations, the reduction in computer time afforded by the implicit schemes made them more suitable for this problem. In particular, the Crank-Nicholson implicit scheme (2) has been used here because of its accuracy and simple formulation.

Figure 1a shows the domain of integration of equation 10. The time domain extends from 0 to ∞, and the spatial domain has a finite length, namely, the depth of the layer undergoing consolidation. A discrete solution at the nodal points of a rectangular mesh (defined by its finite space and time increments, h and k) was sought by means of a difference approximation for the differential operators appearing in equation 10. If we consider a central difference approximation of the derivatives at point P in Figure 1a, a good compromise for the space derivative consists of the following average values for the central difference at j and j+1:

$$\frac{\partial u}{\partial X} = \tfrac{1}{2}\left(\frac{u_{i+1,\,j+1} - u_{i-1,\,j+1}}{2h} + \frac{u_{i+1,\,j} - u_{i-1,\,j}}{2h}\right) \tag{34}$$

$$\frac{\partial^2 u}{\partial X^2} = \tfrac{1}{2}\left(\frac{u_{i+1,\,j+1} - 2u_{i,\,j+1} + u_{i-1,\,j+1}}{h^2} + \frac{u_{i+1,\,j} - 2u_{i,\,j} + u_{i-1,\,j}}{h^2}\right) \tag{35}$$

$$\frac{\partial L}{\partial X} = \tfrac{1}{2}\left(\frac{L_{i+1,\,j+1} - L_{i-1,\,j+1}}{2h} + \frac{L_{i+1,\,j} - L_{i-1,\,j}}{2h}\right) \tag{36}$$

where L stands for $\ell n\ K^*(X)$. For $\partial u/\partial T$, the central difference at point P is

$$\frac{\partial u}{\partial T} = \frac{u_{i,\,j+1} - u_{i,\,j}}{k} \tag{37}$$

Inserting these expressions into equation 10 and denoting the grid parameter k/h^2 by λ, we get

$$\begin{aligned}\frac{16}{\lambda}(u_{i,\,j+1} - u_{i,\,j}) = {} & (L_{i+1,\,j+1} - L_{i-1,\,j+1} + L_{i+1,\,j} - L_{i-1,\,j}) \\ & \cdot (u_{i+1,\,j+1} - u_{i-1,\,j+1} + u_{i+1,\,j} - u_{i-1,\,j}) \\ & + 8(u_{i+1,\,j+1} - 2u_{i,\,j+1} + u_{i-1,\,j+1} + u_{i+1,\,j} - 2u_{i,\,j} + u_{i-1,\,j})\end{aligned} \tag{38}$$

As i varies from 1 (zero depth) to M (full depth of the layer), equation 38 can be viewed as a set of linear equations for each elapsed time j, and these can be expressed as

$$[A]^j\{u\}^{j+1} = \{b\}^j \tag{39}$$

with the following convention:

$$a^j_{k,\,k-1} = L_{k+1} - L_{k-1} - 4 \qquad j = 2, 3, \ldots \tag{40}$$

$$a^j_{k,\,k} = 8(1/\lambda + 1) \qquad k = 2, 3, \ldots, M - 1 \tag{41}$$

$$a^j_{k,\,k+1} = -4 - L_{k+1} + L_{k-1} \tag{42}$$

$$\{u\}^{j+1} = [u_1^{j+1},\ u_2^{j+1} \ldots u_M^{j+1}] \quad j = 1, 2, 3, \ldots \tag{43}$$

$$b_k^j = 8/\lambda u_k^j + (L_{k+1} - L_{k-1})(u_{k+1}^j - u_{k-1}^j) + 4(u_{k+1}^j - 2u_k^j + u_{k-1}^j)$$

$$k = 2, 3, \ldots, M - 1$$

$$j = 2, 3, \ldots \tag{44}$$

The remaining coefficients in equations 40, 41, and 42 are 0, except for the boundary conditions at k=1 and K=M. For the example case of free drainage at both ends, we get

$$a_{1,1} = 1;\ a_{M,M} = 1 \tag{45}$$

and

$$b_1^j = 0;\ b_M^j = 0 \quad j = 2, 3, \ldots \tag{46}$$

Note that the system of equations given by equation 39 is nonsymmetric but is banded; in fact, equations 40, 41, and 42 show that the bandwidth is 3, which allows the required storage and computation to be reduced substantially. The procedure just described does not require a constant time increment. Rather, since the method is stable for large values of the parameter λ, the possibility exists of varying the time increment to reduce the number of steps up to a given time.

Previous known solutions of the consolidation equation with a constant coefficient of permeability or with a deterministic variation of the coefficient of permeability show a decrease in the pore pressure at any point until almost zero excess pore pressure is reached. Not only the pore pressure decreases with time, but the rate of decay also decreases. Therefore, the error in the solution is expected to vary with both the increment of time used and the total elapsed time. This provides a means for maintaining the accuracy of the results approximately constant thoughout the region of integration, provided we adapt the time-dependent function describing the inverse of the time increment to the curve describing the rate of decrease of the excessive pore pressure with time. In reality, a discrete approximation is more suitable for actual applications. Figure 1b shows four successive increments of time computed with this criterion. The curve of $1/\Delta T(T)$ versus T corresponds to the rate of decrease of the degree of consolidation; this actually represents the mean rate of decrease of the excess pore pressure in the layer. If a simplified expression is chosen for the degree of consolidation with constant soil coefficients, we have

$$U = 1 - \frac{8}{\pi^2} \exp\left(-\frac{\pi^2 T}{4}\right) \tag{47}$$

and the rate of decrease of U is proportional to $\exp(-\pi^2 T/4)$. Then, the first time increment, $1/\Delta T_1$, is identified with 1 in the curve of Figure 1b, and the remaining increments are computed according to the number of different time increments desired. Other criteria can be used to find time increments according to the time at which the solution is desired. A computer program was written to perform the simulation of the proposed problem.

Figure 2 shows a simplified flow chart of the simulation process, which includes

(a) the simulation of the ℓn K*(X) process, (b) the strategy used to fix the time increments, (c) the specification of the initial and boundary conditions, (d) the solution of the resulting system of linear equations for each elapsed time, (e) the computation of the derived parameters (mainly the degree of consolidation), and (f) the statistical analysis of the desired quantities.

ANALYSIS OF SPECIFIC CASE

The simulation process associated with the general flow chart shown in Figure 2 can be summarized as follows. First, a sample soil profile with a permeability variation is artificially generated in the computer by the techniques explained. Second, the initial excess pore pressure is allowed to dissipate through this artificially generated medium until a given degree of consolidation is reached; the significant variables of this process (mainly the excess pore pressure and the degree of consolidation) are recorded for each elapsed time. Third, the first two steps are repeated many times to get a statistically satisfactory number of realizations of the time-dependent variations in the excess pore pressure and the degree of consolidation. Finally, a statistical analysis is performed on the set of derived sample populations.

The initial selection of increments in the time domain can be done on the basis of the method previously described. However, if better computer efficiency is desired, more satisfactory time increments can always be obtained for the specific problem under consideration by using a trial process in which the initial selection of increments is used as a starting point. The selection of the spatial increment of the finite difference mesh is, however, more closely related to the probabilistic aspects of the problem. In fact, the criterion for the selection of the space increment should be an accurate representation of the random process defining the natural logarithm of the permeability coefficient. A suitable criterion is suggested by the special form of equation 33, since the oscillations of the process in the X direction are governed by the cosine modulation of this equation. In particular, if F_{max} represents the maximum frequency component of the process describing ℓn K*(X), a maximum number of $F_{max}/2\pi$ cycles per unit of length X would be obtained in a representation of the form given in equation 33. When the number of points n_p needed to numerically define a cycle is fixed, an estimate of the necessary number of layer divisions N_p for a given process with F_{max} is easily computed from

$$N_p = 2F_{max}\, n_p/2\pi \tag{48}$$

since 2 is the maximum dimensionless length in this case.

The preceding development will be demonstrated for a practical situation by analyzing the consolidation of a 66-ft-thick (20-m), randomly heterogeneous clay layer that is freely drained at both ends and the total stress distribution that is uniform with depth. The clay layer is assumed to have a randomly varying (constant mean) permeability distribution with depth, but it can be conveniently represented by a homogeneous random function whose underlying probability distribution is well described by a log-normal model.

This study involves four different values for the coefficient of variation of the permeability process V_{K^*}: 0.1, 0.325, 0.7, and 1.1 corresponding to variances of 0.01, 0.1, 0.4, and 0.8 respectively for the derived ℓn K*(X) process. These values cover the range of variation likely to be encountered in the permeability of relatively homogeneous clayey soils. These cases were approximated in an actual situation by the special form of the normalized (unit area) power spectra density function shown in Figure 3. This function was chosen arbitrarily with the following considerations in mind. Equation 32, which described the autocorrelation function of the ℓn K*(X) process, gives an indication of the frequency content of this process in terms of the behavior of the K*(X) process.

Figure 1. Finite difference approximation.

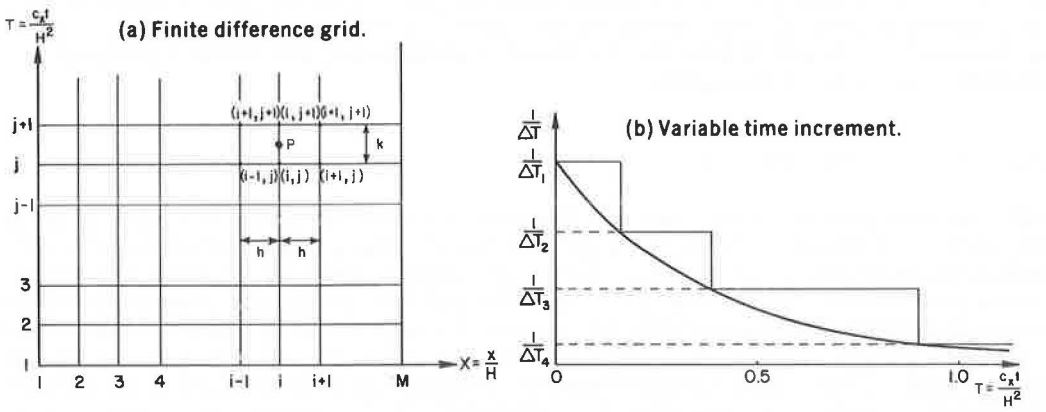

Figure 2. Simulation procedure.

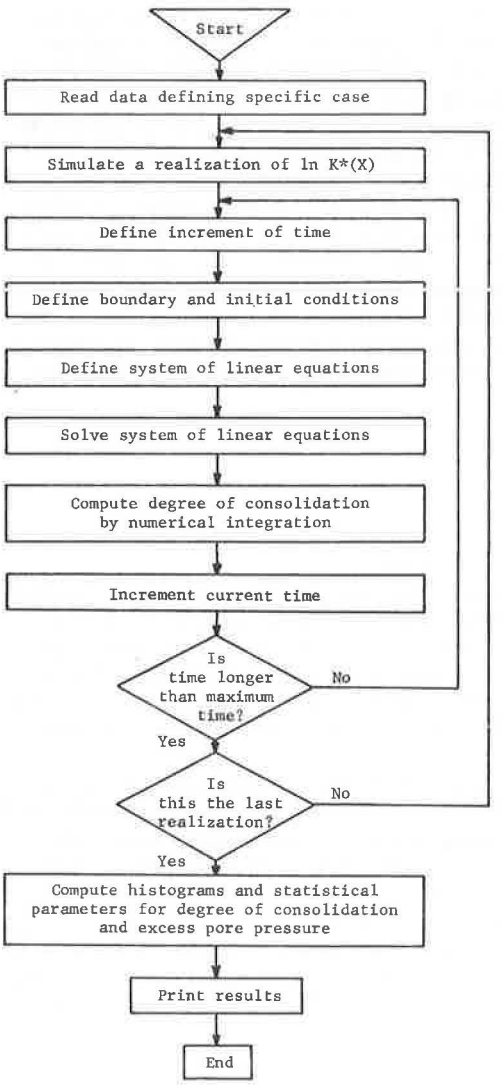

Figure 3. Power spectra function for specific case.

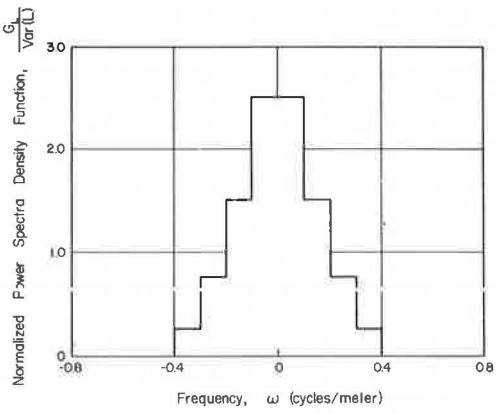

In fact, if μ_{K^*} is considered to be 1, the rate of decay of the autocorrelation function of $\ell n\, K^*(X)$ is $C'_{K^*}(\tau)/[1 + C_{K^*})\tau)]$, where C'_{K^*} is the rate of decay of the autocorrelation function of the $K^*(X)$ process.

For autocorrelation functions, $C_{K^*}(\tau)$, of the form $\exp(-\alpha\tau)$, the derived autocorrelation function of $\ell n\, K^*(X)$ will decay at a slower rate than $C_{K^*}(\tau)$, and consequently the low frequency components of the associated power spectra will be enhanced. Note, however, that this tendency is attenuated for autocorrelation function of the form $\exp(-\alpha\tau)\cos 2\pi\beta\tau$ because of the negative lobes of this representation. In any case, it does not seem that frequencies larger than the maximum ones associated with $K^*(X)$ will appear in $\ell n\, K^*(X)$. However, dominant frequency ranges between 0 and 0.5 m^{-1} were commonly encountered in the analysis of actual field records. Therefore, the hypothetical power spectra function shown in Figure 3 does not seem to differ much from real situations. These considerations have been treated in detail by Alonso and Krizek (1).

According to equation 48, 40 intervals in the definition of the finite difference mesh in the X direction give $n_p = 10\pi$ points for the definition of a cycle in the worst case; this figure was judged to be sufficiently accurate for this analysis. After a number of trials using the classical consolidation equation, the following criteria were used to determine the time increments:

1. $\Delta T = 0.025$, if $0 \leq T < 0.25$;
2. $\Delta T = 0.05$, if $0.25 \leq T < 0.6$;
3. $\Delta T = 0.1$, if $0.6 \leq T < 1.0$;
4. $\Delta T = 0.15$, if $1.0 \leq T < 1.5$; and
5. $\Delta T = 0.25$, if $T \geq 1.5$.

This distribution also satisfies the criteria given previously for the variable time increment. One hundred realizations were performed in each one of the four simulations [corresponding to the four different variances of the $\ell n\, K^*(X)$ process]. For a maximum time factor of 1, it took less than 4 min on a CDC 6400 computer to perform a complete simulation for the above-mentioned conditions.

The relevant results obtained from this simulation are shown in Figures 4 through 9. Figure 4 shows three typical realizations (out of 100 performed) of the degree of consolidation U versus the time factor T for a coefficient of variation of 1.1 for the soil permeability. Histograms of the values assumed for U at a time factor of T = 0.5 are shown in Figure 5 for the four cases studied. Note how the histogram spreads over the values of U when the coefficient of variation for $K^*(X)$ increases. Parallel to this increase in the variance of the soil permeability increases is a reduction in the mean of the degree of consolidation. This tendency is better shown in Figure 6, in which U has been plotted against T for values of $T < 1$. Curves corresponding to the mean values and one standard deviation of dispersion are shown, and the deterministic solution is given by the classical theory. Several histograms are superimposed in these figures to give an idea of the amount of dispersion.

The field equation given by equation 10 shows clearly that the mean value of the excess pore pressure does not satisfy the classical one-dimensional consolidation equation. In fact, by taking expectations of both sides of equation 10, by letting $M(X) = (d/dX)\,[\ell n\, K^*(X)]$, and by interchanging derivation and expectation operators, we get

$$\frac{\partial^2 \bar{u}}{\partial X^2} + E\left[M(X)\,\frac{\partial u}{\partial X}\right] = \frac{\partial \bar{u}}{\partial T} \tag{49}$$

Since M(X) and u(X) are obviously correlated, the second term on the left-hand side of equation 49 is not zero, and consequently it modifies the usual one-dimensional consolidation equation. However, the decrease in the mean degree of consolidation with an increase in V_{K^*} can be explained on the basis of physical grounds only. In fact, when the coefficient of variation of the soil permeability increases, there is a larger dis-

Figure 4. Realizations for degree of consolidation versus time.

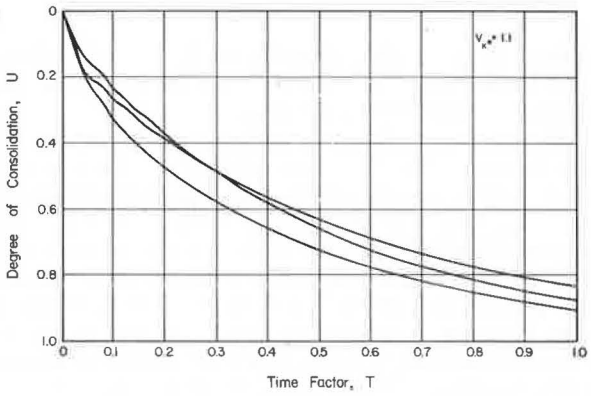

Figure 5. Degree of consolidation at T = 0.5 for four cases.

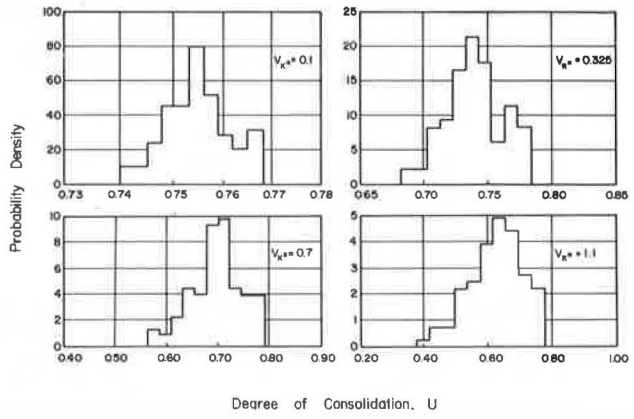

Figure 6. Degree of consolidation versus time.

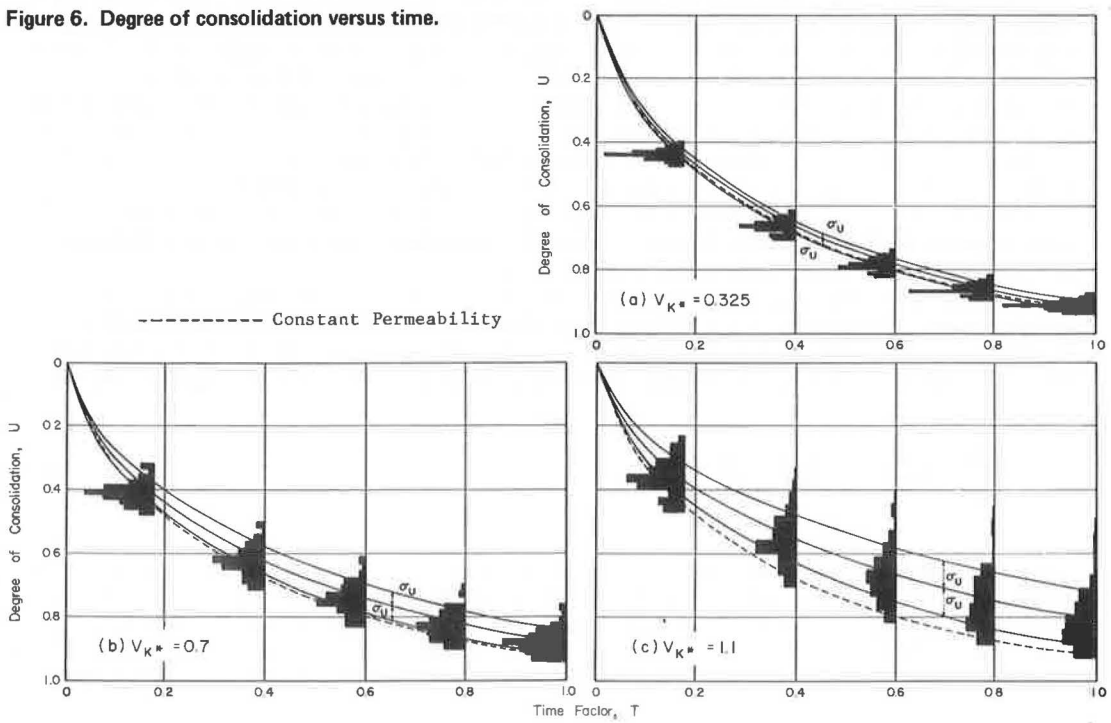

persion of the soil permeability, and this can reach very low values at some places. These low values tend to govern the entire process of consolidation, even though highly permeable regions contribute to a significantly different mean value.

Figure 7 shows the decrease in the mean value of the degree of consolidation for increasing dispersion of the permeability coefficient. If only the mean value ($\overline{U}$ curves) is considered, the curves in Figure 7 represent deviations of nearly 20 percent from the values predicted by classical consolidation theory; however, much larger deviations can be found in the dispersion observed in the histograms. The correct prediction of the degree of consolidation at a given time must be based on some confidence level, and the procedures of significance testing must be used. Figure 7 also shows the increase in the standard deviation of the degree of consolidation, σ_U, with V_{K^*} for several different time factors. The limited information provided by this example indicates that the σ_U versus V_{K^*} relationships are nearly linear in some cases. No regular pattern was observed with respect to the elapsed time.

Figure 8 shows two typical realizations (corresponding to a time factor of 0.5 and a coefficient of variation of soil permeability of 1.1) of the pore pressure developed in the consolidating layer, and these are computed with those realizations predicted by classical consolidation theory. The values of the excess pore pressure at the middepth of the layer were statistically analyzed and plotted against time in Figure 9, and histograms at several time factors are shown to illustrate the variability expected.

In the case of the degree of consolidation, increases in the standard deviation and in the mean values of the pore pressure are observed for increasing dispersion of the soil permeability. Note the skewed character of the histograms for both the degree of consolidation and the excess pore pressure, especially for high values of elapsed time. Any significance testing must take this feature into account, because the skewness of the distributions toward small values of the degree of consolidation and pore pressure increases the chances of reaching smaller degrees of consolidation when compared with the results from symmetrical distributions with the same variance.

SUMMARY AND CONCLUSIONS

A simulation technique has been used to analyze the influence of a randomly heterogeneous soil permeability on the one-dimensional consolidation of a clay layer subjected to a constant load. After the governing field equation was made discrete by an implicit Crank-Nicholson finite difference scheme, a digital computer was used to implement a step-by-step marching procedure in the time dimension. The simulation technique for the process defining the random soil variability depends on the stationary character of the soil permeability and its underlying log-normal probability distribution.

It was assumed that the changes in the coefficient of consolidation of the soil are reflected in the permeability changes; this is approximately the case if the type of soil does not change appreciably within the consolidating layer. If this is not the case, the governing field equation will contain two different correlated random processes as random coefficients, and its simulation will require an explicit knowledge of such a cross-correlation; this latter knowledge is currently difficult to obtain. The simulation procedure involves

1. Generation of a realization of the properties of the soil according to its probability structure,
2. Application of the Crank-Nicholson method to derive a step-by-step procedure that involves the solution of a system of simultaneous linear equations at each step,
3. Use of a numerical integration procedure to obtain the degree of consolidation at each elapsed time,
4. Computation of pore-pressure histograms at selected locations, and
5. Determination of the degree of consolidation with its corresponding statistical parameters (mean and variance).

Steps 4 and 5 are undertaken after the entire simulation has been completed; that is,

Figure 7. Variation of statistical parameters for degree of consolidation.

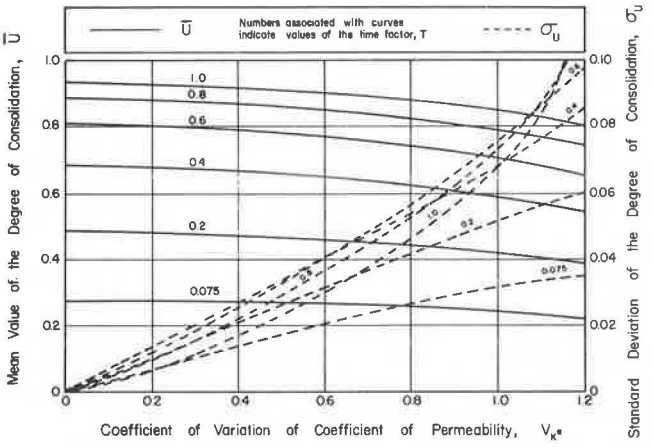

Figure 8. Realizations of pore pressure versus depth.

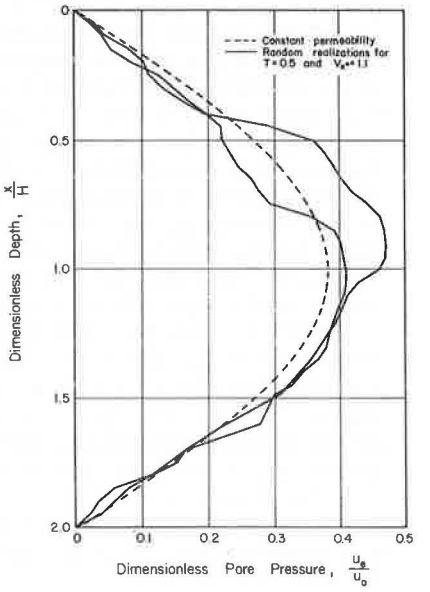

Figure 9. Pore pressure versus time.

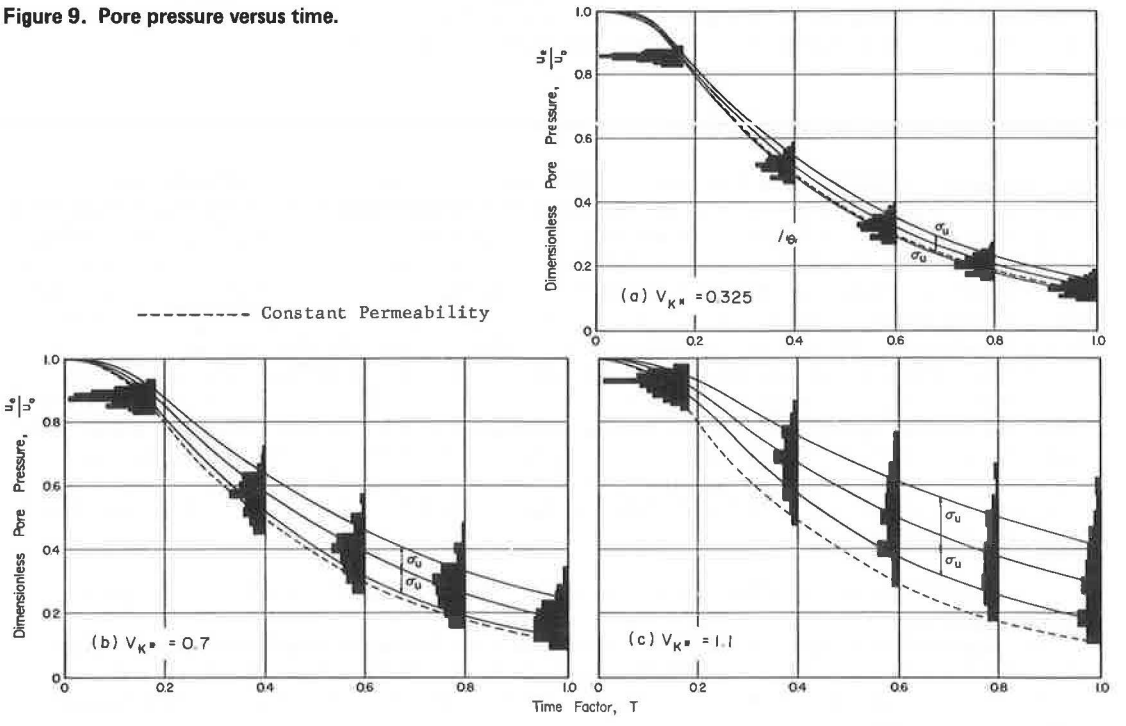

after steps 1, 2, and 3 have been performed the desired number of times. This method has been applied to a particular case, and an attempt has been made to represent as nearly as possible a real situation based on previous results. Four levels of dispersion of the coefficient of soil permeability were successively simulated to evaluate its influence; however, the same power spectra structure of the process describing soil properties was used in all the cases.

Within the limitations given, the following conclusions can be made.

1. The simulation method is a versatile tool for analyzing the influence of heterogeneous soil properties; unlike methods that rely on second-order moments, it is able to give more complete probabilistic answers but is limited in that general conclusions are costly to obtain.
2. The dispersion of soil permeability around its mean value results in a reduction in the degree of consolidation for a given time, as indicated by the mean values, which are progressively smaller than those obtained from the classical one-dimensional equation when the dispersion of the permeability coefficient increases. Therefore, if the true random coefficient of permeability (or its associated coefficient of consolidation) is replaced by its mean value, unsafe results are obtained in that a given degree of consolidation will take more time than predicted.
3. The randomness associated with the degree of consolidation introduces the possibility of obtaining results that are rather different than those predicted by the classical theory. Decisions concerning the amount of settlement expected at a given time should be based on a desired confidence level, and adequate importance must be given to the skewed character (toward smaller degrees of consolidation) of the resulting distributions.
4. Pore pressures behave qualitatively similar to their derived parameter, the degree of consolidation; thus, not only is the dispersion of the pore pressure affected by the dispersion of the coefficient of soil permeability, but also the mean is shifted to a higher value (which results in a lower value of the degree of consolidation) than that predicted by the theory of one-dimensional consolidation. The results may differ substantially from those obtained by the classical theory, and distributions skewed toward increasing values of the pore pressure are observed as time increases.

REFERENCES

1. E. E. Alonso and R. J. Krizek. Stochastic Formulation of Soil Properties. Proc., 2nd International Conference on Applications of Statistics and Probability in Soil and Structural Engineering, Aachen, Germany, 1975.
2. J. Crank and P. Nicholson. A Practical Method for Numerical Evaluation of Solutions of Partial Differential Equations of the Heat Conduction Type. Proc., Cambridge Philosophical Society, Cambridge, England, 1947, pp. 50-67.
3. B. Epstein. The Mathematical Description of Certain Breakage Mechanisms Leading to the Logarithmico-Normal Distribution. Journal of Franklin Institute, Vol. 244, 1947, pp. 471-477.
4. F. Kottler. The Distribution of Particle Sizes. Journal of Franklin Institute, Vol. 250, 1950, pp. 339-356, 419-441.
5. R. L. Schiffman and R. E. Gibson. Consolidation of Nonhomogeneous Clay Layers. Journal of Soil Mechanics and Foundations Division, American Society of Civil Engineers, Vol. 90, No. SM5, 1964, pp. 1-30.
6. M. Shinozuka. Simulation of Multivariate and Multidimensional Random Processes. Journal of Acoustical Society of America, Vol. 49, No. 1, 1971, pp. 357-367.
7. M. Shinozuka and C. M. Jan. Digital Simulation of Random Processes and Its Applications. Journal of Sound and Vibration, Vol. 25, No. 1, 1972, pp. 111-128.

APPENDIX

DISTRIBUTION OF DIMENSIONLESS FREQUENCIES

To find the probability distribution function of the dimensionless frequencies F consider first the influence of the dimensionless variable $X = x/H$ on the two-sided power spectra $S_A(\omega)$ of a homogeneous random process A(x). If $R_A(\tau)$ is the autocorrelation function, we have by definition

$$S_A(\omega) = 4\int_0^\infty R_A(\sigma)\cos 2\pi\omega\tau d\tau \tag{50}$$

If $\tau = \tau^* H$ (where τ^* is a dimensionless lag parameter) and $\omega = F/H$ (where F is a dimensionless frequency), a change of variables allows the expression for $S_A(\omega)$ to be written as

$$S_A(\omega) = 4H\int_0^\infty R_A(\tau^* H)\cos 2\pi F\tau^* d\tau^* \tag{51}$$

where

$$R_A(\tau^* H) = E[A(x)A(x + \tau^* H)] = E\{A(HX)A[H(X + \tau^*)]\}$$
$$= E[A^*(X)A^*(X + \tau^*)] = R_{A^*}(\tau^*) \tag{52}$$

and

$$A(HX) = A^*(X) \tag{53}$$

where the operator denotes the expected value of the operand. Therefore, $S_A(\omega)$ can be written as

$$S_A(\omega) = HS_{A^*}(F) \tag{54}$$

Consider now the new frequency, $F = \omega H$. When $S_A(\omega)$ is known and the probability distribution of F is f_F, the theory of derived distributions can be used to write

$$f_F = \frac{1}{H} S_A\left(\frac{F}{H}\right) = \frac{1}{H} S_A(\omega) = S_{A^*}(F) \tag{55}$$

This result justifies equation 33, where the dimensionless frequencies F_k were distributed with a density function $S_{\ell n K^*}(F)\sigma^2_{\ell n K^*}$ (the division by $\sigma^2_{\ell n K^*}$ normalizes the frequency spectra function to obtain a unit area under the curve).

PROBABILISTIC APPROACH TO PREDICTION OF CONSOLIDATION SETTLEMENT

Ross B. Corotis and Raymond J. Krizek, Technological Institute, Northwestern University; and
Houssam H. El-Moursi, Soil Testing Services of Iowa, Cedar Rapids

The method of derived distributions is used to develop a probabilistic model for predicting the total settlement in a compressible clay layer in terms of uncertain soil compressibility and loads. The settlement ratio (total settlement divided by thickness of compressible layer) is a function of two independent random variables (compressibility factor and load factor). The compressibility factor is a function of two dependent random variables (compression index and initial void ratio), and the load factor is a function of two independent random variables (total stress at the mid-height layer and the preconsolidation stress). The compressibility factor can be described by a normal distribution, and the load factor by a log-normal distribution. The derived distribution of the settlement ratio is also well approximated by a log-normal distribution that approaches a normal distribution as the number of soil samples taken for the settlement prediction increases. Graphs are developed to estimate the settlement ratio parameters in terms of the average dry density of the soil. The effect of the number of samples and the vertical and horizontal correlation on the density function of the settlement ratio is also evaluated.

•MANY design decisions in foundation engineering are made with a great deal of uncertainty (4, 19). Although the determination of reliable and representative settlement parameters for a soil deposit is of fundamental importance in the design of foundations and earthworks, the nature of the soil suggests that these parameters should be described by probability distributions. Furthermore, a probabilistic approach to settlement problems in geotechnical engineering is useful because it provides a systematic insight into the ranges of uncertainty that may be expected for a particular type of settlement problem. Wu and Kraft (22), Folayan, Höeg, and Benjamin (8), Kay and Krizek (12, 13), and Padilla and Vanmarcke (17) have investigated such problems in considerable detail; however, results are generally qualitative because several important uncertainties are not taken into account. Accordingly, this work is directed toward combining the subjective judgment of the engineer with information deduced from collected data to develop the probability distribution for total settlement. The applied loads and the soil compressibility are random variables, and the probability density function for each random variable that affects the settlement prediction is derived. Graphs are presented to help the engineer quantify the risks and economies involved in a decision related to settlement prediction.

PROBLEM DESCRIPTION

The virgin settlement S of a statistically homogeneous compressible soil stratum under-

Publication of this paper sponsored by Committee on Mechanics of Earth Masses and Layered Systems.

lying a foundation is usually computed by use of the equation

$$S = H\left(\frac{C}{1+e}\right)\log\left(\frac{p_o + \Delta p}{p}\right) \tag{1}$$

where H is the thickness of the compressible layer, C is the compression index of the soil, e is the initial void ratio of the soil, p_o is the overburden stress at the midheight of the compressible layer before loading, Δp is the increase in the vertical stress at the midheight of the compressible layer due to the applied load, and p is the preconsolidation stress at the midheight of the compressible layer; in the case of the normally consolidated clay, p equals p_o. For convenience, equation 1 may be rewritten in the form

$$R = \frac{S}{H} = \frac{KL}{2.303} \tag{2}$$

where

$$K = \frac{C}{1+e} \tag{3}$$

$$L = \ln\left(\frac{p_o + \Delta p}{p}\right) = \ln\left(\frac{Q}{P}\right) = \ln(M) \tag{4}$$

The compressibility factor K can take on values between 0 and 1, and the value of the loading term L depends on the magnitude and configuration of the dead and live loads. In contrast to the normal approach to settlement prediction, which involves a deterministic analysis whereby the physical characteristics of the compressible soil are assumed to be constants, probability distributions are used in this study for both the compressibility factor and load ratio to provide appropriate ranges of settlement prediction. Uncertainty associated with equation 1 will not be considered so that the problem can be kept tractable.

SOIL DATA REDUCTION

The probabilistic approach adopted was applied to data from over 700 consolidation tests on undisturbed soils of alluvial, marine, aeolian, and residual origin (2). About three-quarters of these data were obtained from Greece and its environs (tests were performed continuously for about 10 years by Kotzias-Stamatopoulos in Athens), and the rest of the samples were obtained from different parts of the United States (tests were performed by Soil Testing Services, Northbrook, Illinois, and Harza Engineering Company, Chicago). The same test procedure and size of specimen were used in all cases.

The statistical parameters for the soil compressibility parameters and the associated frequency histograms are given in Table 1 and Figure 1 respectively. The whole population was divided into five different groups (A through E, as given in Table 2) to obtain soil groups with similar compressibility properties. These groups were based on the dry density γ_d of each soil sample because dry density is known to be highly correlated with compressibility.

Investigators (2, 11, 15, 16, 22) have reported different distributions to fit almost every

Table 1. Statistical parameters of all samples.

Soil Property	Mean	Median	Standard Deviation	Coefficient of Variation	Skewness	Kurtosis	Number of Samples
Compression index	0.20	0.16	0.14	0.73	1.98	7.98	720
Initial void ratio	0.762	0.680	0.316	0.415	1.307	4.69	723
Compressibility factor	0.104	0.092	0.057	0.548	1.387	6.26	720
Preconsolidation stress, kg/cm^2	2.38	2.00	0.146	0.62	1.47	6.05	707

Note: 1 kg/cm^2 = 9.8 Pa.

Figure 1. Frequency histograms for soil compressibility properties of all samples.

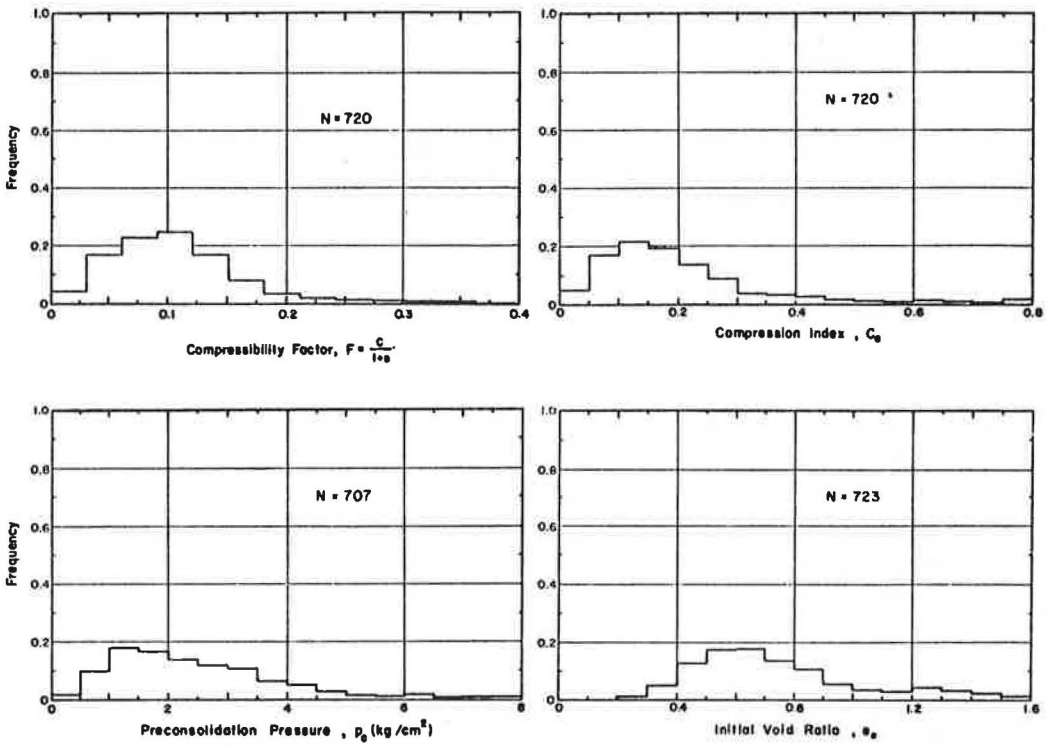

Table 2. Subdivision of soils.

Group	Dry Density (g/cm^3)	Number of Samples
A	$\gamma_d \leq 1.00$	9
B	$1.00 < \gamma_d \leq 1.25$	81
C	$1.25 < \gamma_d \leq 1.50$	153
D	$1.50 < \gamma_d \leq 1.75$	315
E	$1.75 < \gamma_d$	165

Figure 2. Probability density function of compressibility factor for different soil groups.

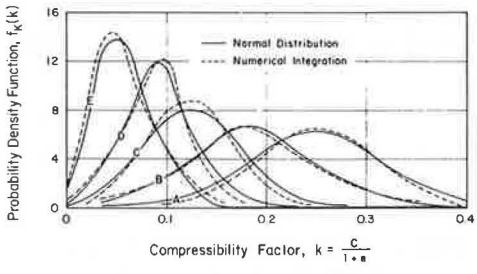

soil property. The general concensus obtained from their studies is that the inherent variations of most of the soil properties can be well explained by either a normal or log-normal distribution. In this work the normal probability density function will be used to describe the inherent variability of the compression index C, initial void ratio e, and the preconsolidation pressure p. Although the histograms in Figure 1 indicate some positive skewness for these properties, this skewness was significantly reduced when the soils were subdivided into groups according to dry density.

COMPRESSIBILITY OF SOIL

As a consequence of the natural processes involved in the formation of soil deposits, the inherent variability of soil, both in material properties and geometry, is well recognized as an important source of uncertainty. Additional uncertainty is introduced by the design and conduct of laboratory tests (9) and the interpretation of data. For a complete probabilistic approach to settlement prediction, one must have reliable estimates of the probabilities of the compression index and the initial void ratio; then, the methods of derived distributions (18, 21) or simulation can be used to find the probabilistic description of the compressibility factor. Since the compression index and initial void ratio have been assumed to be normally distributed, the following probability density functions can be written:

$$f_c(c) = \frac{1}{\sqrt{2\pi}} \frac{1}{\sigma_c} \exp\left[-\frac{1}{2}\left(\frac{C - m_c}{\sigma_c}\right)^2\right] \tag{5}$$

$$f_e(e) = \frac{1}{\sqrt{2\pi}} \frac{1}{\sigma_e} \exp\left[-\frac{1}{2}\left(\frac{e - m_e}{\sigma_e}\right)^2\right] \tag{6}$$

in which m_c and m_e denote the mean values, and σ_c and σ_e denote the standard deviations for the compression index and initial void ratio respectively. If a new variable, $g = 1 + e$, is defined, g has the same distribution as e, but it is shifted by 1; therefore, $m_g = m_e + 1$ and $\sigma_g = \sigma_e$.

Joint Probability Density Function of Compression Index and Initial Void Ratio

To determine a probability statement for the compressibility factor K, one must find an expression for the joint density function of C and e. The results of a two-way χ^2 test (10) are as follows: For the compression index and initial void ratio of the 82 samples $\chi^2 = 30$, $\nu = 19$, and $P_0(\chi^2) = 24$ percent. The results indicate that the joint probability density function of C and e may be assumed to follow the bivariate normal distribution, which can be written in the form

$$f_{c,e}(C, e) = \frac{1}{2\pi\sigma_c\sigma_e\sqrt{1 - \rho^2}} \exp\left\{-\frac{1}{2}\left[\left(\frac{C - m_c}{\sigma_c}\right)^2 - \frac{2\rho(C - m_c)(e - m_e)}{\sigma_c\sigma_e} + \left(\frac{e - m_e}{\sigma_e}\right)^2\right]\right\} \tag{7}$$

where ρ is the correlation coefficient between C and e. It is a characteristic of the normal distribution that $f_{c,g}(C, g)$ is identically equal to equation 7 with e replaced by g and m_e and σ_e replaced by m_g and σ_g.

Probability Density Function of Compressibility Factor

The method of derived distributions enables the probability distribution of K, $f_K(k)$, to be written as

$$f_K(k) = \int_{-\infty}^{\infty} g f_{C,g}(kg, g)dg \tag{8}$$

where $f_{C,g}(C, g)$ is the joint probability distribution of C and g. Since the void ratio cannot be negative, equation 8 simplifies to

$$f_K(k) = \int_{1}^{\infty} g f_{C,g}(kg, g)dg \tag{9}$$

The lower limit for equation 9 can be replaced by zero without affecting the result appreciably, because the probability of g being less than 1 ($e < 0$) is negligible for practical values of m_g and σ_g. By substituting equation 7 into equation 9, by rearranging the power of the exponent, and by using the relations between the moments of e and g, we can rewrite equation 9 in the form

$$f_K(k) = A \exp(-I) \int_{0}^{\infty} g \exp(-Eg^2 - Gg)dg \tag{10}$$

where

$$A = \frac{1}{2\pi\sigma_g\sigma_C\sqrt{1 - \rho^2}} \tag{11}$$

$$E = B\left(\frac{k^2}{\sigma_C^2} - \frac{2\rho k}{\sigma_C\sigma_g} + \frac{1}{\sigma_g^2}\right) \tag{12}$$

$$G = 2B\left[\left(\frac{\rho m_g}{\sigma_g\sigma_C} - \frac{m_C}{\sigma_C^2}\right)k + \left(\frac{\rho m_C}{\sigma_g\sigma_C} - \frac{m_g}{\sigma_g^2}\right)\right] \tag{13}$$

$$I = B\left(\frac{m^2}{\sigma_g^2} + \frac{m_C^2}{\sigma_C^2} - \frac{2\rho m_g m_C}{\sigma_g\sigma_C}\right)$$

$$B = \frac{1}{2(1 - \rho^2)} \tag{14}$$

The analytical solution for equation 10 is

$$f_K(k) = \frac{A \exp(-I)}{2E} \exp\left[G^2/(8E)\right] D_{-2}\left(\frac{G}{\sqrt{2E}}\right) \tag{15}$$

where D_{-2} is the parabolic cylinder function, defined as

$$D_i(z) = \frac{\exp(-z^2/4)}{\Gamma(-i)} \int_0^\infty \exp(-zx - x^2/2)\, x^{-i-1}\, dx \quad \text{for } i < 0 \tag{16}$$

in which i and z denote the parameters of the function and Γ is the gamma function. The probability density function of the compressibility factor is given by equation 15 and is shown in Figure 2 for the different soil groups and a correlation coefficient of 0.8 between the compression index and the initial void ratio. The results of the Kolmogorov-Smirnov one-sample test are given in Table 3 and indicate that the compressibility factor satisfies the normal probability density function for the different soil groups.

The corresponding fitted normal distributions of the compressibility factor for all soil groups are also shown in Figure 2. In view of the good agreement between the actual distribution of K calculated from equation 15 and the normal distribution, the latter will be used for the soil compressibility in evaluating the probability density function of the total settlement ratio R. Finally, the probability function of K can be written as

$$f_K(k) = \frac{1}{\sqrt{2\pi}} \frac{1}{\sigma_K} \exp\left[-\frac{1}{2}\left(\frac{k - m_K}{\sigma_K}\right)^2\right] \tag{17}$$

in which m_K and σ_K denote the mean and standard deviation respectively.

LOAD FACTOR

Applied Loads and Overburden Stress

The applied loads acting on a structure can frequently be treated as random quantities (5, 17, 20), and in the last few years the concept of load variability has been introduced into structural engineering problems through building codes and safety investigations. Since the total applied load is the sum of many relatively small and independent loads, the distribution of the load-induced increase in the vertical stress at the midheight of the compressible layer can be assumed to follow a normal probability density function. Since there is little evidence on which to base a representation of the uncertainty associated with the estimation of stresses in the ground, the value of the overburden stress p_o is assumed to be deterministic. Consequently, the sum of the overburden stresses and the stresses caused by the added loads will follow a normal distribution, and the probability density function of the sum Q can be written as

$$f_Q(q) = \frac{1}{\sqrt{2\pi}} \frac{1}{\sigma_Q} \exp\left[-\frac{1}{2}\left(\frac{q - m_Q}{\sigma_Q}\right)^2\right] \tag{18}$$

where m_Q and σ_Q are the mean and standard deviation respectively.

Preconsolidation Pressure

The preconsolidation stress p may be due to a variety of factors (14): overburden that causes subsequent erosion, desiccation due to exposure of the surface, sustained seepage forces, and tectonic forces due to movement in the earth's crust. The combined influence of these uncertainties in the determination of the preconsolidation stress is assumed to be a normal distribution. Therefore, the uncertainty associated with the preconsolidation stress can be expressed as

$$f_P(p) = \frac{1}{\sqrt{2\pi}} \frac{1}{\sigma_P} \exp\left[-\frac{1}{2}\left(\frac{p - m_P}{\sigma_P}\right)^2\right] \tag{19}$$

where m_P and σ_P are the mean and standard deviation respectively.

Joint Probability Density Function of Applied Loads and Preconsolidation Stress

Since Q and P are statistically independent random variables that follow a normal distribution, the joint distribution will be a bivariate normal distribution (3) that can be written as

$$f_{QP}(q, p) = \frac{1}{2\pi\sigma_Q\sigma_P} \exp\left\{-\frac{1}{2}\left[\left(\frac{q - m_Q}{\sigma_Q}\right)^2 + \left(\frac{P - m_P}{\sigma_P}\right)^2\right]\right\} \tag{20}$$

Probability Density Function of Load Ratio

From equation 4 the load ratio M is defined as M = Q/P, and the method of derived distributions can be used to write the probability distribution of M, $f_M(m)$, as

$$f_M(m) = \int_{-\infty}^{\infty} p f_{Q,P}(mp, p)dp \tag{21}$$

where $f_{Q,P}(q, p)$ is the joint probability density function of Q and P. Since the value of P cannot be negative, equation 21 simplifies to

$$f_M(m) = \int_{0}^{\infty} p f_{Q,P}(mp, p)dp \tag{22}$$

Substituting equation 20 into equation 22 and rearranging the power of the exponent leads to

$$f_M(m) = \bar{A} \int_0^{\infty} p \exp(-\bar{E}p^2 - \bar{G}p)dp \tag{23}$$

where

$$\bar{A} = \frac{1}{2\pi\sigma_Q\sigma_P} \exp\left[-\frac{1}{2}\left(\frac{m_Q^2}{\sigma_Q^2} + \frac{m_P^2}{\sigma_Q^2}\right)\right] \tag{24}$$

$$\bar{E} = \frac{1}{2}\left(\frac{1}{\sigma_P^2} + \frac{m^2}{\sigma_Q^2}\right) \tag{25}$$

$$\bar{G} = -\left(\frac{m_Q}{\sigma_Q^2} + \frac{m_P}{\sigma_P^2}\right) \tag{26}$$

The analytical solution of equation 23 will yield the probability density function of the load ratio M as

$$f_M(m) = \frac{\bar{A}}{2\bar{E}} \exp\left[\bar{G}^2/(8\bar{E})\right] D_{-2}\left(\frac{\bar{G}}{\sqrt{2\bar{E}}}\right) \tag{27}$$

where D_{-2} is the parabolic cylinder function defined by equation 16.

Probability Density Function of Load Factor

Given the distribution function of the load ratio M it is possible to derive the probability density for the logarithm of this ratio. From equation 4

$$L = \ell n(M) \text{ or } M = \exp(L)$$

and the probability density function of L will take the form

$$f_L(\ell) = \frac{dM}{dL} f_M[\exp(\ell)] \tag{28}$$

$$f_L(\ell) = \exp(\ell) f_M[\exp(\ell)] \tag{29}$$

where $f_M \exp(\ell)$ is the probability density function of the load ratio M evaluated at a value equal to $\exp(\ell)$. Figure 3 shows the probability distribution of the load factor L calculated from equations 28 and 29 for mean values of 2, 4, and 6 and for $\frac{\sigma_Q}{\sigma_P}$ equal to 0.75. It appears from Figure 3 that L approximately follows a log-normal distribution, where the value of L is nonnegative and the density function is skewed to the right.

Accordingly, the probability distribution of the load factor will be approximated by the following log-normal distribution in the analysis of settlement prediction:

$$f_L(\ell) = \frac{1}{\ell}\frac{1}{\sqrt{2\pi}}\frac{1}{\sigma_{\ell nL}}\exp\left[-\frac{1}{2\sigma^2_{\ell nL}}(\ell n\ell - m_{\ell nL})^2\right] \tag{30}$$

in which $m_{\ell nL}$ and $\sigma_{\ell nL}$ denote the mean and standard deviation of ℓnL respectively. For a mean load ratio of 1, the exponential distribution shown in Figure 3 described the load factor satisfactorily.

UNCERTAINTY OF SETTLEMENT PREDICTION

Based on the foregoing probabilistic analyses, a normal distribution can be reasonably used to describe the uncertainty associated with the compressibility factor K, and a log-normal distribution can be used to describe the load term L. These two factors will be assumed to be independent in evaluating the effect of their uncertainty on the total settlement ratio R, defined by equation 2. The method of derived distributions will be used to find a probability distribution for R, $f_R(r)$, in the form

$$f_R(r) = 2.303\int_{-\infty}^{\infty}\frac{1}{L}f_{K,L}\left(\frac{2.303r}{\ell},\ \ell\right)d\ell \tag{31}$$

where $f_{K,L}(k, \ell)$ is the joint density function of K and L. Since K and L are assumed to be independent, the joint distribution can be written as

$$f_{K,L}(k, \ell) = f_K(k)f_L(\ell) \tag{32}$$

where $f_K(k)$ and $f_L(\ell)$ are the density functions of K and L respectively. Furthermore, since the value of the compressibility cannot be negative, equation 31 simplifies to

$$f_R(r) = 2.303\int_{0}^{\infty}\frac{1}{L}f_K\left(\frac{2.303r}{\ell}\right)f_L(\ell)d\ell \tag{33}$$

By substituting the corresponding expressions for $f_K(k)$ and $f_L(\ell)$ into equation 33, we obtain

$$f_R(r) = 2.303\int_{0}^{\infty}\frac{1}{\ell}\frac{1}{\sqrt{2\pi}}\frac{1}{\sigma_K}\exp\left[-\frac{1}{2}\left(\frac{\frac{2.303r}{\ell} - m_K}{\sigma_K}\right)^2\right]$$

$$\frac{1}{\ell}\frac{1}{\sqrt{2\pi}}\frac{1}{\sigma_{\ell nL}}\exp\left\{-\frac{1}{2}\left[\frac{1}{\sigma_{\ell nL}}(\ell n\ell - m_{\ell nL})\right]^2\right\}d\ell \tag{34}$$

which, on rearrangement of the exponents, becomes

$$f_R(r) = a\int_0^{\infty}\frac{1}{\ell^2}\exp\left[-\frac{-1}{2\sigma_K^2}\left(\frac{2.303r}{\ell}\right)^2 + \frac{m_K}{\sigma_K^2}\left(\frac{2.303r}{\ell}\right)\right.$$

$$\left. - \frac{1}{2\sigma_{\ell nL}^2}(\ell n\ell)^2 + \frac{m_{\ell nL}}{\sigma_{\ell nL}^2}(\ell n\ell)\right]d\ell \tag{35}$$

where

$$a = \frac{2.303}{2\pi\sigma_K\sigma_{\ell nL}}\exp\left[-\frac{1}{2}\left(\frac{m_K}{\sigma_K^2} + \frac{m_{\ell nL}^2}{\sigma_{\ell nL}^2}\right)\right] \tag{36}$$

A numerical technique was applied to perform the indicated integration, and the probability density function for the settlement ratio R for different soil groups at mean load ratios of 1, 2, 4, and 6 is plotted in Figure 4. As the load ratio M increases and as the dry density of the soil decreases, the mode of the frequency curve is shifted to the right and the mean and standard deviation increase. A heuristic argument, based on the fact that (a) the log-normal distribution can be viewed as a model for the product of independent random variables, and (b) the similarity between the results (Figure 4) and the shape of the log-normal distribution favor the adoption of a log-normal model for the settlement ratio R. Accordingly, the probability density function of R can be expressed as

$$f_R(r) = \frac{1}{r}\frac{1}{\sigma_{\ell nR}}\frac{1}{\sqrt{2\pi}}\exp\left\{-\frac{1}{2}\left[\frac{1}{\sigma_{\ell nR}}(\ell nr - m_{\ell nR})\right]^2\right\} \tag{37}$$

in which $m_{\ell nR}$ and $\sigma_{\ell nR}$ denote the mean and standard deviation of ℓnR respectively.

Analysis Charts

Use of the above probabilistic analysis allows the development of charts to determine the parameters of the log-normal distribution of the settlement ratio for a particular application. These charts (Figure 5) for load ratios 1, 2, 4, and 6 relate the average dry density of a soil to the average and standard deviation of the settlement ratio R.

Effect of Samples

The reduction of inherent uncertainty associated with the determination of R may be approached by calculating both vertical and horizontal correlation structures for the compressibility factor and the preconsolidation stress (17). The vertical correlation is determined by treating each boring (with readings at various elevations) as a sample function of a random process over depth. The autocorrelation as a function of vertical

Table 3. Results of Kolmogorov-Smirnov goodness-of-fit test for compressibility factor.

Group	Number of Samples	Hypothesized Normal Distribution	
		D_2	Probability (percent)
A	9	—[a]	—[a]
B	81	0.06	72
C	147	0.09	26
D	314	0.07	19
E	165	0.08	39

[a]Insufficient data.

Figure 3. Probability density function of load factor for different mean load ratios.

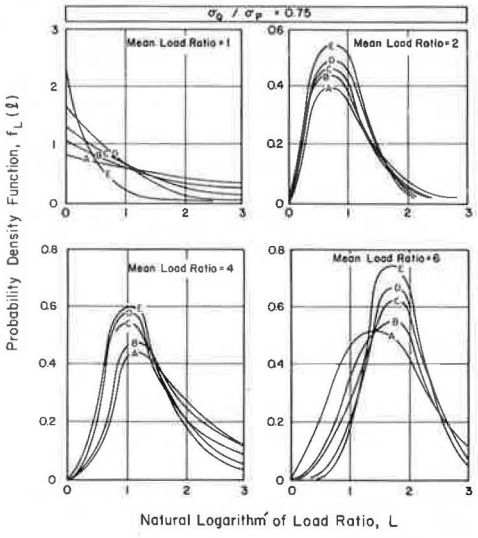

Figure 4. Probability density function of settlement ratio for different soil groups.

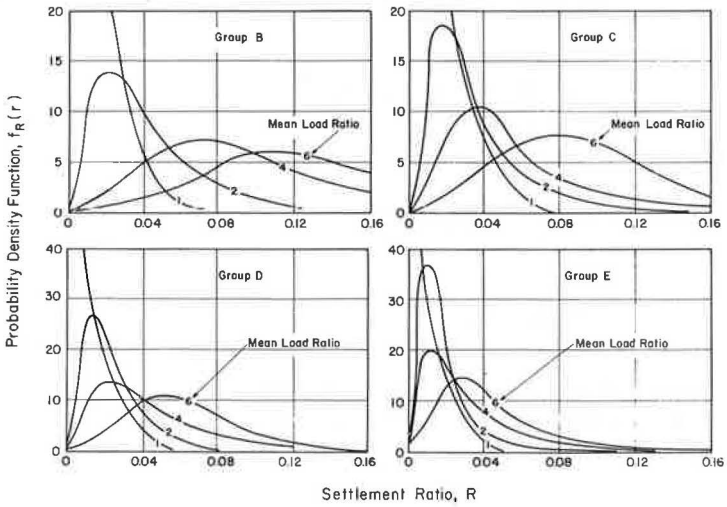

Figure 5. Model parameters of settlement ratio.

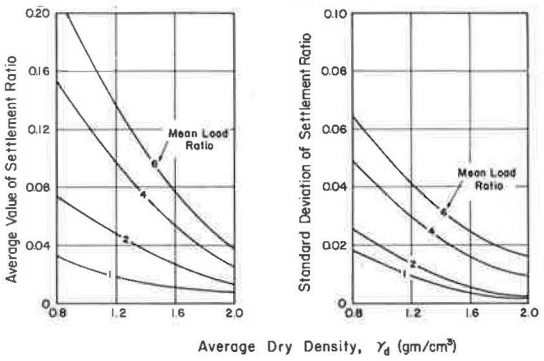

separation is then the vertical correlation, and the horizontal correlation can be obtained in a similar manner by treating the readings within a certain layer from all borings as a sample function of a random process over the horizontal position. In the settlement prediction problem, the variability of the average properties beneath a certain foundation, not the point-to-point variability within the soil mass, is needed. The variability of the average is a function of the spatial correlation structure and the number and location of samples (1) and may be related to an equivalent number of independent samples (6). Figure 6 shows the probability density function of the average value of the settlement ratio m_R as well as the density distribution itself, for 1, 4, 9, and 16 independent soil samples from soil group D. It can be seen from Figure 6 that, as the number of samples increases, the uncertainty associated with the value of R decreases. If n is reasonably large, the distribution of the average will be approximately normal with mean m_R and standard deviation $\sigma_R/\sqrt{n}$, where n is the number of independent samples.

ILLUSTRATIVE EXAMPLE

The application of the foregoing procedure can be best illustrated in an example problem. Consider the case where an 18-ft-thick (6-m) compressible layer is loaded one-dimensionally so that the estimated stress at the midheight of the layer due to both the overburden and the applied load is 3,500 lb/ft^2 (170 kPa). Six consolidation tests from samples taken at random in the layer indicate average values of 0.2 for C, 1.54 g/cm^3 for γ_d, 0.75 for e, and 2,500 lb/ft^2 (120 kPa) for p. Determination of the expected settlement due to primary consolidation is desired. According to the deterministic approach, we obtain

$$S = H\left(\frac{C}{1+e}\right)\log\left(\frac{p_o + \Delta p}{p}\right)$$

$$= 18\left(\frac{0.2}{1+0.75}\right)\log(1.4)$$

$$= 3.6 \text{ in. } (9.2 \text{ cm}) \qquad (38)$$

Figure 6. Effect of number of independent samples on probability density function of settlement ratio.

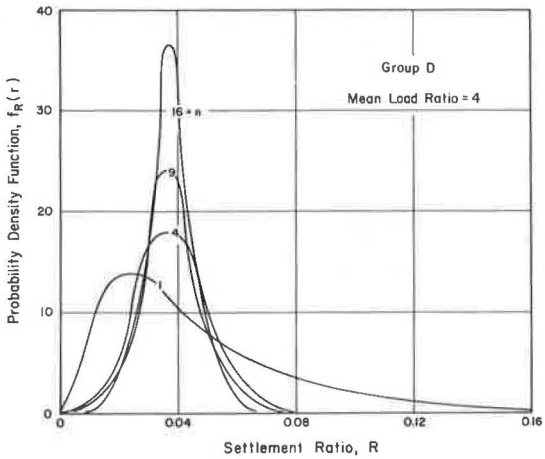

Utilizing the probabilistic approach, we find from Figure 5 that the mean and standard deviation of the settlement ratio are 0.021 and 0.005 for $m_{\gamma_d} = 1.54$ g/cm^3. The average and standard deviation of the total settlement are 4.5 and 1.1 in. (11.5 and 2.7 cm) respectively. The corresponding standard deviation of the natural logarithm of R is 0.241, which is high enough that the log-normal distribution, rather than the simple normal distribution, should be used for the settlement. If the cumulative function of R is evaluated at 0.90, the result will be the settlement for which there is a 90 percent confidence that it will not be exceeded. Since the total settlement is directly proportional to R, the statistics of the total settlement may be used in the log-normal expression to obtain

$$F_u\left[\frac{\ell n\,(S/4.4)}{0.241}\right] = 0.9 \tag{39}$$

or

$$S = 6.0 \text{ in. } (15 \text{ cm})$$

where 4.4 is the median of the total settlement and F_u is the standardized normal cumulative function.

SUMMARY AND CONCLUSIONS

The soil compressibility factor can be quite closely approximated by a normal distribution. Although the most accurate method for determining the mean and standard deviation of the compressibility is to perform a series of consolidation tests on representative undisturbed samples taken at random locations and depths, Elnaggar and Krizek (1) and Azzouz (2) have shown that the compressibility factor is highly correlated to the initial void ratio, and they have provided empirical equations for the determination of the mean. The standard deviation can then be obtained by selecting a value for the coefficient of variation based on a large number of previously obtained test results from soil in the vicinity of the project site. This selection must be tempered by engineering judgment, and the geological aspects of the site must be appropriately considered. The log-normal distribution appeared to be satisfactory for describing the load factor for mean load ratios of 2, 4, and 6. In the case of a mean load ratio of 1, the distribution can be quite closely approximated by an exponential distribution. When the distribution of the load factor was evaluated, σ_Q/σ_P was set equal to 0.75, reflecting somewhat less uncertainty in the sum of the stresses due to the added loads and overburden than in the preconsolidation stress. Finally, the derived distribution for the settlement was in good agreement with the log-normal distribution, the parameters of which were related to the average dry density of the soil at different load ratios.

Based on the probabilistic analyses above, the following conclusions can be made:

1. A prediction model can be developed to yield probabilistic information about the settlement of a clay layer in terms of probabilistic descriptions of soil compressibility and loads.
2. The uncertainty involved in the determination of the soil compressibility can be adequately described by a normal distribution.
3. The log-normal distribution appears to satisfactorily describe the load factor for mean load ratios greater than 1.
4. The total settlement can be expressed in a probabilistic design by a log-normal distribution.
5. As the number of borings increases and the vertical and horizontal correlations are taken into account, the uncertainty involved in the determination of the settlement decreases.

6. If the number of samples is reasonably large, the distribution of the average of the settlement will be approximately normal, and the standard deviation will be inversely proportional to the equivalent number of independent soil samples.

REFERENCES

1. E. E. Alonso. Application of Random Function Theory to Settlement Problems in Soil Engineering. Department of Civil Engineering, Northwestern Univ., PhD thesis, 1973.
2. A. S. Azzouz. Statistical Analyses of Index Properties and Compressibility of Soils. Department of Civil Engineering, Northwestern Univ., MS thesis, 1974.
3. J. R. Benjamin and C. A. Cornell. Probability, Statistics, and Decision for Civil Engineers. McGraw-Hill Book Co., New York, 1970.
4. A. Casagrande. Role of the Calculated Risk in Earthwork and Foundation Engineering. Journal of the Soil Mechanics and Foundations Division, American Society of Civil Engineers, Vol. 91, No. SM4, Proc. Paper 4390, 1965, pp. 1-40.
5. R. B. Corotis. Statistical Analysis of Live Load in Column Design. Journal of the Structural Division, American Society of Civil Engineers, Vol. 98, No. ST8, Proc. Paper 9123, 1972, pp. 1803-1815.
6. R. B. Corotis. Statistical Analysis of Continuous Data Records. Transportation Engineering Journal, American Society of Civil Engineers, Vol. 100, No. TE1, Proc. Paper 10362, 1974, pp. 195-206.
7. H. A. Elnaggar and R. J. Krizek. Statistical Approximation for Consolidation Settlement. Highway Research Record 323, 1970, pp. 87-96.
8. J. I. Folayan, K. Höeg, and J. R. Benjamin. Decision Theory Applied to Settlement Predictions. Journal of the Soil Mechanics and Foundations Division, American Society of Civil Engineers, Vol. 96, No. SM4, Proc. Paper 7390, 1970, pp. 1127-1141.
9. G. M. Hammitt. Statistical Analysis of Data From a Comparative Laboratory Test Program Sponsored by ACIL. Corps of Engineers, U.S. Army Engineer Waterways Experiment Station, Vicksburg, Miss., 1966.
10. P. G. Hoel. Introduction to Mathematical Statistics. John Wiley and Sons, Inc., New York, 1962.
11. R. D. Holtz and R. J. Krizek. Statistical Evaluation of Soils Test Data. Proc., 1st International Conference on Applications of Statistics and Probability to Soil and Structural Engineering, Hong Kong, 1971, pp. 230-266.
12. J. N. Kay and R. J. Krizek. Analysis of Uncertainty in Settlement Prediction. Geotechnical Engineering, Vol. 2, 1971, pp. 119-129.
13. J. N. Kay and R. J. Krizek. Estimation of the Mean for Soil Properties. Proc., 1st International Conference on Applications of Statistics and Probability to Soil and Structural Engineering. Hong Kong, 1971, pp. 279-286.
14. G. A. Leonards. Foundation Engineering. McGraw-Hill Book Co., New York, 1962.
15. P. Lumb. The Variability of Natural Soils. Canadian Geotechnical Journal, Vol. 3, No. 2, 1966, pp. 74-97.
16. P. Lumb. Safety Factors and the Probability Distribution of Soil Strength. Canadian Geotechnical Journal, Vol. 7, No. 3, 1970, pp. 225-242.
17. J. D. Padilla and E. H. Vanmarcke. Settlement of Structures on Shallow Foundations: A Probabilistic Approach. Massachusetts Institute of Technology, Research Rept. R74-9, Soils Publication No. 334, Structure Publication No. 382, 1974.
18. A. Papoulis. Probability, Random Variables, and Stochastic Processes. McGraw-Hill Book Co., New York, 1965.
19. R. B. Peck. Art and Science in Subsurface Engineering. Geotechnique, London, Vol. 12, No. 1, 1962, pp. 60-66.
20. J. C. Peir and C. A. Cornell. Spatial and Temporal Variability of Live Loads. Journal of the Structural Division, American Society of Civil Engineers, Vol. 99, No. ST5, Proc. Paper 9747, 1973, pp. 903-922.

PERFORMANCE OF A LARGE CORRUGATED STEEL CULVERT

Ernest T. Selig, Department of Civil Engineering,
State University of New York at Buffalo; and
Salvatore J. Calabrese, Law Engineering Testing Company, McLean, Virginia

Because few published field data exist to help in the development and evaluation of design criteria for large buried structures, a construction project involving such a structure was instrumented in Thunder Bay, Ontario. The structure was a shallow-buried, elliptical, corrugated-steel pipe with a 16-ft (4.9-m) height and a 27-ft (8.2-m) span. A concrete relief slab was placed on the fill several feet (meters) over the crown to distribute the vehicle loads. Pressures around the structure and under the slab were measured by using embedded stress gauges. Horizontal and vertical extensometers measured strains in the backfill. Radial extensometers inside the structure provided the structural deformation pattern. Data were obtained during construction and during live load tests with heavy vehicles. The results provided information on the magnitudes and distribution of stresses and deformations, the influence of construction procedures, and the apparent moduli of the backfill. Even though the cover over the structure provided by the backfill and slab was only about 20 percent of the span, the deflections and stresses in the pipe from the heavy vehicle loads were much smaller than those produced by the dead weight of material placed over the crown. Many cycles of live loading were required before the culvert system began to respond elastically to the loading. The final soil pressure distribution around the structure and the observed deflections were greatly influenced by the construction procedures.

•THE performance of large buried culverts is difficult to predict because of the complex interaction phenomena involved. The load on the culvert and the deformations are influenced not only by the properties of the structure and the soil but also by the details of the construction process. In addition, few field measurements have been obtained in the past to provide a quantitative evaluation of performance. Therefore, design of most of the large culverts [10- to 50-ft (3- to 15-m) diameter] has involved many assumptions and approximations of unknown validity. This paper describes the results of a field instrumentation study of one such culvert constructed in 1973 in Thunder Bay, Ontario. The purpose of the structure was to provide a road crossing over a stream to replace an old timber bridge.

The culvert was elliptical with a 27-ft (8.2-m) span, a 16-ft (4.9-m) height, and a shallow soil cover (Figures 1 and 2). It was fabricated from 5-gauge, 2 × 6-ft (0.6 × 1.8-m), rolled corrugated-steel plates. Because the design height of soil cover over the crown was initially only 10 percent of the span, the designers specified that a 1-ft-thick (0.3-m), reinforced-concrete slab be placed on top of the soil cover to distribute the concentrated vehicle loads. The structural backfill extending to about 13 ft (4 m) out from each side of the culvert consisted of a compacted granular glacial till.

Publication of this paper sponsored by Soil Mechanics Section.

21. A. A. Sveshnikov. Problems in Probability Theory, Mathematical Statistics and Theory of Random Functions. W. B. Saunders Co., Philadelphia, 1968.
22. T. H. Wu and L. M. Kraft. The Probability of Foundation Safety. Journal of the Soil Mechanics and Foundations Division, American Society of Civil Engineers, Vol. 93, No. SM5, Proc. Paper 5459, 1967, pp. 213-217.

Figure 1. Structure under construction when backfill up to spring line.

Figure 2. End view of completed structure with test load truck, readout station, and relief slab.

Figure 3. Top and end views of instrument layout.

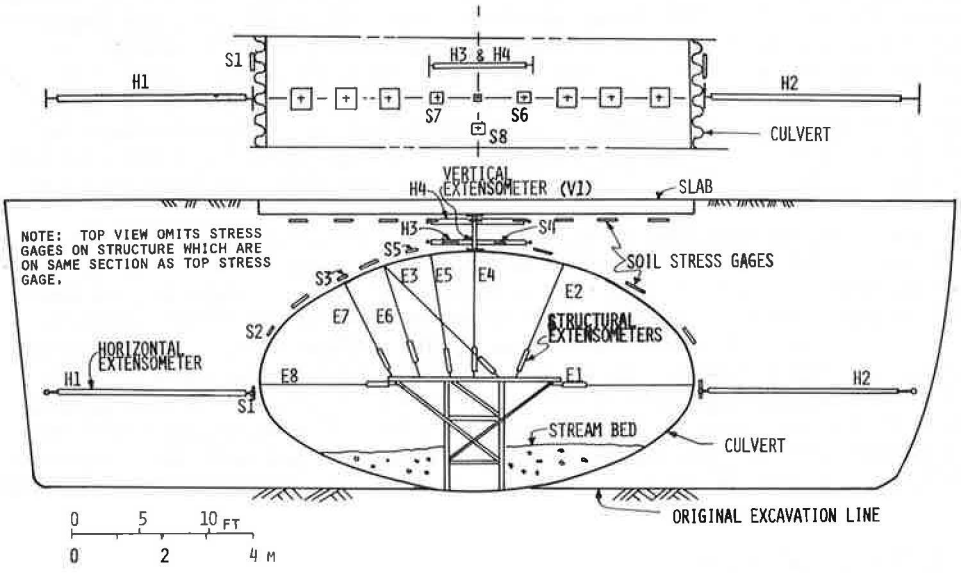

INSTRUMENTATION

The instrumentation layout is shown in Figure 3. Horizontal extensometers measured movements of the sides of the culvert relative to points approximately 13 ft (4 m) away from the structure, at the edge of the granular fill zone. The pressure distribution on the structure from the backfill was measured with embedded stress gauges. The pressure distribution under the slab was also measured with these stress gauges. Horizontal extensometers 6 ft (1.8 m) long were placed in the fill above the crown to help observe how this material deformed. Deflection of the slab relative to that of the crown of the culvert was measured with an embedded vertical extensometer. Radial extensometers inside the culvert gave the magnitude and pattern of deformation of the culvert under vehicle live loads. The instrumentation and installation procedures are described in another paper (1).

STRUCTURAL BACKFILL

The backfill material is classified as a coarse-to-fine gravel and coarse-to-fine sand with a trace of cobbles and silt sizes. The designation of the Unified Soil Classification System is GW-SW, and that of the American Association of State Highway and Transportation Officials is A-1-a. The material was compacted in roughly 1-ft-thick (0.3-m) layers and was covered at least four times by using a small vibratory roller. The moisture content, estimated to be from 5 to 10 percent, was accepted as it came from the borrow pit. Laboratory compaction tests (ASTM D698-70) indicated a maximum dry density of 152 pcf (2430 kg/m^3) and an optimum moisture content of 8 percent after correction for the +¾-in. (19-mm) material. The average material specific gravity was 2.81.

To indicate the compressibility of the backfill, one-dimensional compression tests were conducted on that portion of the material passing the ¾-in. (19-mm) sieve. Because field density and moisture content data were not available, these samples were compacted to 98 percent of the ASTM maximum dry density for the -¾-in. (19-mm) material, at the optimum moisture content, or 131 lb/ft^3 (2100 kg/m^3) and 9.5 percent respectively. The compression tests were conducted in a 12-in.-diameter (30-cm), 8-in.-high (20-cm) cylindrical mold with cycles of pressure between 0 and 11 psi (76 kPa) applied by a 12-in.-diameter (30-cm) circular plate. The one-dimensional compression modulus was 1,200 psi (8300 kPa) for the first load cycle and ranged between about 2,700 and 4,600 psi (18 600 to 31 700 kPa) for the second to nineteenth load cycles.

CONSTRUCTION SEQUENCE

At the location of the structure, the original grade was above the prescribed culvert crown elevation. Therefore the excavation shown in Figure 3 was made first, and then the bottom was shaped to fit the culvert invert. Then assembly of the corrugated plates began, and fill was added to support them. After the entire structure was bolted together, the backfilling was resumed up to the spring line. At this stage (Figure 1), the first instruments were installed. Final bolt tightening with a torque wrench continued toward the crown as the fill elevation increased. By the time the fill reached 70 in. (1.8 m) above the spring line, the bolt tightening was complete, and about 3 ft (0.9 m) of gravel fill was spread, but not compacted, inside the structure to form the streambed. Pairs of heavy timber struts were then wedged upright at 6-ft (1.8-m) intervals along the length of the structure supporting the top plates and butting on the gravel base. The frame for the radial extensometers (Figure 3) was placed inside the culvert and bolted to the invert at the same time. Backfilling over the structure was then completed, and the concrete slab was constructed. The struts were removed after about 1 week of concrete curing. The live load testing of the structure was then conducted, and final grading of the road base over the slab was completed.

MOVEMENTS DURING CONSTRUCTION

The construction events corresponding to the measurements are given in Table 1. Figure 4a shows the change in the two spring-line soil extensometers during construction. The two sides show the same trends. Large inward movement of each side of the culvert [0.35 to 0.5 in. (8.9 to 12.7 mm)] occurred during the 3 ft (0.9 m) of backfilling above the spring-line elevation when the extensometers were placed. Additional fill caused another 0.1-in. (2.5-mm) inward movement on the H1 side but only caused 0.015 in. (0.38 mm) on the H2 side. These differences in magnitude probably resulted from the staging of construction because the filling on the H1 side was usually ahead of the H2 side, and bolt-tightening occurred simultaneously.

Inward movement was small on both sides during the last 2 to 3 ft (0.6 to 0.9 m) of filling up to about 1 to 2 ft (0.3 to 0.6 m) below the crown. Additional fill then caused a movement reversal, and both sides moved outward about 0.15 in. (3.8 mm) by the time the slab was added and the struts removed. During the load test process and final grading, variations within the range of ±0.01 in. (±0.25 mm) were observed. The net outward movement in this phase was a result of both the accumulation of residual strain from the load cycles and the addition of fill on top of the slab.

Figure 4b shows the trends for the pressures on the structure and under the slab during construction and subsequent static load testing. The horizontal stress, measured by gauge S1, at the spring line increased continuously as fill was added and sharply increased again when the slab was poured. A similar trend was observed higher on the pipe by stress gauge S2. The pressure reduction at point A for S2 may be a result of inward structure movement caused by the staging of backfilling. Gauges S1 and S2 showed the highest pressures of all the gauges. Gauges S4 and S5 showed an increase of 1 to 2 psi (6.9 to 14 kPa) as the trench above them was backfilled. Some of the pressure increase during the load-testing phase was caused by the addition of fill over the slab. The remainder was possibly caused by stress redistribution.

On two occasions for most gauges (Figure 4b, D, events 13 and 21) a noticeable pressure drop of up to 1 psi (6.9 kPa) was observed. This drop is believed to be a result of an overnight temperature decrease. Cooling of the steel structure would cause a slight shrinkage, and a pressure relief around the structure would result. Therefore, some of the other minor oscillations in the pressure graphs probably are influenced by temperature change.

All of the gauges showed a pressure increase under the first loading by the 32,800-lb (14 900-kg) truck (event 17) with only a small part of this pressure change generally eliminated after unloading. The additional load cycles during the remaining live load testing produced only a small additional net change in pressure.

The vertical extensometer V1 compressed 0.15 in. (3.8 mm), the upper horizontal extensometer H4 shortened by about 0.05 in. (1.3 mm), and the lower horizontal extensometer H3 extended about 0.03 in. (0.8 mm) from the time that these gauges were placed until the slab was poured and the struts removed. The subsequent movements of these extensometers during load testing were small by comparison (Figure 5a). The two horizontal extensometers exhibited approximately the same trends. The compression change in both when the slab was loaded by the truck indicates either (a) that the composite soil-steel-concrete structure deforms in a bending mode with the neutral axis next to the pipe or (b) that the system is deforming in compression like an arch.

The pairs of struts, installed at 6-ft (1.8-m) intervals along the length of the structure, supported the points shown in Figure 6. These struts were positioned prior to any backfilling over the top of the structure. The struts were removed after the slab was poured and partially cured. The nonuniform pressure distribution shown in Figure 6 was believed to be created under the slab and around the culvert as a result of the stress relief at the strut points when the struts were removed. This distribution did not change when additional fill was placed over the slab. The cross section on which the gauges were located was halfway between two strut cross sections. The average pressures under the slab of 2.9 to 6.8 psi (20 to 47 kPa) for the two situations shown in Figure 6 were about twice the average overburden stress. This indicates a longitudinal redistribution of stress accompanying strut removal, in which the stress

Table 1. Description of construction events corresponding to instrument readings.

Event	Description
0 to 6	Backfill elevation increased from spring line to 40 in. above spring line (56 in. below crown)
7	Backfill increased to 70 in. above spring line (26 in. below crown) and then struts added
8 to 10	Backfill increased to slab level, about 2 ft above crown
11 to 13	Trench dug for installation of gauges above structure and then backfilled
14 to 15	Slab poured and partially cured, then struts removed
17	After first loading with 32,800-lb truck conducted
18 to 21	Additional live load tests conducted
22 to 24	Several more live load tests conducted and addition of 1 to 2 ft of gravel fill placed over slab

Note: 1 in. = 2.5 cm, 1 lb = 0.45 kg.

Figure 4. Measured pressures and deformations during construction.

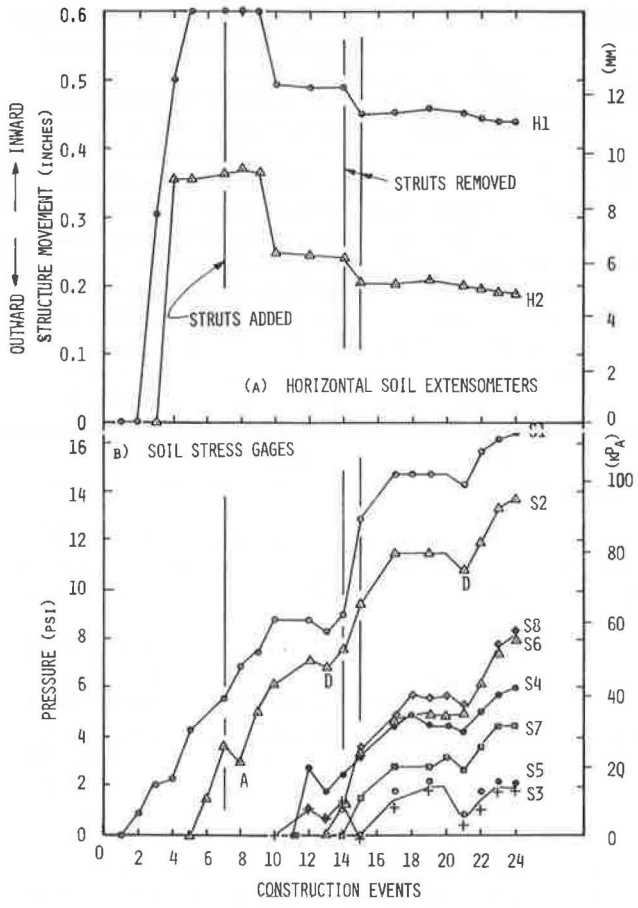

Figure 5. Movements after slab constructed and struts removed.

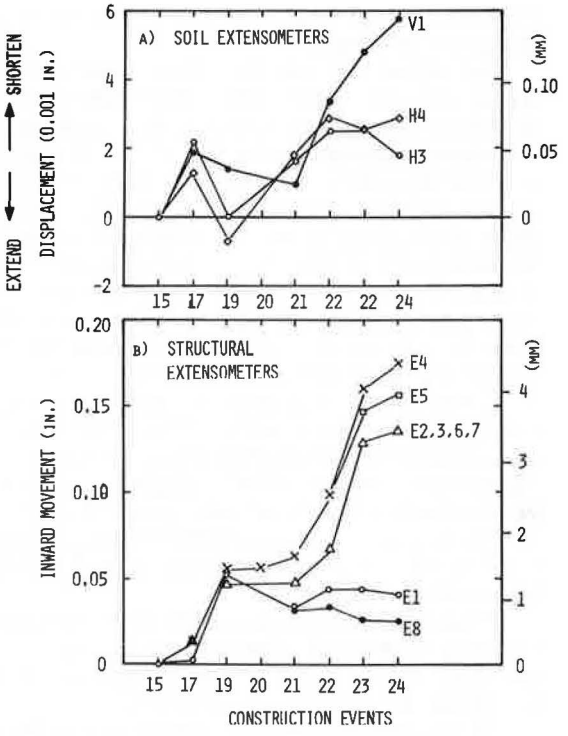

Figure 6. Final pressure distribution around structure and under slab.

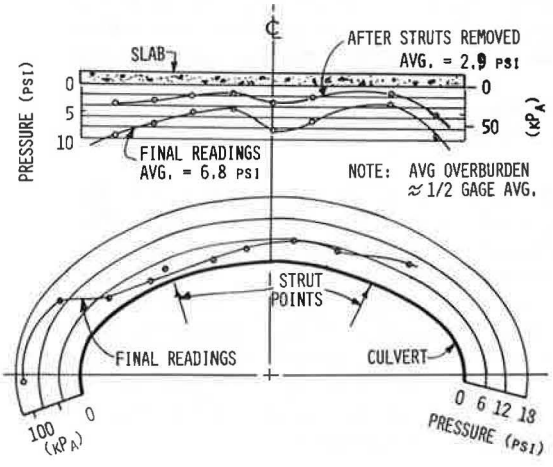

Figure 7. Inward movement of structure during load tests and final filling.

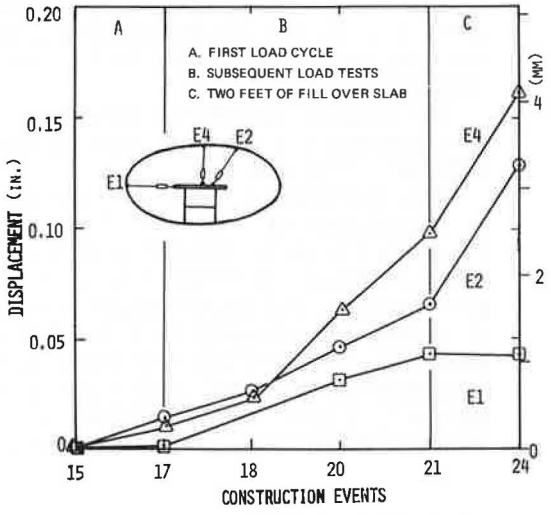

relief at the strut sections caused a stress increase at the intermediate points including the gauge locations.

The structural extensometers were installed after the slab was constructed and the struts removed (event 15). Therefore no information was obtained on the magnitude of structure deflection caused by the construction phases. The measurements for the structural extensometers are shown in Figure 5b. The two horizontal structural extensometers showed little movement during the first loading with the 32,800-lb (14 900-kg) truck (change from event 15 to 17). All of the other extensometers moved about the same amount and generally indicated inward movement under load and a small amount of rebound on unloading. A much larger residual inward movement of about 0.05 in. (1.3 mm) occurred for all extensometers after many additional load cycles in event 18 were completed. The effect of the next series of live load tests (events 19 to 21) appeared to be small. Addition of fill on top of the slab (events 22 to 24) caused outward movement at E1 and E8 and inward movement at the other structural extensometers.

Extensometers E1 and E8 were in good agreement, and this indicates symmetry of conditions on the two sides of the structure. The maximum movement was registered by the vertical extensometer E4, as expected, and the nearest extensometer to it, E5, showed the same trend with slightly smaller deflections. The remaining, vertically inclined extensometers were grouped together in magnitude of movement.

The residual structural deformation after the load tests and final grading was about 0.16 in. (4.1 mm) vertically downward and 0.04 in. (1.0 mm) horizontally inward on both sides (Figure 7).

From the construction measurements for the vertical soil extensometer V1 and the vertical structural extensometer E4, it is apparent that the relative deflection between the slab and the structure is negligible compared with the deflection of the crown of the structure (Figures 5a and 5b).

The readings of the horizontal soil extensometer H measured outside the structure at the spring line are roughly consistent in trend with those for the horizontal structural extensometer E (Figures 4 and 6a). Outward movement of the structure would cause H compression and E extension, for example. However, the magnitudes of the H and E readings are different: Much smaller changes are indicated for H than for E on both sides of the structure. One possible explanation is that the zone of deformation in the soil extends well beyond 13 ft (4 m) from the structure. In addition, the cohesive soil beyond the backfill zone is most likely more compressible than the granular backfill.

The relationship between the pressure under the slab and the crown deflection from the construction process is shown in Figure 8. The average modulus is approximately 26 lb/in.^{3} (7070 kPa/m).

Most commonly used design procedures for culverts require some measure of the horizontal passive resistance of the soil to outward movement of the structure. The dimensions of the associated modulus are pressure per unit deflection. An estimate of this modulus was obtained by plotting the spring-line pressure as a function of the corresponding soil extensometer movement (Figure 9). During the live load test phase, the modulus increased from 17 to 170 lb/in.^{3} (4620 to 46 200 kPa/m). However, because the structural extensometers showed larger lateral movement than the soil extensometers, the actual moduli are probably lower than those shown in Figure 9. During the initial stages of backfilling, the modulus was about 4 lb/in.^{3} (1090 kPa/m). This can be thought of as the active coefficient of backfill reaction.

LIVE LOAD TESTS

Most of the live load tests were conducted by using a gravel-filled dump truck with a gross weight of 32,800 lb (14 900 kg) (Figure 2). The load positions relative to the structure and the instrumented cross section are shown in Figure 10. The first load test consisted of positioning the truck successively in positions D, C, and E and then moving it off the slab to the starting position A. Residual deformations and net pressure increases were observed after the load was removed (Figure 11). The residual

Figure 8. Pressure under slab S8 related to crown deflection E4.

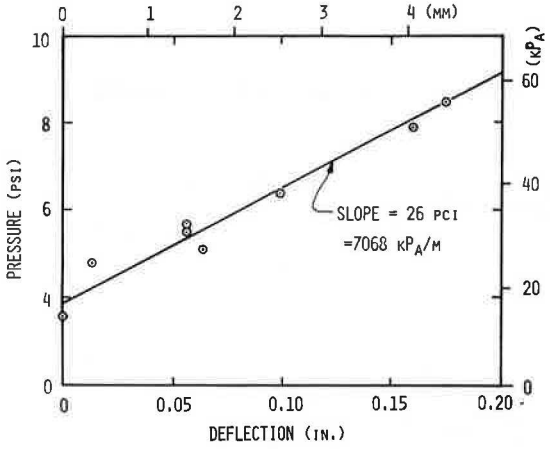

Figure 9. Relationship of spring-line pressure to deformation during construction.

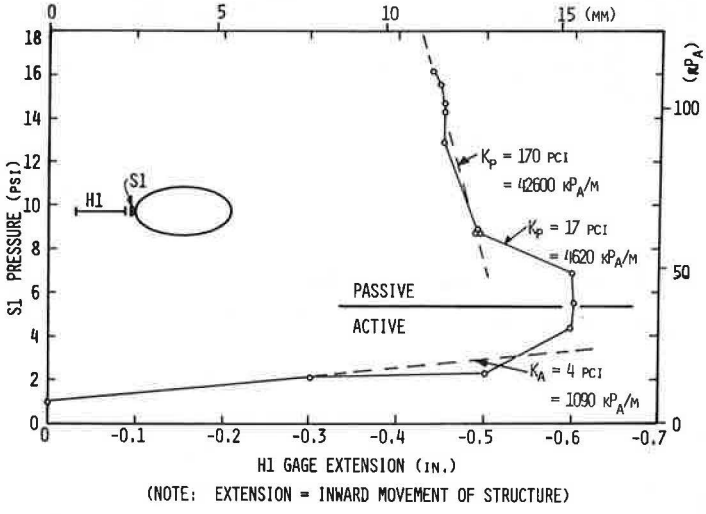

Figure 10. Load positions for 32,800-lb (14 900-kg) truck.

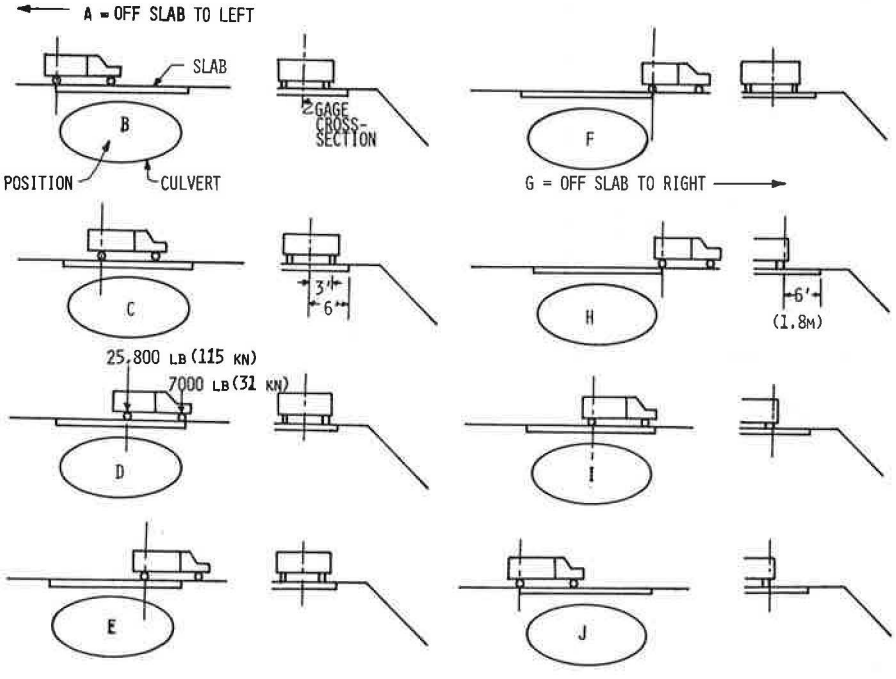

Figure 11. Residual pressures and deflections after first live load test.

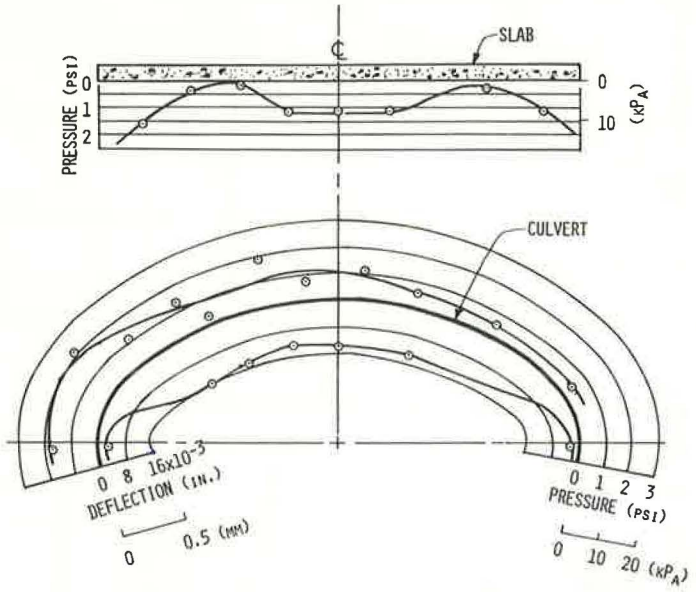

Figure 12. Results from second live load test.

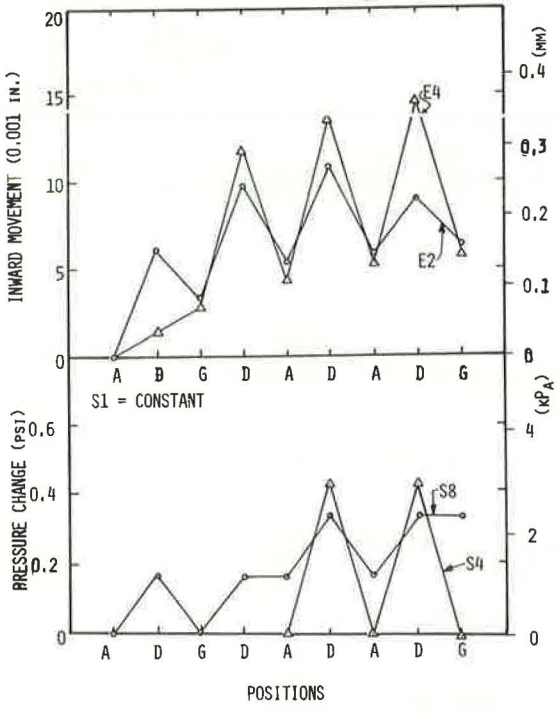

radial deformations were all inward, amounting to 0.003 in. (0.008 mm) at the spring line and 0.014 in. (0.36 mm) at the crown. This pattern suggests slippage at the longitudinal bolted joints in the structure. At the same time residual pressure increases of about 0 to 2.2 psi (0 to 15 kPa) occurred on the structure.

In the second live load test, the truck made a series of passes on and off the slab. The observed elastic and residual pressures and deformations at several locations (Figure 10) are shown in Figure 12. The average ratio of pressure increase under the center of the slab to the crown deflection under the vehicle loading was approximately 47 lb/in.^{3} (12 800 kPa/m). Spring-line movements were less than 0.001 in. (0.025 mm).

In the third live load test, the truck made a pass over the slab from position A to G at a constant speed of about 5 mph (8 km/h). The results are shown in Figures 13, 14, and 15. The residual readings are minor compared with the peak values; therefore, the response is essentially elastic. A reverse pass from G to A gave almost the same results; however, the curves in Figure 13 are not symmetrical about the center position D. The peak dynamic stress around the structure was about 0.15 psi (1.0 kPa) at the crown. The peak stress under the center of the slab was about 0.5 psi (3.4 kPa). The maximum crown deflection was 0.009 in. (0.23 mm), and deflections at all other locations were smaller. None of the soil extensometers changed by more than 0.0005 in. (0.013 mm). The ratio of pressure increase under the center of the slab to crown deflection was 34 lb/in.^{3} (9230 kPa/m).

In the fourth live load test, the vehicle was positioned for a moment in each location in Figure 10. This test gave numerical results similar to those for the previous test with the continuously moving truck for positions A through G. For the reverse pass (positions H through J) in this case, the truck wheels on the right side passed over the gauge section rather than a straddle pass. The trends were similar, but the magnitudes of the peak readings were smaller by an average of 34 percent. The pressure distribution and deflection pattern produced by the truck in position D (center of slab) is shown in Figure 16. The maximum deflection under the 32,800-lb (14 900-kg) load was about 0.012 in. (0.3 mm) at the crown. The maximum pressure on the structure was 0.3 psi (2.1 kPa), and the maximum under the center of the slab was 0.8 psi (5.5 kPa).

The structure was also tested under a live load of 162,000 lb (73 500 kg) produced by the combined weight of three gravel trucks positioned side by side on the slab. The crown deflection under this load was 0.052 in. (1.3 mm), and the ratio of pressure increase under the slab to crown deflection was 33 lb/in.^{3} (8960 kPa/m).

INTERPRETATION OF DIAMETER CHANGES

In interpreting the field data related to the structural extensometers consideration should be given to: (a) the effects of a temperature change on the shape of the structure and the lengths of the connecting cables and metal support frame of the extensometers, (b) a change in the shape of the structure due to bolt slippage, and (c) a change in shape due to the hoop stress in the structure.

A decrease in temperature would cause the cables of the structural extensometers to shorten, which would move the sensing elements of the extensometer apart. The same decrease in temperature would also cause the perimeter of the structure to shorten, which would decrease the lengths of its axes. This will cause the sensing elements of the extensometers to move together so that essentially no net change in extensometer reading would be observed. However, the steel would not be likely to change in temperature as readily as would the structural extensometers because it is in contact with the backfill on one side. Thus air temperature decrease inside of the culvert would show an apparent increase in culvert diameter.

The observed overnight deformation changes with the structural extensometers are shown in Figure 17 both with and without the 0.30-in. (7.6-mm) adjustment for the estimated temperature effect on the extensometers. The adjusted readings indicate a shrinkage of the structure. These readings are consistent with those for the observed pressure reductions (Figure 4).

Figure 13. Soil stress changes during third live load test.

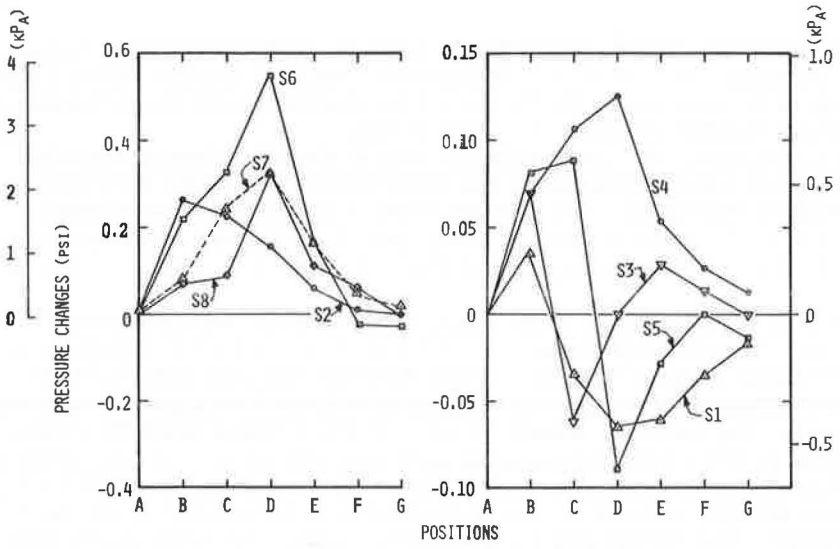

Figure 14. Extensometer changes during third live load test.

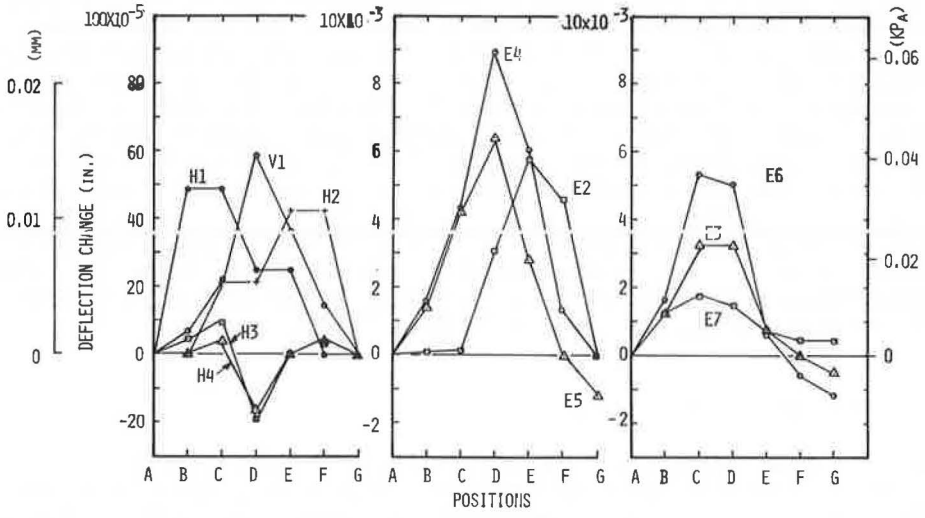

Figure 15. Culvert deflection pattern based on structural extensometers for truck moving over positions indicated.

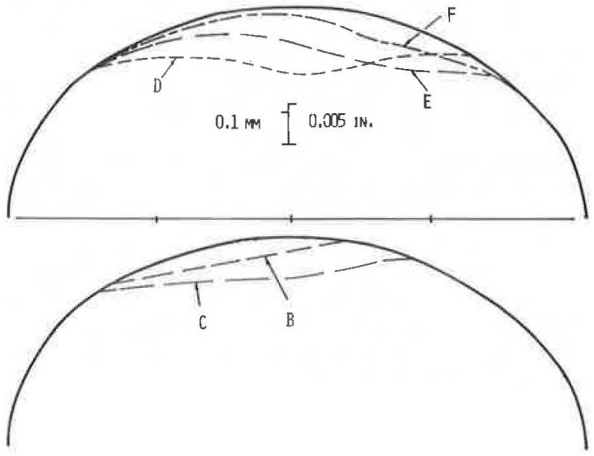

Figure 16. Pressures and deflections for 32,800-lb (14 900-kg) truck in position D.

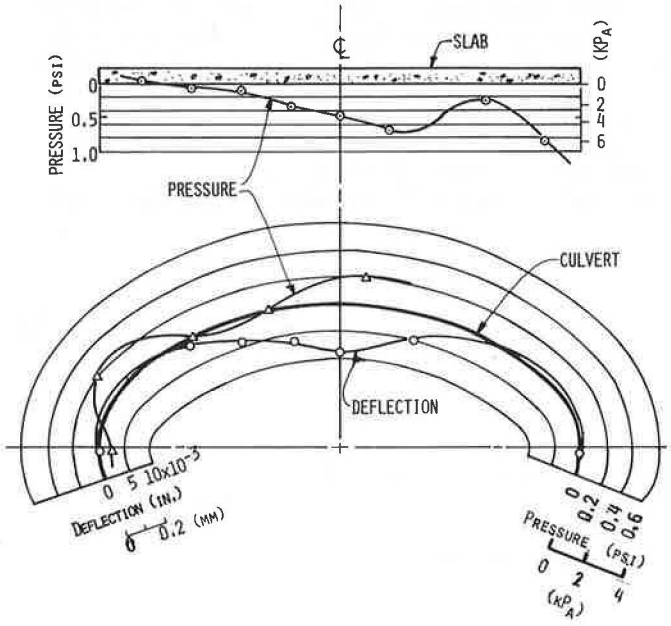

Figure 17. Radial deformations of structural extensometers caused by overnight temperature drop.

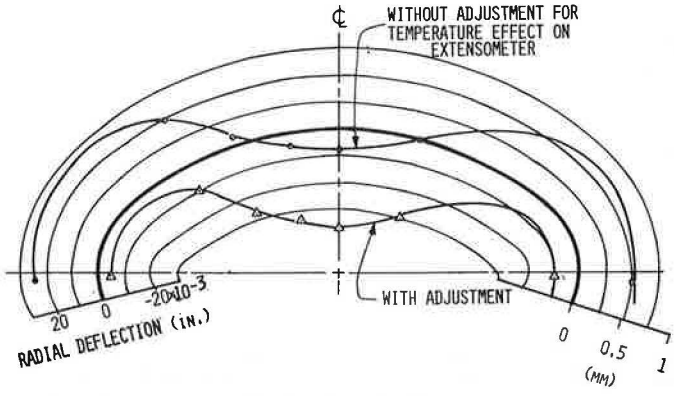

The bolt hole diameter in the plates is 1 in. (2.5 mm), and the bolt diameter is 0.75 in. (19 mm). This leaves an average clearance of 0.125 in. (3.2 mm)/joint. There are a total of 14 longitudinal joints in the pipe. Hence, an average perimeter shortening of 1.75 in. (44 mm) could be expected from slippage if friction were overcome. This would result in a change of 0.35 to 0.19 in. (8.9 to 4.8 mm) in the major and minor diameters respectively. These are much larger movements than those needed to explain the apparent net inward movement at the spring line in Figure 11. Based on an average soil pressure of 8 psi (55 kPa) around the pipe, calculations show that the assumption of slippage at one joint, at least, is reasonable.

If the ring compression theory is used, the thrust T in pounds per foot (kilograms per meter) of length of culvert is

$$T = \frac{pD}{2} \tag{1}$$

where

p = average pressure on pipe from soil in lb/ft^2 (Pa), and
D = average pipe diameter in ft (m).

The stress-strain relationships in the pipe wall give

$$\frac{T}{A}\left(\frac{P}{\Delta P}\right) = E \tag{2}$$

where

E = $30 \times 10^6 \times 144$ in lb/ft^2 (Pa),
P = length of perimeter in ft (m), and
A = area of section in ft^2/ft (m^2/m).

Combining equations 1 and 2 gives

$$\frac{\Delta P}{P} = \frac{pD}{2AE} \tag{3}$$

For the five-gauge, 2 x 6-ft (0.6 x 1.8-m) corrugation, A = 0.022 ft^2/ft (0.0068 m^2/m). The average final backfill pressure on the culvert was about p = 8 x 144 lb/ft^2 (55 kPa). The average diameter is D = 22.5 ft (6.9 m). Thus $\Delta P/P = 0.000135$. The corresponding average diameter change would thus be $\Delta D = 0.003$ ft (0.0009 m) or about 0.04 in. (1 mm). This diameter change is also large enough to account for the apparent residual inward movement at the spring line that resulted in permanent pressure increases around the pipe (Figure 7) after a series of live load tests.

OBSERVATIONS

1. Although a comparison of results with live load tests without the slab was not possible, the results with the slab indicate that the slab was effective in distributing the vehicle load and in stiffening the soil-steel structure. A vehicle load of 162,000 lb (73 500 kg) caused a crown deflection of only about 0.050 in. (1.3 mm).
2. The total inward movement of the spring line of the structure during the stages

of backfilling above the spring line was about 0.3 to 0.6 in. (7.6 to 15 mm). This was much larger than the 0.16 to 0.19-in. (4.1 to 4.8-mm) outward movement accompanying the remainder of construction and load testing. The outward movement of the structure increased the pressure against the fill. The zone of passive resistance apparently extended beyond the 13-ft (4-m) granular fill into the more compressible natural clay stratum at the site.

3. The granular backfill provided stiff lateral support to the structure. The outward movement during the final stages of filling over the crown showed a modulus of 17 lb/in.^{3} (4620 kPa/m). However, during the load testing and final grading after the struts were removed, the modulus increased to 170 lb/in.^{3} (46 200 kPa/m).

4. The stiffness of the fill over the top of the structure was great enough compared with the stiffness of the structure so that the deflection of the slab over the crown was essentially the same as the crown deflection. The subgrade modulus for the center of the slab was thus equal to the pressure under the slab divided by the crown deflection. After a few load cycles, when the soil-structure system began to behave elastically, the modulus under the center of the slab was 25 to 70 lb/in.^{3} (6790 to 19 000 kPa/m). This modulus will increase with distance from the center.

5. The pressures around the structure in the live load tests were an order of magnitude smaller than the dead load values from the slab and fill after construction. The maximum pressure at the center under the slab from the 32,800-lb (14 900-kg) vehicle was estimated to be about 0.7 psi (4.8 kPa). The corresponding maximum pressure on the crown was about 0.3 psi (2.1 kPa). Higher values of pressure were observed under the ends of the slab when the vehicle load was at the quarter point of the slab.

6. The changes in structure diameter in the live load tests were also an order of magnitude less than those from the dead load. When the 32,800-lb (14 900-kg) truck was in the center of the slab, the vertical deflection of the crown was about 0.01 in. (0.25 mm) compared with a total accumulative residual deflection of about 0.2 in. (5.1 mm) during the testing and addition of fill on top of the slab.

7. The first live load test caused a significant residual increase of 0.3 to 1.8 psi (2.1 to 12.4 kPa) in pressure under the slab and an increase of 0.4 to 2.1 psi (2.8 to 14.5 kPa) around the structure. A residual radial inward deformation of the structure also occurred, increasing from 0.004 in. (0.1 mm) at the spring line to 0.016 in. (0.41 mm) at the crown. Apparently this resulted from inelastic soil behavior and possibly from joint movement in the structure.

8. Bolt slippage at the joints of the structure could easily permit a reduction in perimeter of the structure. The timing of construction backfilling with the bolt tightening process could have a big influence on the magnitude and distribution of final pressures. The deformations resulting from thermal strains could also be as large as the live load deformations.

9. Considering the errors inherent in soil pressure measurements, the best estimate of the pressure distributions around the structure and under the slab at the completion of the tests is as shown in Figure 6. Under the slab, the average pressure was 6.8 psi (47 kPa), but it increased from about 8 psi (55 kPa) in the center, to 4 psi (28 kPa) at the quarter points, and to 10 psi (69 kPa) near the ends. The average pressure over the center of the structure was about 4.2 psi (29 kPa), and the maximum at the crown was 5.6 psi (39 kPa). These correspond to an overburden density of about 116 to 155 lb/ft^3 (1860 to 2480 kg/m^3) with a depth of 5.2 ft (1.6 m). This is in the range of the existing average density. The final crown pressure was about 5.6 psi (39 kPa). The pressure decreased to about 2.8 psi (19 kPa) at the strutting support point and increased again to 15.4 psi (106 kPa) at the spring line. The final horizontal pressure at the spring line was about equal to the vertical geostatic stress at that level.

10. The slab-fill-steel pipe composite section at the top of the structure was considered to act as a beam or an arch. The data obtained do not really clarify this; however, a combination of the two models is probably more correct.

11. Field stress measurements in soil are difficult to make accurately, and an uncertainty of ±50 percent exists. Careful laboratory calibration of the gauges in soil is needed, and in-place field calibration checks are desired. For this study, a limited laboratory evaluation was performed. Although this is much more than is usually done,

an additional gauge evaluation program is desirable that includes the effect of having the gauges close to the concrete slab.

12. The staging of strut installation and removal appears to be one of the most important factors in determining the pressure distribution around the structure and under the slab. The slab, when freshly poured, applied a uniform surcharge to the fill. Deflection under this surcharge and the fill on top of the structure was limited at the strut points and probably maximum at the crown. The struts were removed after the slab concrete had hardened. Resulting deflection at the strut points relieved the pressure there and transferred it to the center and haunch zone. The total load carried by the structure also increased and thereby increased the lateral pressure at the spring line.

13. All of the field measurements provided in this study contributed useful information to understanding the soil-structure interaction. It is desirable to obtain similar data on several other projects before generalizing the results. The primary reason is that the results are affected to an unknown degree by the construction details. In such tests, close coordination of the measurements and construction is urged. The influence of the struts should be carefully examined. Temperatures of the structure should also be measured.

ACKNOWLEDGMENTS

Partial support for this research was provided by Westeel-Rosco Ltd. of Toronto under the direction of Ching Fung, who also participated in the field activities, planning, and analysis. Ian Hogg, a student at Lakehead University in Thunder Bay, Ontario, provided the backfill property data. Irvine G. Reinig participated in the development and installation of the field instrumentation.

REFERENCE

1. E. T. Selig. Instrumentation of Large Buried Structures. ASTM Symposium on Performance Criteria and Monitoring for Geotechnical Construction, June 1974.

RAPID COMPACTION CONTROL TESTING USING WET METHOD

Mas Hatano and Travis Smith, California Department of Transportation

The California rapid wet weight method using the sand cone and nuclear gauge for determining the percentage of relative compaction is discussed. Oven drying operations, true density relationships, and optimum moisture determinations were eliminated. This permits test results to be available in a matter of hours instead of by the following day. The validity of the method was confirmed by mathematical calculations and by field correlation tests. Comparisons were made between the wet and the conventional dry method to obtain the percentage of relative compaction. This comparison was made by using the California nuclear procedure in which average test results are used. Using the wet method expedites construction testing in many cases by eliminating the need to determine test maximum density and optimum moisture. This is possible because test results are available as soon as a specimen is compacted and answers do not depend on overnight ovendry moistures. The application of the wet method to tests such as those of the American Society for Testing and Materials and the American Association of State Highway and Transportation Officials, in which fixed volume test molds are used, is demonstrated.

•IN August 1929, the then California Division of Highways was the first organization in the United States to adopt a test procedure for evaluating compaction of soils and aggregates (1). Basically, the method consisted of determining dry in-place density and of relating it to a dry laboratory test maximum density compacted according to a uniform procedure.

The original concept known as relative compaction is still being used by California and other states as a construction control test. Modifications to the test procedure have been made to improve the test and keep pace with the increased production brought about by modern construction methods and equipment. Such things as the use of nuclear gauges, the use of wet weight instead of dry density, and the averaging of test results have improved the test in terms of test accuracy, precision, and time required. The wet weight procedure eliminates all measurement of moisture in the field and laboratory.

This paper deals primarily with the California wet weight method for rapid construction control of compaction. The use of mathematical relationships between the wet and dry methods field correlation tests are discussed. The method was originally used with sand volume testing but was later applied to nuclear testing by using the area concept that averages test results.

In some cases where the material is generally the same, the wet method can still be used, but a moisture correction may be necessary. The application of the wet method to the ASTM and AASHTO test procedures is also presented.

Publication of this paper sponsored by Committee on Compaction.

BACKGROUND

Sand Volume Test

The in-place density is determined with a sand cone. The laboratory test (Calif. 216) maximum density is calculated on compacted specimens 2⅞ in. (72 mm) wide and from 10 to 12 in. (25 to 30 cm) high.

The laboratory test maximum density determination is based on testing all material passing the ¾-in. (19-mm) sieve. A rock correction is applied when the retained ¾-in. (19-mm) fraction exceeds 10 percent. The degree of correction depends on the amount and specific gravity of the retained ¾-in. (19-mm) material.

Wet Method

In 1956, California adopted an optional wet method for determining relative compaction for those soils with less than 10 percent of the material retained on the ¾-in. (19-mm) sieve. This procedure eliminated the need for oven-drying the in-place and laboratory test maximum density samples. Field test results normally became available in several hours instead of by the following day. The procedure eliminated drying equipment, did not require any alteration of existing equipment, simplified the test, made it more accurate by eliminating the variable of moisture, and did not require any special training of test operators. The test results from the wet method are essentially the same as those obtained by the dry method within limits of test variability.

In 1971, the dry method was dropped, and the wet procedure was modified to include those materials that contained more than 10 percent retained on the ¾-in. (19-mm) sieve. The elimination of part or all of the moisture measurements from the compaction test has been reported by other organizations (2, 3, 4).

FUNDAMENTAL CONCEPTS

The original work on the wet method consisted of developing the mathematical relationships to show that the wet and dry methods gave the same test results. True volume measurements were used instead of the traditional unit weights to denote density. Then the same concept was applied by using weight instead of volume. A misconception developed in this case because true densities were not involved in all cases. The details of the method are explained in the following discussions.

A sample of soil is excavated from the earthwork and weighed. The volume of the excavation is determined by filling the hole with calibrated sand. Care is exercised to maintain the moisture content of the excavated material at the condition that prevailed at the time of test. Next, a series of equal weight representative impact test specimens are weighed out of the excavated sample (Figure 1). Being of equal weight and water content, each impact test specimen (A, B, and C) will have the same proportional relationship of soil volume and water as the excavated sample.

$$\frac{W_1}{W_2} = \frac{V_1}{V_2} \qquad (1)$$

where

W_1 = weight of impact test specimen in lb (g),
W_2 = weight of total excavated sample in lb (g),
V_1 = volume of impact test specimen in in.^{3} (cm^3), and
V_2 = volume of total excavated sample in in.^{3} (cm^3).

From this relationship, the volume that A, B, and C occupied in the earthwork can be calculated. Assume that

W_1 = 6 lb (2700 g),
W_2 = 20 lb (8975 g), and
V_2 = 266 in.^{3} (4358 cm^3).

From equation 1,

$$V_1 = \frac{6}{20} \times 266 = 79.8 \text{ in.}^3 (1311 \text{ cm}^3)$$

Impact test specimens A, B, and C are then compacted at different moisture contents to determine the optimum condition. In actual practice, the specimens may be compacted at field moisture, by adding water or by drying the specimen out. Changing the water content affects the void water content but does not affect the volume of soil solids in the impact test specimens.

After the specimens are compacted in the impact test apparatus, the specimen with the smallest test volume is related to the volume that the specimen occupied in the earthwork. The resultant value is multiplied by 100 for an end result in terms of the percentage of relative compaction (RC). Figure 1 shows specimen B as the impact test specimen with the minimum volume.

$$RC = \frac{V_3}{V_1} \times 100 \qquad (2)$$

where

V_1 = volume that impact test specimen occupied in the earthwork, in in.^{3} (cm^3), and
V_3 = smallest volume determined after compacting specimens in the impact test, in in.^{3} (cm^3).

Assume that V_3 = smallest impact specimen B_1 = 73 in.^{3} (1196 cm^3). Therefore,

$$RC = \frac{73}{79.8} \times 100 = 91$$

The above discussion on the determination of RC eliminated soil drying procedures and direct density relationships.

The current procedure uses the more common weight relationships. The mathematical relationship here is

$$D_w = \frac{W_1}{V} \qquad (3)$$

where

D_w = wet weight of compacted specimen,
W_1 = batched wet weight of test specimen before adjustment for water, and
V = volume of compacted specimen.

Therefore,

$$RC = \frac{D_t}{D_w} \tag{4}$$

where D_t = in-place wet density D_w from equation 4.

Table 1 gives comparisons of the percentage of relative compaction calculations based on wet and dry methods using the California procedure. Table 1 is based on the following assumptions (1 lb/ft^3 = 0.016 g/cm^3):

In-place wet density = 100 lb/ft^3,
Moisture content = 10.0 lb/ft^3 = 11.1 percent, and
In-place dry density = 100 - 10.0 = 90 lb/ft^3.

Lines 8 and 9 show the same RC for the dry and wet methods. In normal practice, the compaction curves are plotted for the data on line 6 or 7, and the maximum value is used to calculate RC for the test.

SINGLE SPECIMEN TESTS

For construction control purposes, there are occasions when only one impact test specimen is needed. If the first test result indicates a percentage of relative compaction below the specified minimum, there is no reason to compact additional specimens. If the second specimen showed a higher test result, it would only lower the percentage of relative compaction that already failed to meet specification. Thus, the complete compaction curve is not always necessary.

The single specimen test is easily adaptable to the wet method because no moisture measurements are made but is not readily adaptable to the dry method because of the time required to obtain ovendry moistures.

NUCLEAR TEST

In November 1966, California adopted the nuclear procedure (Calif. 231-F) for determining relative compaction. The adoption of the nuclear method for determining in-place density caused considerable discussion about the precision of the nuclear gauge and comparison with the sand volume test. Studies by Utah (6), California (7), and others indicate the nuclear test to be equal to or have less variability than the sand volume test. In terms of accuracy, studies by California (8), Minnesota (9), and others have shown the nuclear test to be more accurate than the sand volume test.

Some pertinent features of test method Calif. 231-F are as follows:

1. The wet method is used exclusively,
2. All testing is performed in the direct transmission mode,
3. Nuclear gauges are calibrated from standard blocks (6),
4. The area concept is used,
5. A composite sample is used for test maximum determination, and
6. A common test maximum is used where conditions permit.

AREA CONCEPT

The area concept evolved from a statistical study performed on embankment material (10, 11). Figures 2 and 3 from the study (10) show random sand volume tests taken from jobs that had uniform and varied materials. The sand volume tests were

Figure 1. Wet method based on volume comparison.

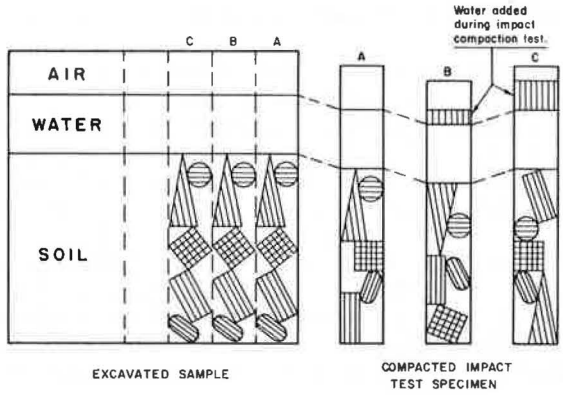

Table 1. Percentages of relative compaction based on wet and dry methods using the California procedure.

Line Number	Item	Impact Specimen A	B	C
1	Equal weight of batched representative wet test specimen from excavated sample, lb	5.0	5.0	5.0
2	Dry weight[a], lb	4.5	4.5	4.5
3	Adjustment for water to determine optimum, lb	0	-0.22	+0.22
4	Total wet weight before compaction[b], lb	5.0	4.78	5.22
5	Compacted volume determined from test, ft^3	0.050	0.051	0.052
6	Dry density of compacted specimen[c], lb/ft^3	90.0[d]	88.2	86.5[d]
7	Wet value of compacted specimen[e]	100.0	98.0	96.2
8	Relative compaction (dry basis)[f], percent	100	102	104
9	Relative compaction (wet basis)[g], percent	100	102	104

Note: Moisture adjustments were made but not included in calculations. 1 lb = 453.6 g. 1 ft^3 = 0.03 m^3. 1 lb/ft^3 = 0.016 g/cm^3.

[a] Line 1 - field moisture.
[b] Line 1 + line 3.
[c] Line 2/line 5.
[d] Not true densities.
[e] Line 1/line 5.
[f] ($90 lb/ft^3$)/line 6 x 100.
[g] ($100 lb/ft^3$)/line 7 x 100.

Figure 2. Statistical study results based on random selection of uniform materials.

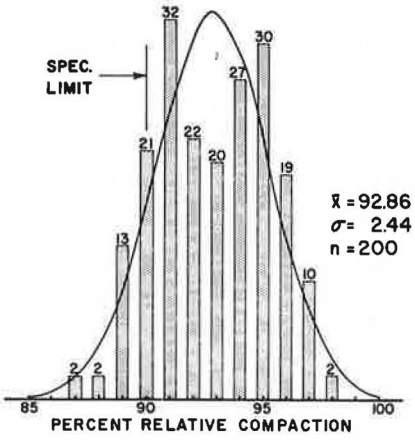

Figure 3. Statistical study results based on random selection of nonuniform materials.

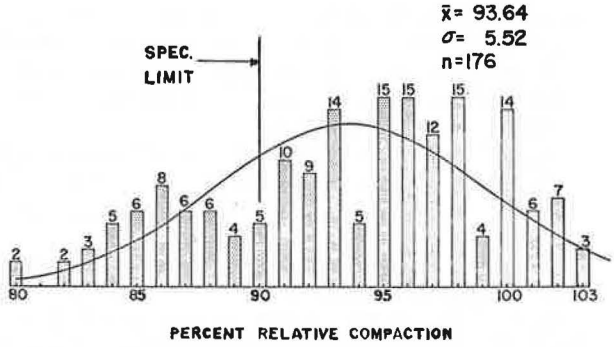

performed after construction personnel had tested and accepted the compacted area as meeting specifications.

Data indicated that highways are constructed with a number of tests that do not meet specifications and that there is considerable variation in compaction (6, 12, 13, 14). The conclusion from these studies clearly showed that one test is not a satisfactory criterion for checking specification compliance. A more realistic approach is to average a small number of tests that would more nearly tend to reflect the average obtained if a large number of tests were performed in a given area. The average value would also tend to give a better picture of what is actually being constructed.

Initially, an area of work is carefully delineated. This area may be either very small, such as backfill around pipes, or more than 0.5 mile (0.8 km) of roadway. Some factors to consider when an area is selected are uniformity of materials, conditions of production, and compaction. Portions of the area that may be observed or that are suspected to be different are excluded from the total area and are treated as separate small areas.

A minimum of five test sites are randomly selected for areas greater than 1,000 yd^2 (836 m^2), and a minimum of three test sites are randomly selected for areas less than 1,000 yd^2 (836 m^2).

MAXIMUM DENSITY TEST

Equal representative portions of material from each test site are combined to form one composite sample. A laboratory wet test maximum value is determined on the composite sample and is related to the average wet in-place density to get a percentage of relative compaction. In many cases when the material is generally the same from one area to the next, a common wet composite test maximum value may be used. A moisture correction may be necessary.

In some cases, a single test specimen is satisfactory where it signifies a failing test. The compaction of additional specimens to determine a test maximum value would not be necessary since the test had already failed to meet the minimum specification.

PRINCIPLES OF WET METHOD

The principles of the wet method for compaction control are the same for the nuclear test and the sand volume test. However, since the California procedure uses multiple in-place tests, a composite test maximum value, and a common density, further discussion on the wet method is presented.

Figure 4 shows comparative field test data from one area evaluated on the basis of both wet and dry methods. The use of composite test maximum values compared with individual test maximum values is also compared.

Line 1 shows the percentage of relative compaction calculated by dividing the individual dry in-place density by the individual dry test maximum density. This average is 90.9 for the six test sites.

Line 7 shows the percentage of relative compaction calculated for each test site by dividing the individual wet in-place density by the composite test maximum density. This average is 91.3 percent, which compares closely to the 90.9 percent relative compaction for the dry method.

Figure 5 shows data from 75 test areas where the comparative percentages of relative compaction based on the wet and dry methods were determined as described previously. The scatter diagram indicates that there is no significant difference between the wet and dry methods when a composite test maximum and average in-place density are used instead of individual tests.

Figure 4. Test plan data of comparison of percentage of relative compaction based on wet and dry methods.

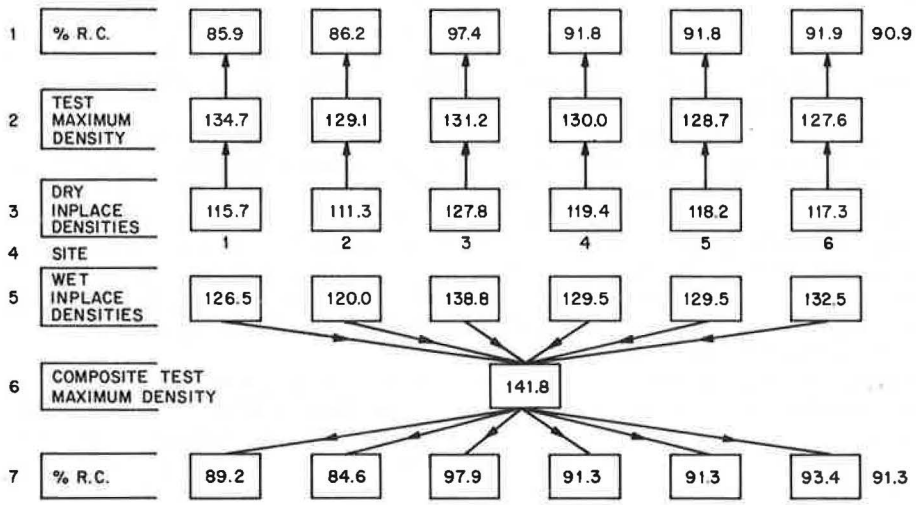

Figure 5. Nuclear gauge tests for wet versus dry method.

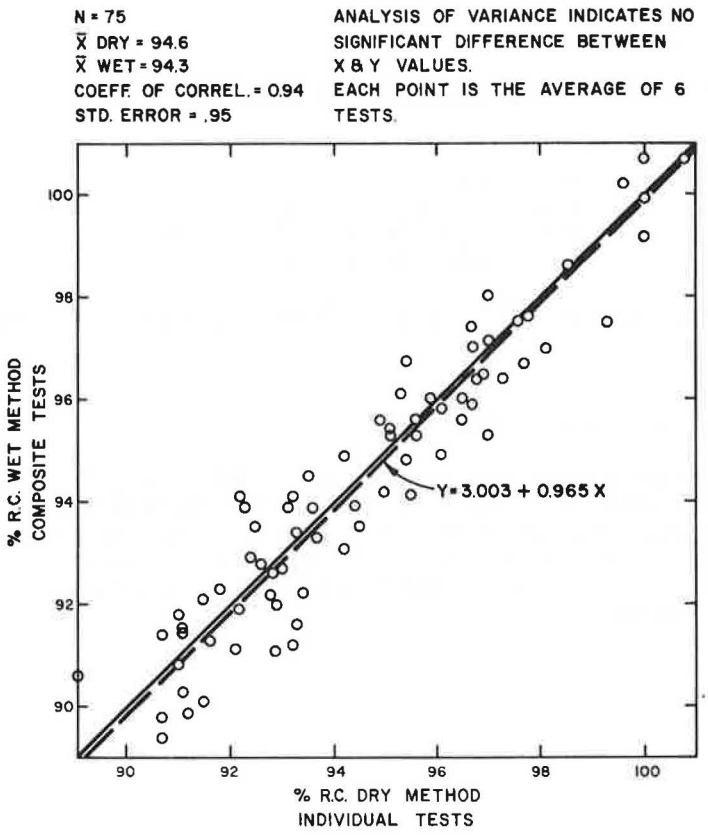

COMMON DENSITY

In many cases where the material from one area to the next is generally the same, a common density may be used, and a laboratory compaction test need not be run. Some of the criteria used for a common density are that the material must be from the same general source, must generally have the same visual characteristics, and must have the same moisture content.

A common density is established by averaging wet composite test maximum values from two consecutive areas. The difference in average moisture contents between the two consecutive areas must also be within 31.25 lb/ft^3 (0.05 g/cm^3) of the common value. Checks are performed at least every 7 days, and if the moisture content and test maximum values are within 31.25 lb/ft^3 (0.05 g/cm^3) of the common values, the two values are averaged to establish a new common test maximum value and moisture. If the previous criteria are not met, a compaction test is performed for each area being tested. Since a judgment factor is involved, an operator must be trained and experienced to effectively use the common density.

When a common density is used, the moisture content between areas must be the same, or adjustments must be made so that the wet procedure will be valid. In these cases, an average moisture content is determined for each area by nuclear tests at the same time the density tests are being performed. Nuclear moisture tests need only indicate the average relative difference between areas. Therefore, no special calibration relating to a standard such as ovendry moisture is necessary. No moisture determinations are necessary for the laboratory test maximum specimens.

Following is an example of the moisture correction method (1 lb/ft^3 = 0.016 g/cm^3):

Common composite test maximum value = 137.5 lb/ft^3,
Average moisture = 6.9 lb/ft^3,

These data are used to complete the moisture content method for the test area:

Average in-place wet density (five tests) = 135 lb/ft^3,
Average in-place moisture (five tests) = 8.8 lb/ft^3,
Moisture correction = 6.9 - 8.8 = -1.9 lb/ft^3,
Adjusted in-place wet density = 135 - 1.9 = 133.1 lb/ft^3, and
RC = (133.1/137.5) × 100 = 97.

This method became standard on April 2, 1973, and is now being used for all contracts using the nuclear method.

APPLICATION TO AASHTO AND ASTM METHODS

The same type of analysis made previously can be applied to the AASHTO and ASTM methods. The difference between the California method and the other methods is that the California method uses a fixed weight of material and measures the volume of compacted soil but the latter methods use a variable weight of material and a fixed volume.

Equation 5 shows the mathematical relationship between the wet and dry methods when the fixed volume molds are used:

$$RC = \frac{D_W}{T_M} \times 100 \qquad (5)$$

where

D_W = in-place wet density by tests such as the sand cone or nuclear test, and
T_M = laboratory compacted test specimen with highest wet weight as determined by the AASHTO or ASTM procedure.

T_M is calculated as shown in figure 6.

Based on Figure 6, the following relationships are developed:

$$\frac{B}{F} = \frac{S}{T_M}$$

$$T_M = \frac{F \times S}{0.033B} \qquad (6)$$

where 0.033 ft^3 (943.9 cm^3) = constant volume based on a mold of the same size.

Assume that (1 lb = 453.6 g)

F = 4.75 lb,
S = 5.29 lb, and
B = 5.63 lb.

Therefore,

$$T_M = \frac{4.75 \times 5.29}{0.033 \times 5.63} = 135 \text{ lb/ft}^3 \ (2.16 \text{ g/cm}^3)$$

Let (1 lb/ft^3 = 0.016 g/cm^3)

D_M = 130 lb/ft^3 and
T_M = 135 lb/ft^3 = the highest wet density of a laboratory compacted test specimen.

Therefore,

$$RC = \frac{130}{135} \times 100 = 96$$

Table 2 gives comparisons of the percentage relative compaction calculations based on wet and dry methods using the 0.033-ft^3 (934.5-cm^3) mold. Table 2 is based on the following assumptions (1 lb/ft^3 = 0.016 g/cm^3):

In-place moisture content = 10.0 percent,
In-place wet density = 134.2 lb/ft^3, and
In-place dry density = 122.2 lb/ft^3.

CONCLUSIONS

1. Mathematical calculations indicate that the wet and dry procedures for determining percent relative compaction give the same results.
2. Test data indicated that the wet method applied to multiple nuclear testing and use of a composite sample for determining laboratory test maximum density are essentially the same as the average of single tests when the dry method is used.
3. Application of the wet method to a common density by making moisture adjustments based on nuclear gauge measurements was developed.
4. In many cases, the wet method permits determination of specification compliance without the development of a compaction curve. Therefore, results can be obtained in several hours instead of by the following day.

Figure 6. Calculation of T_M.

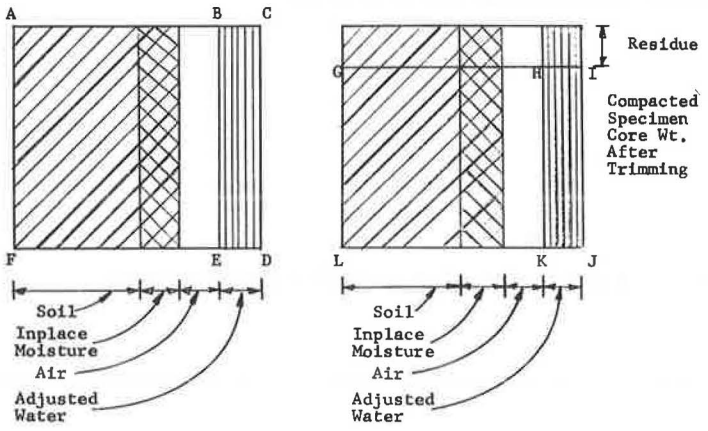

Note:
ABEF = S = initial batched specimen weight in lb/ft^3 (g/cm^3) that has the moisture content that prevailed at the time of the in place test;
ACDF = B = initial batched specimen in lb (g) adjusted for added or subtracted water;
GIJL = F = final compacted core weight in lb(g) after trimming; and
GHKL = T_M = laboratory test specimen wet weight, an unknown value.

Table 2. Percentages of relative compaction based on wet and dry methods using the 0.033-ft^3 (934.5-cm^3) mold.

Line Number	Item	Impact Specimen		
		A	B	C
1	Equal weight of batched representative wet test specimen from excavated sample, lb	5.07	5.07	5.07
2	Dry weight, lb	4.61	4.61	4.61
3	Adjustment for water to determine optimum, lb	-0.11	0	+0.11
4	Total wet weight before compaction[a], lb	4.96	5.07	5.18
5	Final compacted core weight after trimming, lb	4.46	4.63	4.63
6	Wet weight[b], lb	136.8	138.9	136.0
7	Dry density[c], lb/ft^3	124.2	126.3[d]	123.6[d]
8	Relative compaction (wet basis)[e], percent	98	97	99
9	Relative compaction (dry basis)[f], percent	98	97	99

Note: Moisture adjustments were made but not included in calculations. 1 lb = 453.6 g, 1 lb/ft^3 = 0.016 g/cm^3.

[a]Line 1 + line 3.
[b](Line 5 x line 1) 30/line 4.
[c](Line 5) 30/percentage of moisture.
[d]Not true densities.
[e]In-place wet density/line 6.
[f]In-place dry density/line 7.

5. The wet method could be applied to such tests as the ASTM or AASHTO procedures where a fixed volume mold is used to determine the laboratory test maximum density.

REFERENCES

1. T. E. Stanton. Highway Fill Studies and Soil Stabilization. California Highways and Public Works, Vol. 16, June-July 1938.
2. J. W. Hilf. A Rapid Method of Construction Control for Embankments of Cohesive Soils. Bureau of Reclamation, U.S. Department of the Interior, Denver, Oct. 1959.
3. R. Schonfeld. The Constant Dry Weight Method—A No Weighing Field Compaction Test. Ontario Department of Highways, D.H.O. Rept. RR141, Sept. 1968.
4. W. H. Peak. Rapid Test Method for Earthwork Compaction Control. New York State Department of Transportation, Albany, Nov. 1972.
5. Method of Developing Density and Moisture Calibration Tables for the Nuclear Gage. Materials Manual of Testing and Control Procedures, Transportation Laboratory, California Department of Transportation, Test Method Calif. 911B, April 2, 1973.
6. G. F. Neilson. Characteristics of Compacted Bases and Subbases. Utah State Highway Department, Aug. 1967.
7. T. Smith. Effect of Plus ¾-Inch Rock and Other Field Variables on Nuclear Gage Moisture and Density Determinations. California Division of Highways, Jan. 1970.
8. R. A. Forsyth, A. D. Hirsch, and M. Hatano. Structure Backfill Testing. California Department of Transportation, Jan. 1974.
9. M. S. Kerston and E. L. Skok. Evaluation of Nuclear Moisture Density Gages. Univ. of Minnesota, June 30, 1966.
10. G. B. Sherman, R. O. Watkins, and R. H. Prysock. A Statistical Analysis of Embankment Compaction. Highway Research Record 177, 1967, pp. 157-185.
11. W. G. Weber, Jr., and T. Smith. Practical Application of the Area Concept to Compaction Control Using Nuclear Gages. Highway Research Record 177, 1967, pp. 144-156.
12. F. J. Davis. Quality Control of Earth Embankments. Proc., 3rd International Conference on Soil Mechanics and Foundation Engineering, Vol. 1, Zurich, 1953.
13. T. G. Williamson. Embankment Compaction Variability—Control Techniques and Statistical Implications. Indiana State Highway Commission, Aug. 1968.
14. J. L. Jorgenson. The Statistical Approach to Quality Control. North Dakota State Highway Department, Nov. 1968.

FACTORS INFLUENCING VIBRATORY COMPACTION OF COHESIONLESS SOILS

M. F. Howeedy, Faculty of Engineering, Ain Shams University, Cairo, Egypt; and
A. R. Bazaraa, Faculty of Engineering, Cairo University, Egypt

Field data are given for 22 test fills made of medium-to-fine uniform sand and compacted by 7 models of vibratory compactors. The final relative density is correlated with lift thickness, number of coverages, total static plus dynamic force applied by the compactor, towing speed, and operating frequency. There is considerable scatter in these correlations because of difficulties in determination of in situ relative density, heterogeneity in the degree of compactness of sand, variation of the depth at which the relative density is determined, and lack of sufficient data when a single variable is studied and other variables are fixed. However, the data indicate that the final relative density increases as operating frequency, total applied force, or the number of coverages increases. The variation in lift thickness up to 1 ft (0.3 m) has no significant effect on this density, but an increase in towing speed reduces it. A study of the trends of the relationships between final relative density and the various variables and a dimensionless and statistical analysis establish a correlation between the final relative density and a factor expressing the joint effect of the important properties of the soil, compactor, and compaction procedure. Such correlations, when available and justified, help in the choice of the compactor or compaction procedure for a given job.

•VIBRATORY compaction of cohesionless soils, used as early as the 1930s (1), is influenced by resonant frequency of compactor-soil system, number of load cycles, variation of shear strength during vibration, and magnitude of dynamic stresses generated by the vibrator.

Improvements in construction and construction efficiency are partially based on experience and well-documented studies. Full-scale field experiments are badly needed. This paper presents field data for 7 models of vibratory compactors used to compact 22 test fills made of medium-to-fine sand at the Pumped Storage Project at Ludington, Michigan (6).

The objectives of the analysis of the field test results are

1. To evaluate specific variables, such as lift thickness, number of coverages, total force applied by the compactor, operating frequency, and towing speed, that influence the final relative density of the compacted sand.
2. To explore feasible relationships between the final relative density and one factor that can express variations in compaction procedure, compactor characteristics, and properties of soil.

CONSTRUCTION OF TEST FILLS

Test fills were constructed of the site sand that is a light brown, uniform, medium-to-fine sand having a uniformity coefficient of about 2. It is classified as SP according

Publication of this paper sponsored by Committee on Compaction.

to the Unified Soil Classification System. The overage value of the fraction passing the No. 200 sieve ranges, for the various test fills, is between 1.4 and 5.5 percent, and the representative value is 2.4 percent. Range of grain size distribution curves of this sand is shown in Figure 1. The average placement water content for the sand in the various test fills varied between 1.1 and 6.1 percent and averaged close to 4.2 percent.

Each test fill had plan dimensions of 30 by 160 ft (9 by 49 m). There were four to eight lifts, and the compacted lift thickness varied from 0.45 to 1.00 ft (0.14 to 0.3 m). Test pits were made at about 6 or 9 ft (1.8 or 2.7 m) from the centerline of the test fill.

The in situ density after compaction was determined at depths of 1.25, 2.25, and 3.25 ft (0.4, 0.7, and 0.99 m) by using the water balloon and sand cone methods. In each test fill, from 8 to 49 tests (an average of 30 tests) were performed. The total number of tests performed in the test fills was 663.

The final relative density D_r (ASTM D2049) for each test fill, after compaction, is given in Table 1.

TECHNICAL DATA FOR VIBRATORY COMPACTORS

Vibratory compactors in these tests were all towed by a tractor at speeds between 1.5 and 4.5 mph (2.4 and 7.2 km/h) (Table 1). They can be classified according to their static weights as follows (1 T = 0.9 t):

Compactor Type	Static Weight (ton)
Light	<2
Medium	2 to 4
Heavy	4 to 7
Very heavy	>7

All the vibratory compactors used in this investigation are, according to this classification, either heavy or very heavy.

The vibrations of the roller or drum are produced by an eccentric weight mounted on a rotating shaft within the drum. The frequency of the rotating shaft can be altered by a throttle setting. The operating frequency of the compactors varied between 1,100 and 2,250 vibrations/min.

Vibrations of the drum produce a centrifugal dynamic force F_{dyn} that depends on the weight and eccentricity of the eccentric weight in the drum and also on the square of the maximum operating frequency of the vibration. The sum of the static weight of the compactor and its dynamic force is the total applied force. In general, the total applied force by tractor-towed compactors is two to three times the static weight of the vibrator (1).

A summary of the available technical data for the compactors used in the test fills is given in Table 2.

FIELD TEST RESULTS

There are two ways to present the field test results. The first is to determine the influence of one variable only on the final relative density while all other factors are kept constant. The second is to study the influence of one variable on the final relative density regardless of the variation in the other variables. The first approach is scientifically accepted. The second approach indicates the general trend and probably the overriding influence of the variable under consideration. In Figures 3 and 6, a refers to the first approach and b refers to the second approach. It is natural that, in general, the scatter in Figures 3b and 6b is much greater than that in Figures 3a and 6a.

Figure 1. Grain size curves for site sand.

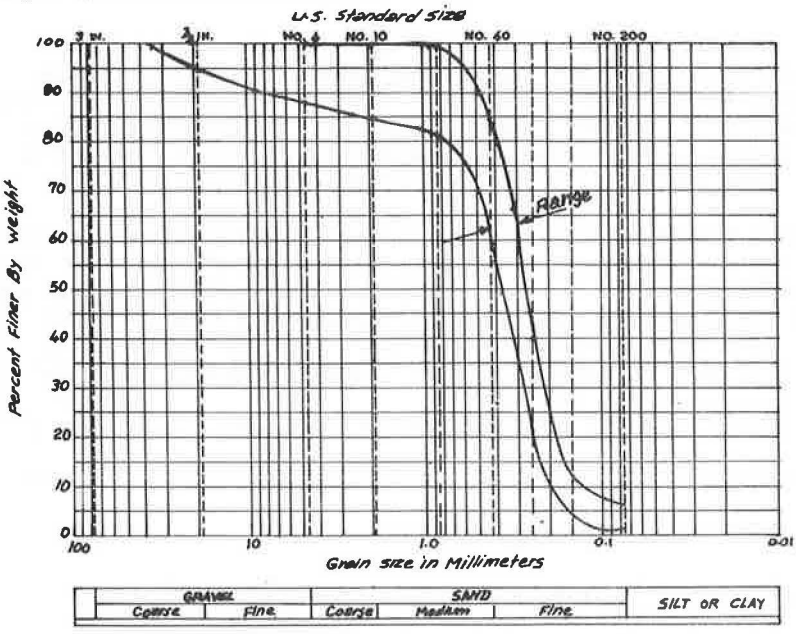

Table 1. Vibratory compaction field test data from test fills at Ludington, Michigan.

Compactor Model[a]	Lift Number	Lift Thickness[b] (ft)	Number of Coverages	Towing Speed (mph)	In Situ Density Test Type	In Situ Density Test Number	Final D_r (percent)
CF-43	4	1.00	3	1.5	SC[c], W[d]	22	80
CF-43	4	1.00	6	1.5	SC, W	23	79
CF-43	8	1.00	6	1.5	SC, W	23	91
CF-43	4	1.00	10	1.5	SC, W	20	88
VP-22D	4	1.00	3	1.5	SC, W	20	87
VP-22D	4	1.00	6	1.5	SC, W	20	79
VP-22D	4	1.00	10	1.5	SC, W	8	98
CH-43	5	1.00	6	1.5	SC, W	20	92
CF-43	5	1.00	6	1.5	SC, W	22	86
RVT-200	4	1.00	6	1.5	SC, W	22	96
CH-43	4	1.00	6	1.5	SC, W	22	90
CF-43	4	1.00	6	3.0	W	30	80
CF-43	4	1.00	6	4.5	W	30	81
VP-22D	4	1.00	6	3.0	W	27	97
SV-70	4	1.00	6	1.5	W	27	90
CF-43	8	1.00	6	1.5	W	40	101
RVT-100	8	0.55	6	1.5	W	47	88
CF-43	8	0.45	6	1.5	W	47	90
RVT-100Z	8	0.70	6	1.5	W	48	92
CF-43	8	0.77	6	3.0	W	49	87
RVT-100Z	8	0.72	6	3.0	W	48	98
RVT-100	8	0.68	6	3.0	W	48	85

Note: 1 ft = 0.3 m, 1 mph = 1.6 km/h.

[a]Table 2 gives data on compactors.
[b]After compaction.
[c]Sand cone method.
[d]Water balloon method.

Table 2. Technical data for vibratory compactors used in test fill.

Type	Model	Drum Width (in.)	Drum Diameter (in.)	Foot Length (in.)	Vibrating Power (hp)	Operating Frequency (cycles/min)	Static Weight (lb)	Dynamic Force[a] (lbf)	Total Force[a] (lbf)
Smooth drum	VP-22D	78	60	—	66	1,100 to 1,300	22,750	41,400	64,150
	RVT-100	76	56	—	55	1,350 to 2,250	13,500	33,000	46,500
	RVT-200	76	56	—	73	1,350 to 2,250	17,800	40,000	57,800
	CH-43	75	47	—	30	1,400 to 1,600	10,000	23,000	33,000
Sheep's-foot	CF-43	75	47	7.9	30	1,400 to 1,600	12,000	23,000	35,000
	SV-70	75	49	7.2	74	1,500 to 1,800	14,500	30,850	45,350
	RVT-100Z	76	56	7.9	55	1,350 to 2,250	13,500	33,000	46,500

Note: 1 in. = 2.5 cm. 1 hp = 0.746 kPa. 1 lb = 0.45 kg. 1 lbf = 4.4 N.

[a]At maximum operating frequency.

Influence of Lift Thickness on Final Relative Density

The relationship between lift thickness and relative density for all test fills is shown in Figure 2. The range of lift thickness studied was 0.45 to 1.00 ft (0.14 to 0.3 m). The data indicate that, within the limits of lift thickness, the value of D_r did not vary as the lift thickness varied. This may be explained by the overvibration phenomenon (2) that occurs near the vibrated surface of each layer and that may tend, for small lift thicknesses, to compensate the increase in the degree of compactness of the sand for the reduction of the lift thickness.

Since the variation in lift thickness from 0.45 to 1.00 ft (0.14 to 0.3 m) did not influence the final relative density, it was more economical to use a 1-ft (0.3-m) lift thickness. Extension of this conclusion beyond a 1-ft (0.3-m) thickness is not appropriate.

Influence of Number of Coverages on Final Relative Density

The relationship of the number of coverages and D_r for all test fills is shown in Figure 3. The data show that the final relative density increases as the number of coverages increases. The rate of increase beyond six coverages was smaller than that from three to six coverages.

The increase in relative density that occurs as the number of coverages increases is expected and agrees with previously published data (5). The increase in number of coverages represents an increase in the compactive effort. However, when the sand gets dense enough, an increase in the compactive effort may not be effective enough to produce densification of the soil.

Influence of Total Force Applied by Compactor on Final Relative Density

The relationship between total applied force and D_r for all test fills is shown in Figure 4. An increase in this force causes an increase in the dynamic stress applied to the soil. This is an important factor in causing densification of the soil (2).

The data show an increase in D_r for a total force of 35,000 to 46,500 lbf (156 to 207 kN). An additional increase in the total force up to 64,150 lbf (285 kN) did not cause any further change in D_r.

Previous data show good correlations between degree of compaction and static weight per unit width of the roller (4).

Influence of Operating Frequency of Compactor on Final Relative Density

The frequency of the compactors used in this investigation varied from 1,200 to 1,800 cycles/min.

The relationship between operating frequency and D_r, shown in Figure 5, is for test fills in which only the frequency varied. Each lift in these fills received six coverages from compactors towed at 1.5 mph (2.4 km/h). The figure indicates that the final relative density increases as the frequency of the compactor increases.

Previous studies indicated that the increase in operating frequency up to 1,200 cycles/min caused an increase in D_r for medium-to-fine sand (2). For well-graded sand, dry density increased as frequency increased up to 2,400 cycles/min and then decreased as frequency further increased (5). This agrees generally with the relationship between frequency and dynamic force on the soil surface (1, 2).

Figure 2. Final relative density versus lift thickness.

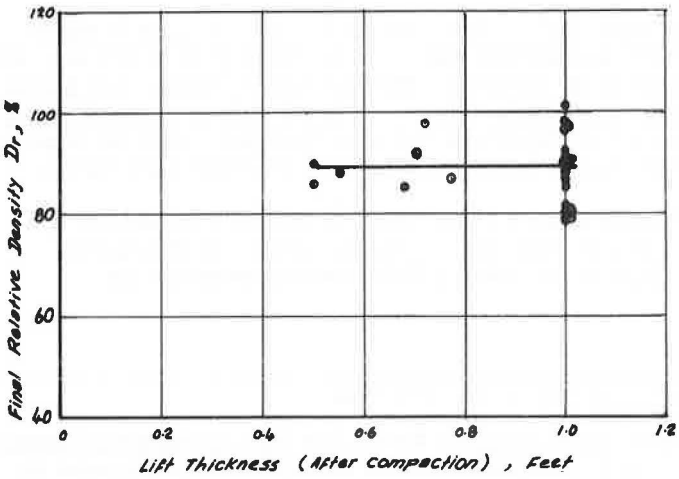

Figure 3. Final relative density versus number of coverages for (a) CF-43 vibratory compactors towed at 1.5 mph (2.4 km/h) and (b) various vibratory compactors and different towing speeds.

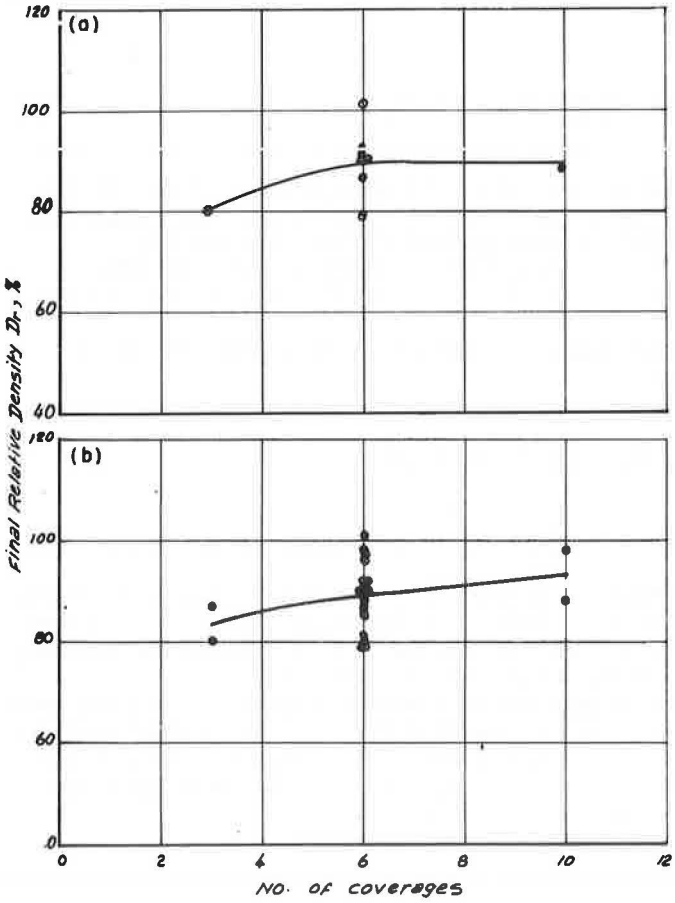

Figure 4. Final relative density versus applied force for various compactors and different towing speeds.

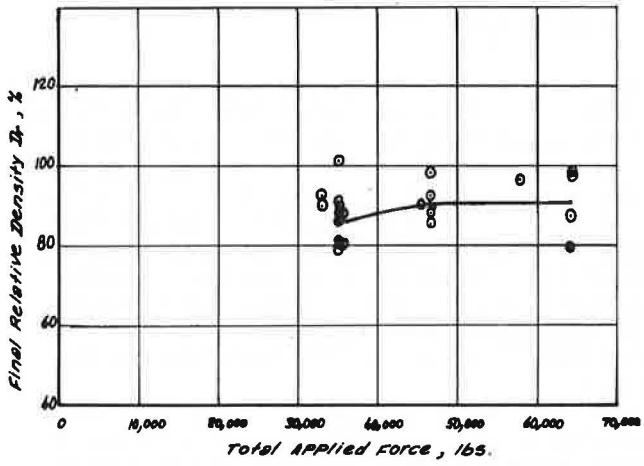

Figure 5. Final relative density versus operating frequency based on six coverages of vibrating compactors towed at 1.5 mph (2.4 km/h).

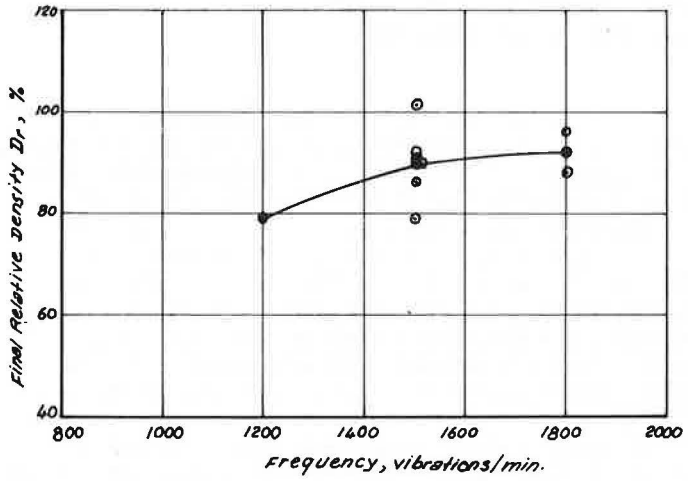

Figure 6. Final relative density versus towing speed for (a) test fills placed on 1-ft-thick (0.3-m) compacted lifts and (b) all test fills.

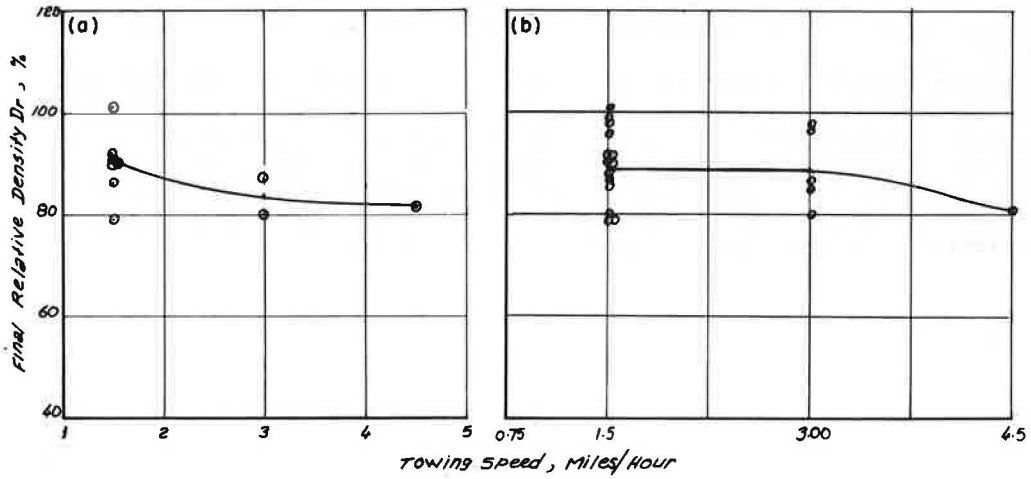

Influence of Towing Speed on Final Relative Density

The compactors were towed at speeds between 1.5 and 4.5 mph (2.4 and 7.2 km/h). Figure 6a shows the relationship of towing speed and D_r for test fills placed in 1-ft-thick (0.3-m) compacted lifts. Each lift received six coverages of vibratory compactors operating at a frequency of 1,500 cycles/min. The relative density decreases as the towing speed increases. A similar relationship, shown in Figure 6b, was obtained for all test fills. The lack of sufficient field data at a towing speed of 4.5 mph (7.2 km/h) is apparent; however, the relative density decreased when the towing speed increased beyond 3 mph (4.8 km/h). Thus, although the increase in towing speed is economically desirable, it causes a decrease in the final relative density. (Towing speed reflects the rest periods between the cycles if the frequency is the same.)

The increase that occurs in the final relative density as towing speed decreases agrees with previously published data (3).

The considerable scatter in the correlations shown in Figures 2 to 6 may be due to difficulties in determination of in situ relative density, heterogeneity in the degree of compactness of the sand, variation of the depth at which the relative density is determined, and lack of sufficient data when a single variable is studied while other variables are fixed.

CORRELATION OF SOIL PROPERTIES WITH COMPACTION PROCEDURE AND CHARACTERISTICS OF VIBRATORY COMPACTORS

It is difficult to establish general guidelines for selecting vibratory rollers or compaction procedures for cohesionless soils. Many variables are involved that may have appreciable effect on the result of compaction. Some of these variables are associated with properties of the compacted soil such as the content of fines, initial dry density, placement water content and size, roughness, and gradation of particles. A second group of variables pertain to the technical data of the vibrator. For example, the static weight of the compactor, the mass and eccentricity of the eccentric weight in the drum, the maximum operating frequency of the shaft and, hence, the maximum centrifugal radial force, the drum width, and diameter may all affect compaction. A third group of variables is related to details of the compaction procedure such as the frequency of the rotation of the shaft, the number of coverages, the towing speed, the lift thickness, and the number of lifts.

The data from the test fills at Ludington, Michigan, present an opportunity to explore the feasibility of establishing some type of relationship among some of the factors involved in the compaction of cohesionless soils. From the first group of variables, the dry density of the soil was considered to be one of the variables that may reflect some of the other variables pertaining to the soil properties. From the second group of variables, the force per unit width of the drum was speculated to be an important variable (4). The main variables pertaining to the compaction procedure, namely frequency, number of coverages, towing speed, and lift thickness, were all considered in the analysis.

A good criterion that can be used for comparing the performance of the vibratory compactors in cohesionless soils is the final relative density of the compacted soil. Data shown in Figures 2 to 6, previously published data (1, 2, 3, 4, 5), and intuition suggest that this relative density should increase as total force (F_{total}) per unit width of drum, number of coverages, and frequency increase and as towing speed, lift thickness, and initial (or final) dry density of the soil decrease. A dimensionless relationship between D_r and these variables can be given in the form:

$$D_r = K \alpha^a \qquad (1)$$

Figure 7. Final relative density versus dimensionless factor α.

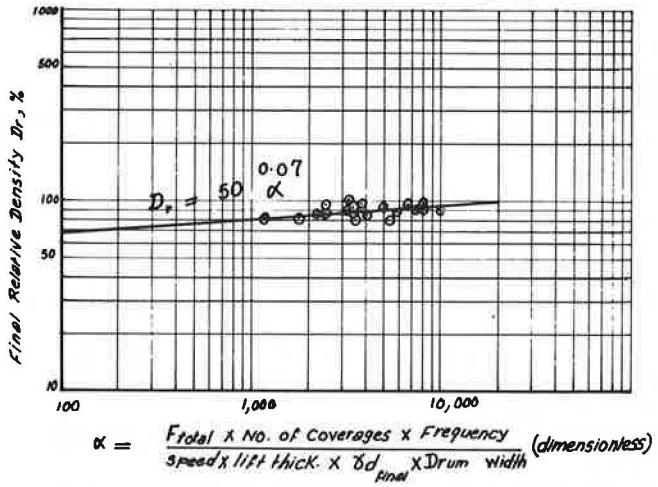

where

K and a = constants, and

$$\alpha = \frac{F_{total} \times \text{number of coverages} \times \text{frequency}}{\text{speed} \times \text{lift thickness} \times \alpha d_{final} \times \text{drum width}} \quad (2)$$

The data available from the test fills at Ludington were used to calculate the values of α in equation 2. The variation in D_r in relation to α is shown in Figure 7 on log-log scale. Figure 7 shows that the proposed equation 1 is a good representation of the data. A statistical study of the data shown in Figure 7 gives K = 50 and a = 0.07. Thus the data obtained from the test fills constructed of poorly graded medium-to-fine sand at Ludington, Michigan, lead to the following relationship between α and D_r:

$$D_r = 50\ \alpha^{0.07} \quad (3)$$

CONCLUSIONS

1. Relative density can be used as a measure of the effectiveness of various variables involved in the vibratory compaction of cohesionless soils.
2. For the poorly graded medium-to-fine sand used in the test fills at Ludington, Michigan, the following are valid: (a) The variation of the compacted lift thickness between 0.45 and 1.00 ft (0.14 to 0.3 m) did not significantly influence D_r, (b) D_r increased as the number of coverages (up to six), the operating frequency, and the total force applied by the compactor increased, and (c) D_r decreased as the towing speed increased.
3. A statistical relationship exists between D_r and the dimensionless factor α. This reflects some of the important properties of the soil, vibratory compactor, and compaction procedure. This relationship is given by the equation, $D_r = 50\ \alpha^{0.07}$.

ACKNOWLEDGMENTS

We would like to thank the Public Power Company (Cooper Nuclear Station), Consumer Power Company, the Detroit Edison Company, and Ebasco Engineering Corporation (Ludington Pumped Storage Project) for permission to publish the data from their projects. Yves Lacroix and Dennis Leary of Woodward—Moorhouse and Associates, Inc., supplied the data and encouraged us during the preparation of the paper.

REFERENCES

1. B. B. Broms and L. Forssblad. Vibratory Compaction of Cohesionless Soils. Proc., 7th International Conference on Soil Mechanics and Foundation Engineering, Mexico, Vol. 1, 1969, pp. 1-19.
2. D. J. D'Appolonia, R. U. Whitman, and E. D'Appolonia. Sand Compaction With Vibratory Rollers. Proc., Soil Mechanics and Foundations Division, ASCE, Vol. 95, No. SM1, paper 6366, 1969, pp. 263-284.
3. L. Forssblad. Investigation of Soil Compaction by Vibration. ACTA Polytechnica Scandinavica, Ci 34, Stockholm, 1965.
4. A. W. Johnson and J. R. Sallberg. Factors That Influence Field Compaction of Soils. HRB Bulletin 272, 1960, 206 pp.
5. W. A. Lewis. Recent Research Into the Compaction of Soil by Vibratory Compaction Equipment. Proc., 5th International Conference on Soil Mechanics and Foundation Engineering, Paris, Vol. 1, 1961.
6. C. F. Whitehead and D. Ruotolo. Ludington Pumped-Storage Project Wins 1973 Outstanding CE Achievement Award. Civil Engineering, ASCE, June 1973, pp. 64-68.

STRESS-STRAIN CHARACTERIZATION OF TWO COMPACTED SOILS

Roy V. Sneddon, Department of Civil Engineering, University of Nebraska

This study defines a triaxial test method for controlling or measuring the variables that govern stress-strain behavior of partially saturated, compacted soil in compression. Triaxial data for Peorian loess and Hastings silt loam from Nebraska are combined into a useful, compact form by using exponential functions. Stress-strain curves representing a wide range of initial densities and moisture contents are reasonably well characterized by a hyperbolic stress-strain function. The two coefficients of this function are shown to be exponential functions of void ratio and degree of saturation. Techniques are given for determining elastic (secant) moduli as functions of the level of stress difference, degree saturation, and void ratio. These moduli can be used in flexible pavement design procedures requiring a subgrade stiffness for any reasonable assumed in situ subgrade condition of dry density and moisture content for the soils tested.

•THE primary cause of premature flexible pavement failure is cumulative plastic strain in the subgrade caused by repetitive, high-axle loads applied during periods of near saturation of the subgrade soil. Current concepts of flexible pavement design (1, 2, 3, 4, 5) predict the required depth of asphalt concrete to control these strains within acceptable limits. Designs are based on traffic and environmental conditions and laboratory tests of representative, compacted soil samples. Tests are conducted according to procedures purported to permit evaluation of subgrade strength and stiffness. Many of these tests neither measure nor control the known variables affecting the behavior of partially saturated, compacted soil (6, 7, 8). Current triaxial testing techniques can control or measure these variables. The triaxial test (9, 10, 11) is the most widely available test that is consistent with well-established principles of theoretical soil mechanics that have this capability. Currently, it appears to be the most appropriate test for routinely evaluating stress-strain behavior of compacted samples.

The specific test configuration for controlling both the relevant test variables and the synthesis of test data into a compact form is described in this paper. Possible applications of these data to flexible pavement design are shown.

STRESS-STRAIN CHARACTERISTICS OF COMPACTED SOILS

The physical state of a partially saturated soil depends on variables such as void ratio e, degree of saturation S_r, and soil structure λ. This indicates that it depends on the arrangement of soil particles and the electrical forces between adjacent particles (12) and invariants of the applied stress system (8).

Vertical strain ϵ in a partially saturated soil sample in triaxial compression ($\sigma_2 = \sigma_3$) can be given by a function of the form

Publication of this paper sponsored by Committee on Strength and Deformation Characteristics of Pavement Sections.

$$\epsilon = H(p_a, q, u_c, e, S_r) \tag{1}$$

where

σ_1 = major principal stress (compression +),
σ_3 = minor principal stress (confining pressure),
$p_a = \frac{\sigma_1 + 2\sigma_3}{3} - u_a$ = mean stress,
$2q = (\sigma_1 - \sigma_3)$ = stress difference,
$u_c = u_a - u_w$ = suction pressure,
u_a = pore air pressure, and
u_w = pore water pressure.

It can be shown that u_w at small strains and initial soil structure λ_i (of compacted samples having a mineralogical and grain size composition C and molding water content w) are equivalent considerations (13, 14, 15) under certain limiting conditions, namely, the compaction procedure used, time of aging, and specimen temperature during aging and testing. After large strains have been applied, the effects of initial structure are largely obliterated, and the maximum stress difference is principally a function of molding water content w (13). Therefore, from equation 1, for a given compaction procedure and a range of moisture contents, if σ_3, u_a, and C are held constant, for small strains

$$\epsilon = H_1(q, S_{r_i}, e_i) \tag{2}$$

and for large strains

$$\epsilon = H_2(q, S_{r_f}, e_f) \tag{3}$$

where S_{r_i}, e_i are initial values in the sample and S_{r_f}, e_f are so called ultimate values that are reached after large strains (15).

Nonlinear triaxial stress-strain curves for sands and clays have been successfully approximated by a hyperbolic function of the form

$$\sigma_1 - \sigma_3 = \frac{\epsilon}{a + b\epsilon} \tag{4}$$

where a and b are coefficients to be determined (16, 17, 18, 19, 20, 21). Coefficients a and b are geometric properties of the laboratory stress-strain curve. It has been shown (15) that

$$a = h_1(S_{r_i}, e_i) \tag{5}$$

and that

$$b = h_2(S_{r_f}, e_f) \tag{6}$$

A relationship similar to equation 5 can be found elsewhere (22).

EXPERIMENTAL DETERMINATION OF COEFFICIENTS a AND b

Sample Description and Testing

Two aeolian soils, Peorian loess and Hastings silt loam, were selected for study. Typical soil properties are given in Table 1, and compaction characteristics are shown in Figure 1.

Two types of triaxial test were used to control or to measure sample variables (23). A consolidated constant water content test was used to test samples with $S_{r_i} < 100$ percent. Sample volume was measured periodically during testing (6, 7, 8) so that S_r and e could be calculated from known values of initial water content and dry density. Saturated specimens were tested in a consolidated undrained saturated test. All data were reduced by using a FORTRAN program TRIAX (23).

Correlating Functions

Hyperbolic stress-strain coefficients a and b were determined for the 17 Peorian and 12 Hastings samples tested. Semilog plots of a and b as functions of $e_i\sqrt{S_{r_i}}$ and $e_f\sqrt{S_{r_f}}$ respectively were linear as shown for a in Figure 2. Three different curves representing different compaction energies are shown in Figure 2. The slope of these curves was an exponential function of the degree of saturation at optimum moisture content S_{r_o} for each compactive effort (15). A composite equation for the a coefficient is given by

$$a = C_1 \exp (2.303\ m_1\ e_i\sqrt{S_{r_i}}) \tag{7}$$

where

$m_1 = C_2 \exp (2.303\ m_2\ S_{r_o})$ and
$C_1 = C_3 \exp (2.303\ m_3\ S_{r_o})$.

Numerical values of C_2, C_3, m_2, and m_3 are given elsewhere (15). It was also found that $e_i\sqrt{S_{r_i}}$ and $e_f\sqrt{S_{r_f}}$ are linearly related (15).

DATA USE

Two examples of possible ways in which these correlating functions can be used are given below. When equations 4 and 7 are used together with the equation for the b parameter, triaxial stress-strain curves can be computed for the soils tested for any impact compacted sample (Proctor to modified Proctor energy). Initial and final values of e and S_r must be known for the sample.

Five identical samples of Peorian loess have initial dry densities of 100 lb/ft^3 (1.60 g/cm^3), $w_i = 17.0$ percent, and $S_{r_o} = 76.8$ percent (Figure 1). The secant modulus of each sample at $\epsilon = 0.002$ must be determined if four samples increase in water content at constant dry density as shown in Figure 1. The a and b parameters for each sample can be computed as described above (15). A plot of the secant modulus versus S_r at the final water content is shown for these samples and for five Hastings samples in Figure 3.

Subgrade moduli (secant moduli) for various strains can be generated as shown above

Table 1. Sample description.

Sample Name	Classification	Sand (percent)	Silt (percent)	Clay (percent)	ω_L	I_p	G_s
Peorian loess	CH	0	72	28	50	24	2.73
Hastings silt loam	CH	1	66	33	60	38	2.68

Figure 1. Compaction curves for Peorian loess.

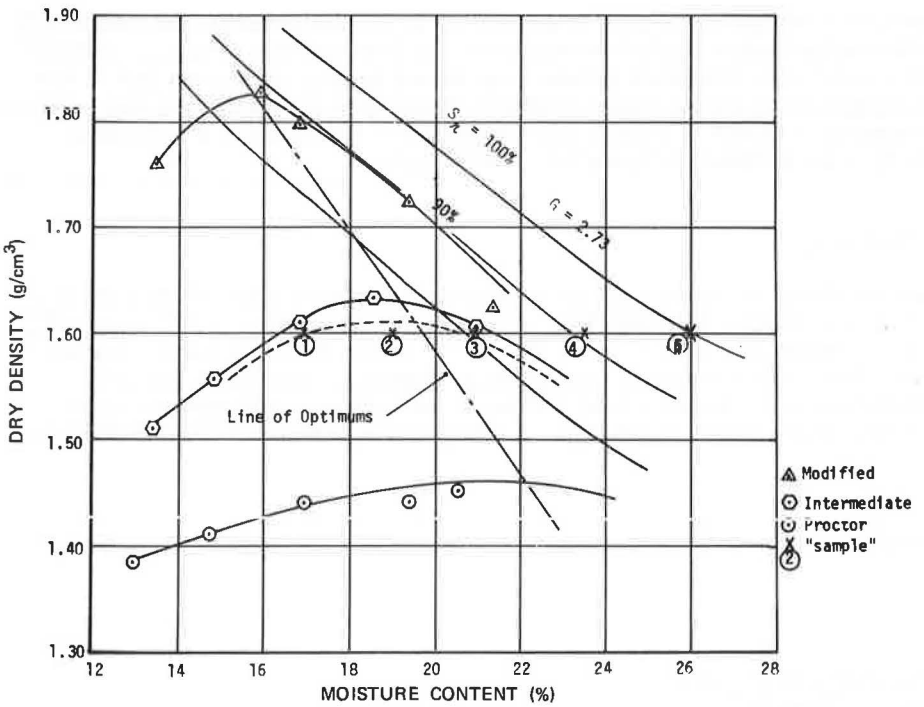

Figure 2. Correlation of coefficient a for Peorian loess.

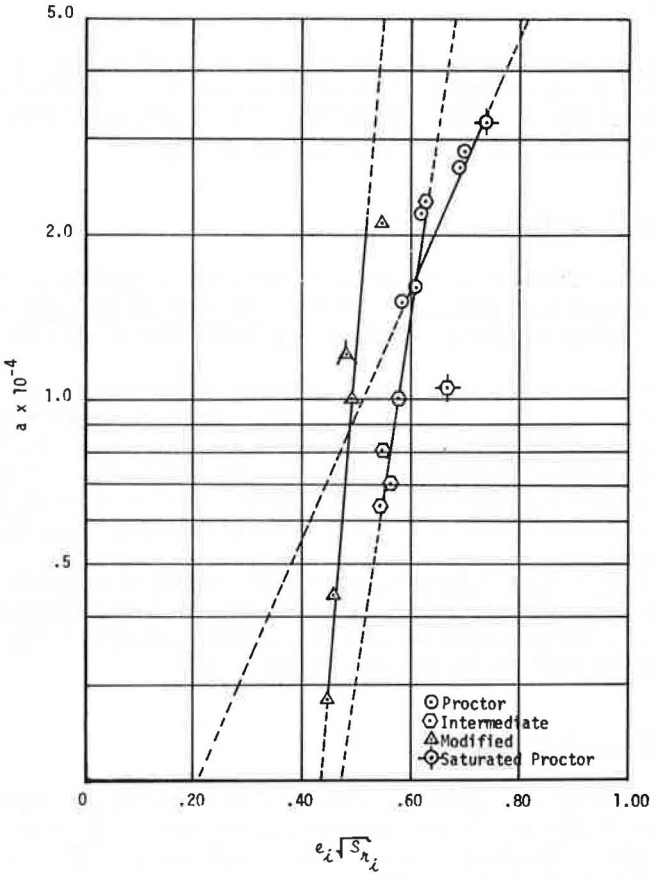

Figure 3. Secant modulus versus S_r calculated at 0.002 strain.

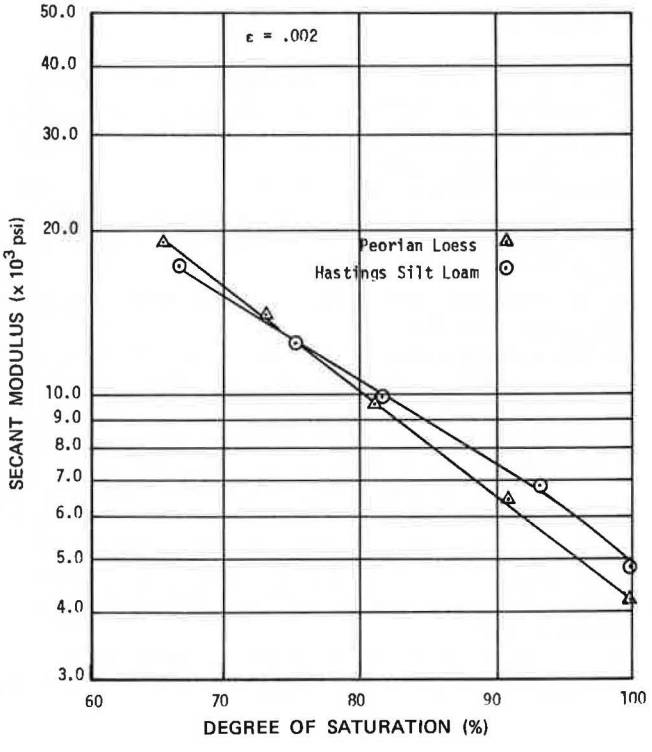

for use in a flexible pavement design procedure similar to the Kansas method (3). The value of the secant modulus depends on the assumed strain since soil has a nonlinear stress-strain curve. Therefore, a trial and error procedure is required (3, 24). Such a procedure has been given elsewhere (15).

CONCLUSIONS

A triaxial testing method was demonstrated for determining the stress-strain curves of compacted, partially saturated, or saturated subgrade soil capable of controlling or measuring those variables that determine static compression stress-strain behavior.

Stress-strain curves representing a wide range of densities and moisture contents for Peorian loess and Hastings silt loam from Nebraska were reasonably approximated by a hyperbolic stress-strain function. The two coefficients of this function, a and b, were nonlinear functions of S_{r_o}, $e_i\sqrt{S_{r_i}}$ and $e_f\sqrt{S_{r_f}}$. Use of these nonlinear functions produced a compact form for determining a and b and, therefore, for generating stress-strain curves over wide ranges of initial density and degree of saturation for the soils tested.

The design of flexible pavements, based on subgrade stiffness criteria, can be accomplished for a broad range of assumed in situ subgrade conditions of density and degree of saturation for the soils tested, and there is no need to test samples that have been brought to the assumed design state.

ACKNOWLEDGMENT

This study was made possible through a grant from the U.S. Department of Transportation, Federal Highway Administration, and the Nebraska Department of Roads. The opinions, findings, and conclusions are those of the author and not necessarily those of the sponsoring agencies.

REFERENCES

1. F. N. Hveem and R. M. Carmany. The Factors Underlying the Rational Design of Pavements. HRB Proc., Vol. 28, 1948, pp. 101-136.
2. Interim Guide for Design of Flexible Pavement Structures. AASHO Committee on Design, Oct. 1962.
3. Kansas State Highway Commission. Design of Flexible Pavement Using the Triaxial Compression Test. HRB Bulletin 8, 1947.
4. C. McDowell. Triaxial Tests in Analysis of Flexible Pavements. HRB Research Rept. 16-B, 1954, pp. 1-28.
5. N. W. McLeod. Flexible Pavement Thickness Requirements. Proc., AAPT, 1956, pp. 199-291.
6. A. W. Bishop and G. E. Blight. Some Aspects of Effective Stress in Saturated and Partly Saturated Soils. Geotechnique, Vol. 13, 1963, pp. 177-197.
7. A. W. Bishop and I. B. Donald. The Experimental Study of Saturated Soil in the Triaxial Test. Proc., 5th International Conference on Soil Mechanics and Foundation Engineering, Vol. 1, 1961, pp. 13-21.
8. E. L. Matyas and H. S. Radhakrishna. Volume Change Characteristics of Partially Saturated Soils. Geotechnique, Vol. 18, 1968, pp. 432-448.
9. A. W. Bishop and D. J. Henkel. The Measurement of Soil Properties in the Triaxial Test, 2nd Ed. Edward Arnold Ltd., London, 1962.
10. Research Conference on the Shear Strength of Cohesive Soils. Proc., ASCE, Boulder, 1960.
11. E. J. Yoder and C. R. Lowrie. Triaxial Testing Applied to Design of Flexible Pavements. HRB Proc., Vol. 31, 1952, pp. 487-498.

12. T. W. Lambe. The Structure of Compacted Clay. Journal of the Soil Mechanics and Foundations Division, ASCE, Vol. 84, No. SM2, Paper 1654, 1958.
13. H. B. Seed and C. K. Chan. The Structure and Strength Characteristics of Compacted Clays. Journal of the Soil Mechanics and Foundations Division, ASCE, Vol. 85, No. SM5, 1959, pp. 87-128.
14. H. B. Seed and C. K. Chan. The Undrained Strength of Compacted Clays After Soaking. Journal of the Soil Mechanics and Foundations Division, ASCE, Vol. 85, No. SM6, 1959, pp. 31-47.
15. R. V. Sneddon. Strength and Stiffness Characteristics of Compacted Nebraska Soils. Interim Rept., Prepared for Nebraska Department of Roads, Study 63-14, 1973.
16. R. L. Kondner. Hyperbolic Stress-Strain Response: Cohesive Soils. Journal of the Soil Mechanics and Foundations Division, ASCE, Vol. 89, No. SM1, 1963, pp. 115-143.
17. R. L. Kondner and J. M. Horner. Triaxial Compression of a Cohesive Soil With Effective Octahedral Stress Control. Canadian Geotechnical Journal, Vol. 2, No. 1, 1965, pp. 40-52.
18. R. L. Kondner and J. S. Zelasko. A Hyperbolic Stress-Strain Formulation for Sands. Proc., 2nd Annual Pan-American Conference on Soil Mechanics and Foundation Engineering, Vol. 1, 1963, pp. 289-324.
19. R. L. Kondner and J. S. Zelasko. Void Ratio Effects on the Hyperbolic Stress-Strain Response of Sand. In Laboratory Shear Testing of Soils, ASTM STP 361, Ottawa, 1963.
20. J. M. Duncan and C. Y. Chang. Nonlinear Analysis of Stress and Strain in Soils. Journal of the Soil Mechanics and Foundations Division, ASCE, Vol. 96, No. SM5, 1970, pp. 1629-1953.
21. F. H. Kulhawy and J. M. Duncan. Finite Element Analysis of Stresses and Movements in Dams During Construction. Office of Research Services, Univ. of California, Berkeley, Rept. TE 69-4, 1969.
22. P. T. DaCruz. Shear Strength Characteristics of Some Residual Compacted Clays. Proc., 2nd Annual Pan-American Conference on Soil Mechanics and Foundation Engineering, Vol. 1, 1963, pp. 73-102.
23. A. Rodriguez. Strength and Stiffness Characteristics of Compacted Peorian Loess. Univ. of Nebraska, MS thesis, 1971.
24. E. J. Yoder. Principles of Pavement Design. John Wiley and Sons, Inc., New York, 1959.

SPONSORSHIP OF THIS RECORD

GROUP 2—DESIGN AND CONSTRUCTION OF TRANSPORTATION FACILITIES
W. B. Drake, Kentucky Department of Transportation, chairman

COMPACTION AND STABILIZATION SECTION
Eugene B. McDonald, South Dakota Department of Transportation, chairman

Committee on Compaction
John R. Sallberg, Federal Highway Administration, chairman
Mehmet C. Anday, Robert C. Deen, Delon Hampton, C. M. Higgins, J. M. Hoover, Eugene Y. Huang, James E. Kelly, T. F. McMahon, William O'Sullivan, Charles H. Shepard, William J. Sisiliand, Travis W. Smith, Robert J. Weaver, William G. Weber, Jr., Anwar E. Z. Wissa

SOIL MECHANICS SECTION
John A. Deacon, University of Kentucky, chairman

Committee on Strength and Deformation Characteristics of Pavement Sections
Richard D. Barksdale, Georgia Institute of Technology, chairman
Stephen F. Brown, Bert E. Colley, Hsai-Yang Fang, F. N. Finn, Jim Hall, Jr., R. G. Hicks, Frank L. Holman, Jr., Ignat V. Kalcheff, Bernard F. Kallas, William J. Kenis, Thomas W. Kennedy, Milan Krukar, H. Gordon Larew, Kamran Majidzadeh, Fred Moavenzadeh, William M. Moore, Quentin Robnett, Eugene L. Skok, Jr., Ronald L. Terrel

Committee on Embankments and Earth Slopes
Lyndon H. Moore, New York State Department of Transportation, chairman
Raymond A. Forsyth, A. Alexander Fungaroli, David S. Gedney, Roger D. Goughnour, Wilbur M. Haas, William P. Hofmann, Henry W. Janes, Philip Keene, Charles C. Ladd, Richard E. Landau, Harry E. Marshall, Glen L. Martin, R. M. Mattox, Melvin W. Morgan, Lyle K. Moulton, John D. Nelson, Robert L. Schuster, Edgar Pierron Ulbricht, Walter C. Waidelich, William G. Weber, Jr., Donald L. York

Committee on Mechanics of Earth Masses and Layered Systems
Russell A. Westmann, University of California, Los Angeles, chairman
Richard G. Ahlvin, Richard D. Barksdale, Michael I. Darter, A. Alexander Fungaroli, Charles M. Gerrard, Delon Hampton, M. E. Harr, Robert L. Kondner, Raymond J. Krizek, Fred Moavenzadeh, Keshavan Nair, Gerald P. Raymond, Robert L. Schiffman, Awtar Singh, Robert D. Stoll, Aleksandar S. Vesic, Harvey E. Wahls, William G. Weber, Jr., T. H. Wu

SOIL AND ROCK PROPERTIES AND GEOLOGY SECTION
L. F. Erickson, Idaho Department of Highways, chairman

Committee on Exploration and Classification of Earth Materials
Robert L. Schuster, U.S. Geological Survey, Denver, chairman
Robert C. Deen, Edward A. Fernau, Albin D. Hirsch, William P. Hofmann, Frank L. Jagodits, Robert B. Johnson, Ralph W. Kiefer, Robert D. Krebs, Clyde N. Laughter, R. M. Mattox, Donald E. McCormack, Olin W. Mintzer, R. Woodward Moore, Arnold C. Orvedal, David L. Royster, A. Rutka, Robert B. Sennett, William W. Shisler, Preston C. Smith, Ernest G. Stoeckeler, J. Allan Tice, Walter H. Zimpfer

John W. Guinnee, Transportation Research Board staff

Sponsorship is indicated by a footnote on the first page of each report. The organizational units and the chairmen and members are as of December 31, 1974.